Universität Rostock Traditio et Innovatio

Universitätsmedizin Rostock

Defective myelination and its relative mechanism in Niemann-Pick type C disease

Inauguraldissertation

zur

Erlangung des akademischen Grades

Doktor der Medizinwissenschaften

der

Universitätsmedizin Rostock

Vorgelegt von

Fan Yang, Geb am 21.08.1986 in Rizhao, V. R. China

Rostock, 2022

https://doi.org/10.18453/rosdok_id00003713

DOKTORARBEIT

UNIVERSITÄTSMEDIZIN ROSTOCK

Gutachter:

PD Dr. Jiankai Luo, Universitätsmedizin Rostock, Sektion für Translationale Neurodegeneration „Albrecht Kossel“ der Klinik und Poliklinik für Neurologie

Prof. Dr. med. Rüdiger Köhling, Universitätsmedizin Rostock, Oscar Langendorff Instituts für Physiologie

Prof. Dr, rer. nat. Thomas Pufe, Universitätsklinikum Aachen, Instituts für Anatomie und Zellbiologie

Jahr der Einreichung: 2019

Jahr der Verteidigung: 2022

Contents

1. Introduction

1.1. Niemann–Pick type C disease

Niemann–Pick type C (NPC) disease is a rare neurovisceral disorder characterized by the accumulation of unesterified cholesterol and glycosphingolipids in the late endosomal and lysosomal (LE/LY) compartments. Generally, NPC occurs as a result of mutations in the gene of NPC intracellular cholesterol transporter 1 (*npc1*) or 2 (*npc2*) [1,2]. Its incidence is approximately 1/150,000 live births [3], with the age at onset being very heterogeneous among patients. The classic visceral pathology of NPC includes hepatomegaly and splenomegaly, whereas its neurological symptoms include cerebellar ataxia, dysarthria, dysphagia, and progressive dementia. Moreover, vertical supranuclear gaze palsy (VSGP) is observed in most cases, and psychiatric disturbances are frequently detected in late-onset patients [4]. Corresponding to the various neurological symptoms, neuron degeneration and myelin disruption in the central nervous system (CNS) have been considered as the main defects in both patients and animal models of NPC [5-8].

1.1.1. History of NPC

Niemann–Pick diseases were first described by Albert Niemann in 1914 [9], and its pathological defects, including enlarged liver, spleen, and lymph nodes, were later described by Ludwig Pick in the 1930s [10]. Moreover, an accumulation of lipids was reported in the liver, spleen, lungs, bone marrow, and brain [5]. In the late 1950s, Niemann–Pick diseases were classified into four groups according to their clinical manifestations: NPA, NPB, NPC, and NPD [11,12]. Both NPA and NPB were recognized as a disease that involves sphingomyelin accumulation, which is caused by a deficiency in acid sphingomyelinase (*smpd1*), whereas NPC was recognized as a disease that involves lipid accumulation in the LE/LY caused by abnormalities of intracellular transport of unesterified cholesterol (Fig. 1) [13]. In addition, NPD, relatively common in southwestern Nova Scotia (Canada), has been confirmed as an allelic variant of NPC in 1998 [14].

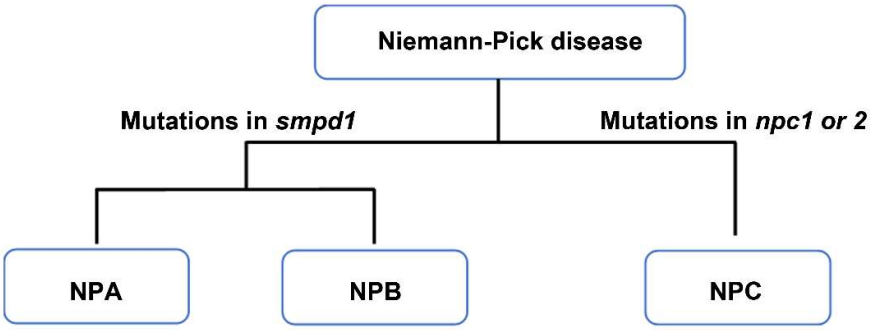

Fig. 1. Niemann–Pick disease types

Niemann–Pick diseases comprise three types: type A (NPA), type B (NPB), and type C (NPC). Both NPA and NPB are caused by mutations in the gene of acid sphingomyelinase (*smpd1*), whereas NPC is caused by mutations in the gene of either NPC intracellular cholesterol transporter 1 (*npc1*) or 2 (*npc2*).

1.1.2. The causes of NPC

Mutations in either the *npc1* or *npc2* gene lead to the accumulation of cholesterol in the LE/LY, which ultimately leads to NPC [1,15]. Approximately 95% and 5% of known cases of NPC are due to mutations in *npc1* and *npc2*, respectively (Fig. 2) [3]. Both NPC1 and NPC2 are mainly located in the LE/LY. NPC1 is an integral membrane protein, and NPC2 is a soluble lumenal protein. The human NPC1 protein consists of 1,278 amino acids and contains 13 presumed transmembrane domains and a sterol-sensing domain, which is homologous to 3-hydroxy-3-methylglutaryl-CoA reductase(HMG-CoA), sterol regulatory element-binding protein cleavage-activating protein (SCAP), NPC1-like protein-1 (NPC1L1), and Patched receptor. On the other hand, the human NPC2 protein is composed of 151 amino acids. In the LY/LE, NPC1 and NPC2 can bind cholesterol and transport it to the plasma membrane and cellular organelles, although the mechanism underlying this process has not yet been completely clarified [16,17].

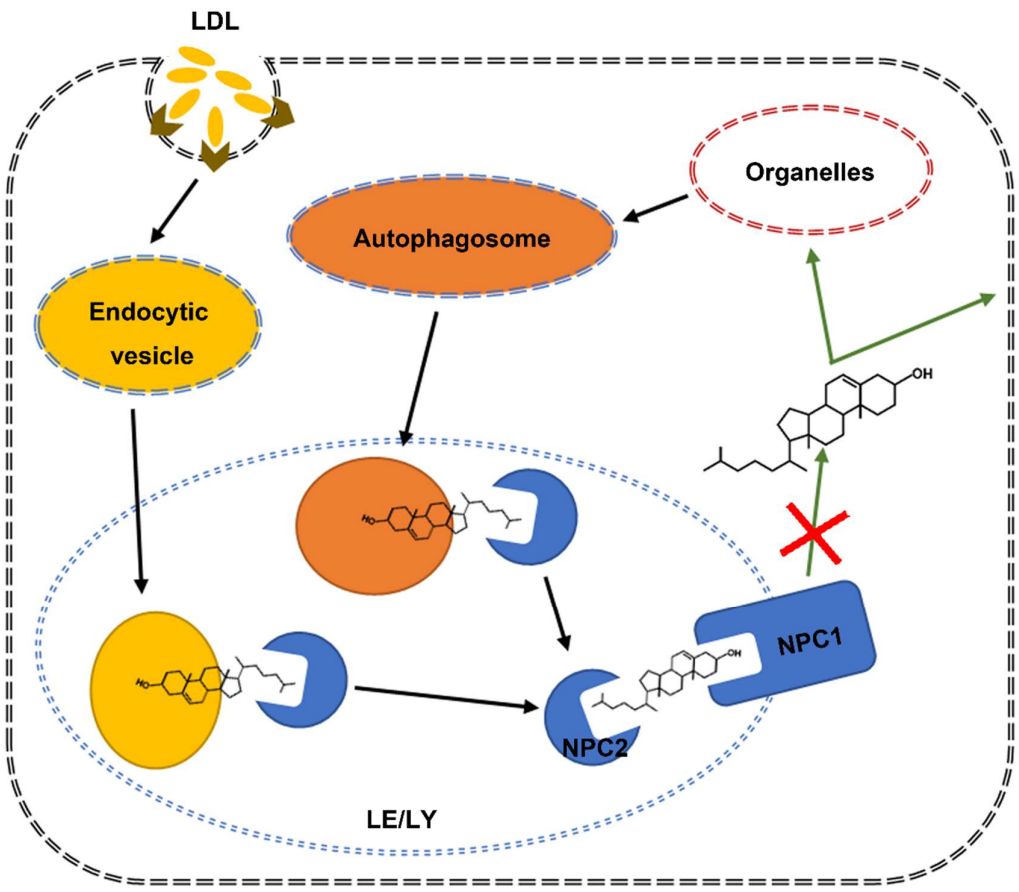

Fig. 2: Schematic diagram of cholesterol transport by NPC1 and NPC2

Cholesterol from either endocytosis or autophagy in the LE/LY is extracted by NPC2, passed to NPC1 (hydrophobic hand-off transfer model), and then transferred by NPC1 to the plasma membrane or organelles. Mutations in *npc1* or *npc2* gene disrupt the transport of cholesterol (red cross) and lead to NPC.

Notably, the main cellular pathology of NPC is the accumulation of unesterified cholesterol in the LE/LY, which can be detected using filipin staining [18]. Besides cholesterol, other sphingolipids, including sphingomyelin, gangliosides (especially GM2 and GM3), and sphingosine, are also deposited in *npc1* mutant ($NPC1^{-/-}$) cells. However, the reason why various lipids are accumulated in $NPC1^{-/-}$ cells is still debated. Gondre-Lewis et al. believed

that the accumulation of cholesterol in NPC1-deficient neurons depends on gangliosides [19]. However, the reduced ganglioside accumulation in NPC1-deficient mice by intercrossing with GM2/GD2 or GM3 synthase-deficient mice did not reduce the accumulation of cholesterol or improve the clinical phenotypes in $NPC1^{-/-}$ mice [20]. Other studies have suggested that dysregulated lysosomal calcium due to sphingosine accumulation secondarily leads to the storage of cholesterol and sphingolipids [21]. However, given that different types of sphingolipids are accumulated in the LE/LY in sphingolipid storage diseases, Simons and Gruenberg postulated the involvement of lipid rafts in lysosomal storage diseases, in which one overloaded lipid component of lipid rafts in the LE may slowly trap other components [22]. Notably, the cholesterol processed in the LE/LY originates from not only the receptor-mediated uptake of exogenously supplied lipoproteins (e.g., low-density lipoproteins [LDLs]), but also recycled membrane and organellar components from endocytosis and autophagy. Moreover, lipids in the LE/LY, especially in the CNS, are extensively supplied from recycled cell membranes, because of the insulation from the blood-brain barrier, which limits the supplementation of circulating LDLs [23,24]. Sandhoff et al. suggested that membrane lipids in the LE/LY can be degraded by hydrolytic enzymes only after cholesterol is extracted from the membranes [23,25], and they also suggested that high-level cholesterol inhibits the activity of lysosomal lipid-binding and lipid-transfer proteins, such as saposin-A (Sap-A), saposin-B (Sap-B) [26,27], and sphingomyelinase [28]. Therefore, the blockage of cholesterol exclusion from the LE/LY, due to the dysfunction of NPC1 or NPC2, attenuates the lysosomal function and leads to the accumulation of other lipids in the lysosome.

1.1.3. Neuronal degeneration in NPC

In 1958, Crocker and Farber [5] described cortical atrophy and distended neurons in patients with NPC. Subsequently, a loss of volume in vast brain regions, such as the gray and white matter of the cerebellum [29], hippocampus, thalamus, and cortex, has been reported [8]. In addition, neurofibrillary tangles, which are ultrastructurally identical to those reported in Alzheimer's disease, have been detected in the cerebellar cortex, hippocampus, hypothalamus, thalamus, and basal ganglia in patients with NPC [30,31]. Atrophy of the cerebellum, especially the loss of Purkinje cells, is regarded as the most prominent feature in the pathology of NPC [6,32]. Recently, a volume change in the cerebellum has been associated with the impairment of saccadic gain and motor control in adult patients with NPC [29]. In the mouse model of NPC, neuronal degeneration has been detected as early as postnatal day 9 (P9) [33], with severity

varying among different regions. For example, 96% of Purkinje cells, 28% of neurons in the prefrontal cortex, 20% of neurons in the thalamus, and 63% of glial cells in the corpus callosum were found to be degenerated in 11-week-old NPC1$^{-/-}$ mice when compared to the controls [6].

1.1.4. Myelin disturbance in NPC

Myelin disturbance is another obvious but less investigated pathology in NPC and is equivalent to the reduction of white matter in the cortex and cerebellum of patients with NPC [8] and particularly in the mouse model of NPC [7,34]. Myelin disturbance was reported in NPC1$^{-/-}$ mice as early as in the 1980s [35]. In 2004, Takikita et al. suggested a pathological feature of hypomyelination in NPC1$^{-/-}$ mice and proposed that disturbed myelination contributes to axonal injury [7]. In 2013, Yu and Lieberman reported that specific *npc1* knockout in either neurons or oligodendrocytes arrests the maturation of oligodendrocytes and delays myelination, proving the essential role of *npc1* in both neurons and oligodendrocytes during development [36]. However, myelination is affected unequally in different regions in NPC1$^{-/-}$ mice (e.g., it is severely affected in the cortex and corpus callosum but is mostly intact in the brainstem and optic nerves) [7]. Pathological diversity is possibly correlated with the onset of myelination in different regions. Generally, myelination is controlled spatiotemporally during development in the CNS, and its duration varies among different regions. Myelin formation starts caudorostrally in the brain but rostrocaudally in the spinal cord. Moreover, myelination starts at birth in the spinal cord and continues until around P60 in the mouse cortex [37]. It should be noted that regions myelinated later are more vulnerable to be affected in NPC. Therefore, to reveal the regulatory role of *npc1* in myelination, a comprehensive evaluation of myelin development is necessary.

1.1.5. Therapeutic strategies in NPC

Currently, the treatments available for NPC are limited, and most of the therapeutic strategies are targeted at neuron loss, with fewer ones targeting the restoration of myelination. Miglustat, an inhibitor of glycosphingolipid synthesis, reduces the accumulation of gangliosides, delays the onset of neurological dysfunction, and increases the average lifespan of treated NPC1$^{-/-}$ mice [38]. It has been observed that the survival of Purkinje cells is prolonged in miglustat-treated cats [39]. In a 24-month trial involving miglustat treatment, patients with NPC showed mild clinical improvement or stabilization [40]. Several benefits for using histone deacetylase inhibitors and antiapoptotic agents to treat NPC1$^{-/-}$ animals have been reported [41].

Notably, the use of 2-hydroxypropyl-β-cyclodextrin (CD), an oligosaccharide with a hydrophobic pocket, is one of the most exciting and promising approaches for the treatment of NPC [3]. Generally, CD has a high affinity for cholesterol and can include cholesterol in its internal cavity. Although the mechanism of its function in NPC is still under debate [42], many data suggest that CD, which enters cells via endocytosis, depletes cholesterol from the LE/LY and delivers it to other cellular compartments [43,44]. Single-dose CD, which is used for the treatment of $NPC1^{-/-}$ mice, can significantly decelerate neurodegeneration and increase the lifespan [45]. Early (at P7) long-term administration of CD delays the onset of ataxic gait and tremor in $NPC1^{-/-}$ mice and greatly reduces the accumulation of cholesterol, glycosphingolipids, and sphingosine in neurons [46]. However, different concentrations of CD exhibit opposite effects on cholesterol homeostasis. For example, 0.1 mM CD mobilizes trapped cholesterol from the LE/LY to the endoplasmic reticulum (ER), 1 mM CD primarily extracts cholesterol from the plasma membrane and reduces ER cholesterol, and 10 mM CD shows profoundly neurotoxic effects [47].

In contrast to the vague mechanisms of CD, lovastatin, an agent used to prevent cardiovascular disease, reduces the synthesis of cholesterol by inhibiting 3-hydroxy-3-methylglutaryl-CoA reductase (HMGCR). Generally, lovastatin reduces the accumulation of cholesterol and GM3 gangliosides and diminishes astrogliosis in the brain of $NPC1^{-/-}$ mice [48]. Additionally, it has been suggested that lovastatin promotes the differentiation of oligodendrocyte progenitor cells (OPCs) and increases remyelination by increasing the activation and expression of both peroxisome proliferator-activated receptor-γ (PPAR-γ) and phosphatidylinositol 3,4,5-trisphosphate 3-phosphatase and dual-specificity protein phosphatase (PTEN) in multiple sclerosis [49].

1.2. Myelin regulation

Myelin is a membrane structure that extends from oligodendrocytes in the CNS and from Schwann cells in the peripheral nervous system (PNS). By wrapping axons with their multilamellar structures, oligodendrocytes generate electrically insulating myelin to increase the velocity of signal conduction and fulfill the metabolic requirements of ensheathed neurons [50,51].

Myelin contains a huge amount of lipids (70% of dry myelin weight), with approximately 26% of total lipids being cholesterol [52]. The approximate surface area of

myelin formed by one oligodendrocyte is about 20×10^5 μm^2 [52]. Myelin biosynthesis is extraordinarily fast; for instance, oligodendrocytes in zebrafish generate new myelin sheaths just within five hours [53]. Thus, a large amount of cholesterol is required in oligodendrocytes to form the most lipid-concentrated structure during myelination. Blockage of sterol biosynthesis via the conditional knockout of a specific enzyme, squalene synthase (SQS), in oligodendrocytes delays myelination and reduces the myelin thickness, which proves the essential role of a high cholesterol level during myelination [54]. In addition, the transportation of proteolipid protein (PLP) to the myelin sheath is strictly regulated by the cholesterol level in oligodendrocytes [55]. Furthermore, the dysmyelination due to overexpressed PLP in Pelizaeus–Merzbacher disease (PMD) can be restored by a cholesterol-rich diet [56]. Regarding the essential role of cholesterol in myelination, oligodendrocytes are considered one of the most vulnerable cell types in NPC.

1.2.1. Myelin structural proteins

Beside lipids, myelin contains various distinctive proteins. Generally, both PLP and DM20, its smaller splice isoform, are considered the most abundant myelin proteins, constituting approximately 17% of the total proteins, as estimated using proteomics on a purified myelin fraction from a mouse brain [57]. Despite its high abundance in myelin, PLP is not a requisite component during myelination, since mice lacking PLP/DM20 can be fully myelinated [58], which has recently been detected from the compensatory effect of glycoprotein M6B [59]. However, the absence of PLP/DM20 alters the ultrastructure of myelin [60], leading to axonal swelling and length-dependent degeneration in older mice [61,62]. In contrast, the overexpression of PLP results in hypomyelination [63], which is the most frequent cause of PMD [56]. Although their functions have not been completely revealed, it has been proposed that PLP and DM20 sequester and transport cholesterol to create a high cholesterol content in myelin [59].

Myelin basic protein (MBP) is another major myelin protein that constitutes approximately 8% of the total myelin proteins [57]. Generally, MBP is an indispensable myelin structural protein whose mutation leads to severe myelin deficiency in shiverer mice [64]. It is assumed that the function of MBP is to bring opposing inner membranes together and form a cohesive protein meshwork to extrude most proteins and other contents of the cytosol and compress the myelin membrane into a lipid-enriched insulating structure [65]. Therefore, the expression of MBP is controlled sophistically. During myelination, the mRNAs of MBP are

transported to the perikaryon and assembled with the machinery of protein synthesis to form granules [66], which are then transported along microtubules in a translationally silenced state to the myelin membrane of the oligodendrocyte [67]. Signals from the interacted axon initiate the translation of MBP locally [68], and the newly synthesized MBP is integrated immediately into the myelin sheath [69].

Myelin sheaths contain other highly abundant proteins, such as 2′,3′-cyclic nucleotide phosphodiesterase (CNP), myelin-associated glycoprotein (MAG), and myelin oligodendrocyte glycoprotein (MOG). First, CNP is mainly present in the paranodal loops and cytoplasm of noncompact myelin, but not in compact myelin. Similar to PLP, CNP-knockout mice can form normal myelin, but they also develop axonal swelling and neurodegeneration [70]. Second, MAG is essential for the maintenance of the cytoplasmic collar and periaxonal space of myelinated axons [71]. Third, MOG is a surface marker for oligodendrocyte maturation and is mainly located on the extracellular surface of myelin sheaths [72]. Using proteomic analysis in purified myelin fractions, in 2009, Jahn et al. reported 342 myelin and myelin-associated proteins [57]. In 2013, Gopalakrishnan et al. compared human and murine myelin fractions and identified 284 common lipids and 257 proteins [73]. Panfoli et al. pointed out that 1,280 proteins have been reported in 12 published proteomic studies until 2014 [74]. It should be noted that other myelin proteins may not have been identified because of the technical limitations in the current proteomic methodology.

1.2.2. Myelination during development

Oligodendrocytes differentiate from OPCs. Three subpopulations of OPCs originate successively from different germinal zones during development in the mouse brain. Since all subpopulations are replaceable, if one subpopulation is abolished, myelination remains intact [75]. To myelinate axons in the entire brain, OPCs need to migrate from their germinal zones toward their final destination. As observed in zebrafish, OPCs continuously extend and retract their filopodium-like structures to survey the environment and then finally spread uniformly in the CNS during migration [76]. Individual oligodendrocytes generate new myelin sheaths in a short time window [75,76]. Multiple processes extend and up to 50 sheaths can be generated from a single oligodendrocyte to wrap different axons [52]. At the same time, numerous myelin proteins are synthesized coordinately with lipids, including cholesterol, and then assembled and transported to myelin sheaths.

1.2.3. Interactions between neurons and oligodendrocytes

The interactions between neurons and oligodendrocytes are considered to be important in myelination. Signals from axons mostly control the myelination process rigorously and spatiotemporally *in vivo* (Fig. 3) [77], although oligodendrocytes in culture can wrap paraformaldehyde (PFA) fixed neurons [78] and even Matrigel-coated glass and Vicryl microfibers in proper diameters [79]. The proliferation of OPCs in zebrafish is influenced by the neuronal electrical activity [80], and the blockage of action potentials by tetrodotoxin (TTX) reduces the number of oligodendrocytes and inhibits myelination [81,82]. In addition, the proliferation or differentiation of OPCs in the corpus callosum of mice can be induced correspondingly via electrical stimuli with different frequencies [83]. During myelination, the number of OPCs produced is exceeded; for example, in the optic nerves at least twice the number of oligodendrocytes required is produced during myelination [84,85]. Since neurons guide oligodendrocytes to wrap target axons at the proper time, redundant oligodendrocytes undergo apoptosis during development [77,86]. Moreover, in the CNS, only axons larger than 0.2 μm in diameter can be myelinated [77,87], with the thickness of the myelin sheaths correlating with the diameter of the wrapped axons [88]. Myelin sheaths are not evenly spaced in single myelinated axons, and several unmyelinated regions interspersed with myelinated segments have been reported in neocortical pyramidal neurons [89]. Recently, in an *in vivo* study on zebrafish, it has been shown that elongation of myelin sheaths occurs after the elevation of cellular Ca^{2+} in oligodendrocytes induced by neuronal activity [90]. Furthermore, the nonreceptor tyrosine kinase focal adhesion kinase (FAK) in oligodendrocytes integrates multiple axonal signals and regulates downstream signaling pathways, which are involved in oligodendrocyte survival, cytoskeleton stabilization, and myelin protein synthesis [91].

Besides contact signals, secretory factors from neurons also modulate myelination, although these factors have not yet been fully identified. In zebrafish, the number of myelin sheaths from individual oligodendrocytes is regulated via synaptic vesicle release [92]. During myelination, axon selection is directed by activity-dependent secretion from axons, and blockage of vesicle-associated membrane protein 2-dependent exocytosis abolishes the preference for activating axons [93]. Treatment with a neuron-conditioned medium (CdM) increases the expression of MBP in oligodendrocytes [94] and triggers the transport of PLP

from the LE/LY to the plasma membrane [55]. Most likely, neurons from distinct CNS regions utilize different factors to regulate the development of oligodendrocytes [95].

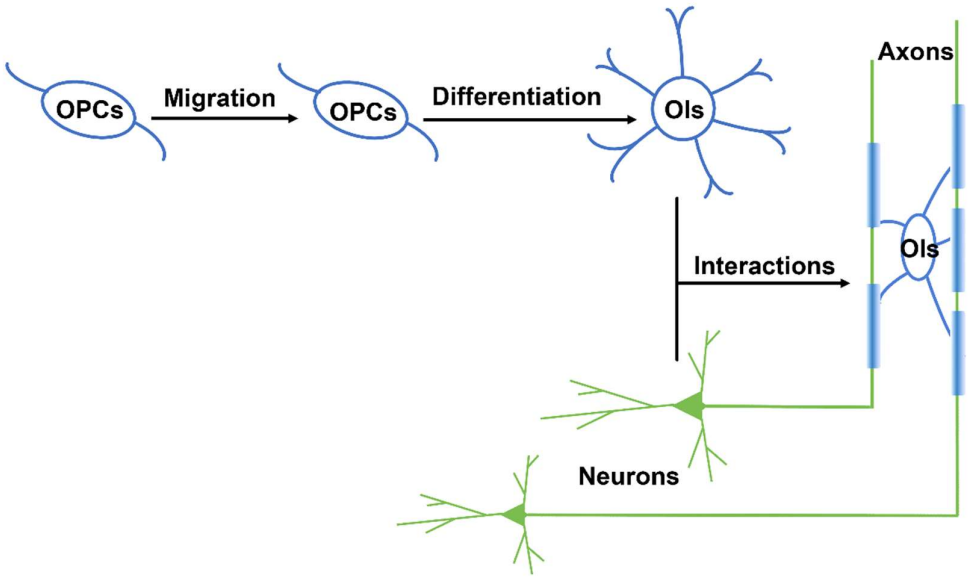

Fig. 3: Myelination during development

Generally, OPCs migrate from germinal zones and differentiate into oligodendrocytes. The interaction between oligodendrocytes and neurons facilitates the wrapping of axons by myelin sheaths from oligodendrocytes.

1.2.4. Signal cascades in myelination

Many signaling pathways are involved in the coordination of complex regulatory processes during myelination and the regulation of the production of myelin sheaths, which contain diverse lipids and proteins. For example, platelet-derived growth factor (PDGF), sonic hedgehog (SHH), and fibroblast growth factors (FGFs) regulate oligodendrocyte specification from multipotential neural progenitor cells. Moreover, PDGF and FGFs also promote the proliferation and migration of OPCs through different signal cascades [96]. Both inhibiting and promoting signals influence the differentiation and maturation of oligodendrocytes. Leucine-

rich repeat and immunoglobulin domain-containing 1 (LINGO-1) blocks the differentiation of OPCs via a homophilic intercellular interaction [97], and G-protein-coupled receptor 17 (GPR17) regulates DNA-binding protein inhibitors 2 and 4 (ID2/ID4) [98]. Triiodothyronine (T3) also promotes differentiation [99], and its deficiency disrupts myelination in patients with hypothyroidism [100].

Several transcription factors promote the differentiation of OPCs, such as oligodendrocyte transcription factor 1 (Olig1), Olig2, SRY-related HMG-box 10 (Sox10), and myelin gene regulatory factor (Myrf) [101-104]. Recently, Olig2 has been identified to recruit the chromatin-remodeling enzyme transcription activator BRG1 (Smarca4/Brg1) to distinct subsets of myelination regulatory genes and to precisely initiate and establish a transcriptional program that promotes the differentiation of OPCs into oligodendrocytes and subsequent myelination in the CNS [105]. Generally, Myrf is a transcription factor in specific postmitotic oligodendrocytes that has been identified by comparing transcriptomes of oligodendrocytes with neurons and astrocytes [106]. Full-length Myrf is located in the ER. After self-cleavage, its N-terminal domain (N-Myrf) is transported into the nucleus to activate the transcription of various myelin-related genes [107,108]. In general, Myrf is critical for oligodendrocyte maturation and myelination in the CNS, and its knockout leads to severe hypomyelination in mice [104]. Cyclin-dependent kinase inhibitor 1C protein (p57Kip2) inhibits the differentiation of oligodendrocytes in the nucleus [109] but promotes myelin formation when translocated from the nucleus into the cytosol [110]. Moreover, the intracellular calcium level, which is either mediated by voltage-operated Ca^{2+} channels (VOCCs) [111] or released from the ER, can modulate myelination, which is necessary in Schwann cells. For example, the elevated cytoplasmic Ca^{2+} level stimulated by neuregulin activates the nuclear factor of activated T-cell protein (NFAT) via calcineurin and activates Krox20, resulting in the myelination of Schwann cells [112]. It has also been found that the myelination of oligodendrocytes in the CNS is regulated by a similar mechanism [113].

1.2.5. Dysfunction of NPC1 protein in oligodendrocytes disrupts myelination

The accumulation of cholesterol in $NPC1^{-/-}$ oligodendrocytes impairs the LE/LY system and consequently disrupts signaling pathways (see i in Fig. 4). However, how the NPC1 protein affects myelination in the lysosomes remains to be elucidated. Schwend et al. reported that early embryonic cell movement is delayed as a result of the abnormal actin cytoskeleton

network in NPC1-deficient zebrafish [114]. Insufficient oligodendrocytes, resulting from either reduced proliferation or impaired migration of OPCs, can result in hypomyelination. Autophagic dysfunction and inhibited proteolysis are related to lipid accumulation in NPC1$^{-/-}$ cells [115,116]. The signals regulating autophagy have also been reported to regulate myelination, such as serine/threonine-protein kinase mTOR (mTor) [117]. Moreover, dysregulated lysosomal calcium may contribute to myelin disruption [21,118].

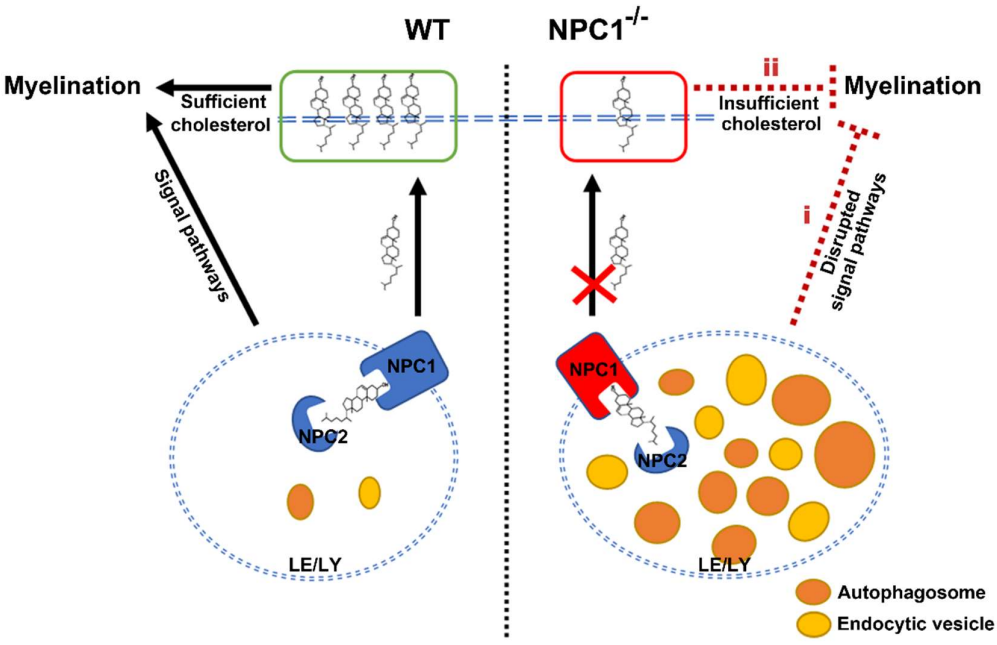

Fig. 4: Hypotheses of myelination disorders in NPC

In WT oligodendrocytes, NPC1 and NPC2 transport cholesterol from the LE/LY to support myelination, whereas the signaling pathways from the LE/LY regulate myelination. However, in NPC1-mutant (NPC1$^{-/-}$) oligodendrocytes, dysfunction of NPC1 either (i) overloads the LE/LY and disrupts the signaling pathways or (ii) blocks cholesterol supplementation from the LE/LY and causes cholesterol deprivation, resulting in the inhibition of myelination.

Alternatively, blocking cholesterol transport provokes its accumulation in the LE/LY and presumably restricts its supplementation to other cellular compartments. Although the level of cholesterol is a rate-limiting factor in myelination and its accumulation has been reported in various cell types, cellular cholesterol distribution has rarely been investigated in NPC1$^{-/-}$ oligodendrocytes. In NPC1$^{-/-}$ neurons, the level of cholesterol decreases in distal axons, despite

its heavy accumulation in cell bodies [119]. Furthermore, axonal growth in NPC1$^{-/-}$ neurons cannot be sustained by external cholesterol [120]. Given its massive requirement and rate-limiting role, cholesterol insufficiency resulting from disorientated transport may disrupt myelination (see ii in Fig. 4). However, the link between the dysfunction of cholesterol transport protein (either NPC1 or NPC2) and disrupted myelination remains to be elucidated.

1.3. Investigating myelination using an *in vitro* system

To investigate the signaling pathways involved in myelination, some *in vitro* systems have been established. Such an investigation of *in vitro* myelination started via tissue culture in the 1950s. In the 1980s, a primary oligodendrocyte culture was established, followed by the identification of different stage-specific markers. Thereafter, neurons isolated from different sources were added to a co-culture with oligodendrocytes [121]. For example, neurons from dorsal root ganglia have been commonly used in co-culture systems [122,123] because these neurons can be easily extracted and purified, but they are not CNS neurons. Retinal ganglion cells [124], on the other hand, are a type of CNS neurons that are difficult to obtain from a relatively small number of animals. Pang et al. described a mixed-culture system from embryonic spinal cord and cerebral cortex. However, neurons and oligodendrocytes are not separate, which is why manipulating a single cell type is impossible in this culture system [125]. Cheli et al. cultured cortical neurons from P1 mice and co-cultured them with cortical OPCs at day *in vitro* (DIV) 7, and only close contact was observed between the axons and processes of oligodendrocytes, but not myelin sheaths [126]. Gottle et al. used embryonic rat cortical neurons and observed myelin sheaths at DIV26 [110]. Oligodendrocytes from the cortex have been mostly used in co-culture systems [110,122,126] and seldom from optic nerves [99,124]. Notably, when cultured in the absence of growth factors, OPCs differentiate into oligodendrocytes spontaneously [99,127] and generate membrane structures that structurally and biochemically resemble myelin sheaths without neurons [128]. Therefore, primary oligodendrocyte culture systems allow the exploration of intrinsic signals, whereas co-culture systems facilitate the comprehension of the intercellular interactions between oligodendrocytes and neurons prior to and during myelination.

1.4. Aims of this study

Generally, progressive neurological impairments, including neuronal degeneration, dysmyelination, and gliosis, are found in the CNS of patients with NPC [129]. Although neuronal alterations have been widely investigated, the mechanisms underlying myelin deficiency are still mostly unknown, although dysmyelination has been reported as early as in the 1980s in a mouse model [35] and later in humans [8]. Therefore, in the present study, we chose the corpus callosum, one of the most myelin abundant structures, to investigate myelination by comparing the expressions of myelin structural and regulatory proteins in both wild-type (WT) and $NPC1^{-/-}$ mice. Primary oligodendrocytes were used to evaluate the differentiation of OPCs, relative signaling pathways, and pathophysiological roles of cholesterol in myelination in $NPC1^{-/-}$ mice.

Therefore, the goals of this study are as follows:

- To investigate whether mutations in NPC1 cause hypomyelination or demyelination in mice
- To investigate the cellular mechanisms of myelin deficiency and relative signaling pathways
- To assess the involvement of cholesterol metabolism in myelin deficiency

2. Materials and Methods

2.1. Animals

Heterozygous NPC1 (HZ, $NPC1^{+/-}$) mice (BALB/cNctr-Npc1m1N/J) were purchased from the Jackson Laboratory and used to generate NPC1-mutant (NPC, $NPC1^{-/-}$) and WT (WT, $NPC1^{+/+}$) mice. All experiments were approved by the local ethical committee and performed according to the *Guide for the Care and Use of Laboratory Animals*.

2.2. Materials

2.2.1. Equipment

Name	Company	Model number
Criterion™ Cell	Bio-Rad Laboratories	1656001
LightCycler®	Roche Diagnostics	Nano
Microscope	Keyence	Biozero
Odyssey Infrared Imaging System	LI-COR Biosciences	9120
Photometer	Amersham Biosciences	Ultrospec 3100
Trans-Blot® Turbo™ Transfer Starter System	Bio-Rad Laboratories	17001915

2.2.2. Chemicals

Name	Company	Order number
Biotin	Sigma	B4639
BrdU	Abcam	142567
Bromophenol blue	Carl Roth	A512.1
BSA	Roche Diagnostics	8076.4
Ceruloplasmin	Calbiochem	239799
DNase I	Roche Diagnostics	1010159001
EDTA	Sigma	E5134
EGTA	Sigma	G4378
Filipin	Sigma	F4767
Glycerol	Merck	1.04094.1000
Hydrocortisone	Sigma	H0888
Insulin	Sigma	I6634
L-Glutamine	Invitrogen	25030
Lovastatin	Calbiochem	438185
NaCl	Carl Roth	3957.2
NaF	Merck	1.06688.0100
NaOH	Carl Roth	6771.3

PDL	Sigma	7405
Progesterone	Sigma	P6149
Putrescine	Sigma	P5780
SDS	Carl Roth	2326.2
Skim milk powder	Sigma	BCBT8091
Sodium deoxycholate	Sigma	T7284
Sodium pyrophosphate tetrabasic decahydrate	Sigma	S6422
Sodium selenite	Sigma	S5261
T3	Sigma	T6397
Transferrin	Sigma	T1147
Tris	Carl Roth	4855.2
Tris-HCl	Carl Roth	9090.2
Triton X-100	Roche Diagnostics	10789704001
Tween 20	Carl Roth	9127.3
Vitamin B_{12}	Sigma	V6629
CD	Sigma	H107
β-Mercaptoethanol	Sigma	M3148

2.2.3. Kits and reagents

Name	**Company**	**Order number**
B27 supplement	Invitrogen	17504
Criterion™ TGX Precast Midi Gel 12-well	Bio-Rad Laboratories	567-1083
Criterion™ TGX Precast Midi Gel 18-well	Bio-Rad Laboratories	567-1084
DMEM	Invitrogen	11960
FastStart Essential DNA Green Master	Roche Diagnostics	6402712001
FBS	Thermo Fisher Scientific	10091-148
Goat serum	Dako	X0907
Hibernate w/o Ca^{2+} medium	BrainBits LLC	HA-Ca
Hibernate-A medium	BrainBits LLC	HA
MEM	Life Technologies	12360-038
Mounting medium	Vector	H1200
Neurobasal-A	Invitrogen	10888
OptiPrep 1.32	Sigma	D1556
Papain suspension	Worthington	LS003126
PBS buffer	Merck	L1825
Pen/Str stock solution	Invitrogen	15140
PhosSTOP	Roche Diagnostics	04906845001

Pierce BCA Protein Assay	Thermo Fisher Scientific	23225
Protease inhibitor cocktail	Roche Diagnostics	4693159001
QuantiTect Reverse Transcription Kit	Qiagen	205311
RNeasy Plus Micro Kit	Qiagen	74034
Taq PCR Core Kit	Qiagen	201225

2.2.4. Primers

Gene	Sequence	Tm
NPC1 WT	Fr: CTG TAG CTC ATC TGC CAT CG	59.4
	Re: TCT CAC AGC CAC AAG CTT CC	59.4
NPC1 mutant	Fr: TGA GCC CAA GCA TAA CTT CC	57.3
	Re: GGT GCT GGA CAG CCA AGT A	58.8
GAPDH	Fr: AGT ATG TCG TGG AGT CTA CTG	60.7
(NM_008084)	Re: GAG TTG TCA TAT TTC TCG TGG T	60.4
PPIA	Fr: CAG ACA AAG TTC CAA AGA CAG	59.4
(NM_008907)	Re: ATT ATG GCG TGT AAA GTC ACC	60.7
PLP	Fr: CTT CAA TAC CTG GAC CAC CT	60.2
(NM_011123)	Re: GGG AGA ACA CCA TAC ATT CTG	60.1
MBP	Fr: CAC ACG AGA ACT ACC CAT TA	59.1
(NM_010777)	Re: CGA GGT GTC ACA ATG TTC TT	60.6

2.2.5. Antibodies

Name	Company	Host	Order number	Dilution
Anti-BrdU	Roche Diagnostics	Mouse	11170376001	1:200
Anti-Caspr	NeuroMab	Mouse	75-001	1:500
Anti-GAPDH	Abcam	Mouse	ab8245	1:10,000
Anti-MBP	BioLegend	Mouse	SMI-99	1:1,000
Anti-MOG	Merck	Mouse	MAB5680	1:200
Anti-Myrf-C	Abcam	Rabbit	ab93040	1:500
Anti-Myrf-N	Abcam	Rabbit	ab96444	1:500
Anti-Nav1.6	Alomone Labs	Rabbit	ASC009	1:500
Anti-NF	BioLegend	Mouse	SMI31	1:1,000

Anti-NG2	Abcam	Mouse	ab5000	1:200
Anti-Olig1	Santa Cruz Biotechnology	Mouse	sc-166257	1:200
Anti-Olig2	Merck	Rabbit	ab9610	1:500
Anti-p57Kip2	Sigma	Rabbit	P0357	1:800
Anti-PLP	Abcam	Rabbit	ab28486	1:500
Anti-Sox10	Abcam	Rabbit	ab27655	1:500

Anti-mouse IgG IRDye-800	Rockland	Goat	610-131-121	1:10,000
Anti-rabbit IgG IRDye-680	Rockland	Goat	926-68021	1:10,000
Anti-mouse IgG Alexa Fluor-488	Invitrogen	Goat	A-11029	1:500
Anti-rabbit IgG Alexa Fluor-568	Invitrogen	Goat	A-11031	1:500

2.2.6. Solutions

All solutions were grouped according to their application.

(1) Genotyping

(a) 50× base solution

NaOH 2.5 g and EDTA-2Na·2H_2O 186 mg in water to 50 mL, pH 12. Dilute with water to 1× base solution for use.

(b) 50× neutralization solution

Tris-HCl 15.76 g in water to 50 mL, pH 5. Dilute with water to 1× neutralization solution.

(2) Western blot

(a) Radioimmunoprecipitation assay (RIPA) buffer

Tris 0.24 g, NaCl 0.8 g, sodium dodecyl sulfate (SDS) 0.1 g, sodium deoxycholate (SDC) 0.5 g, Triton X-100 1 mL, glycerol 10 mL, ethylenediaminetetraacetic acid (EDTA) 0.0744 g, egtazic acid (EGTA) 0.038 g, NaF 0.004 g, and sodium pyrophosphate tetrabasic decahydrate 0.89 g in water to 100 mL. Add protease inhibitor cocktail and PhosSTOP before use.

(b) 5× Laemmli buffer

2 M Tris-HCl (pH 6.8) 12.5 mL, SDS 10 g, glycerol 30 mL, β-mercaptoethanol 5 mL, and 1% bromophenol blue 2 mL in water to 100 mL.

(c) 10× electrophoresis buffer

Tris 30.3 g, glycine 141 g, and SDS 10 g in water to 1 L. Dilute with water to 1× working solution before use.

(d) 10× Tris-buffered saline (TBS) solution

Tris-HCl 10.42 g and NaCl 87.66 g in water to 1 L. Dilute to 1× TBS + Tween 20 (TBST) solution by adding 100 mL of 10× TBS stock solution and 1 mL of Tween 20 in water to 1 L.

(e) Blocking buffer

Skim milk powder 3 g or bovine serum albumin (BSA) 2 g in 100 mL of 1× TBST solution.

(3) Cell culture

(a) 10× Poly-D-Lysine (PDL)

Phosphate-buffered saline (PBS) 5 mL into a PDL bottle (5 mg). Incubate at 37℃ until being completely dissolved. Dilute to 1× solution by PBS and sterilize by filtration before use.

(b) DMEM-20S solution

Fetal bovine serum (FBS) 40 mL and 10,000 U Pen/Str stock solution 1 mL in 159 mL of Dulbecco's modified Eagle's medium (DMEM). Sterilize by filtration and store at 4℃.

(c) Papain for oligodendrocytes

Papain suspension 346 μL in minimum essential medium (MEM) to 12 mL. Incubate at 37℃ until the papain dissolves completely. Add DNase (5 mg/mL) 60 μL. Sterilize by filtration and store at 4℃ before use.

(d) Papain for neurons

Papain suspension 346 µL and L-glutamine 30 µL in Hibernate w/o Ca^{2+} to 12 mL. Incubate at 37℃ until the papain dissolves completely. Add DNase (5 mg/mL) 60 µL. Sterilize by filtration and store at 4℃ before use.

(e) Hibernate medium

B27 supplement 2 mL and L-glutamine 250 µL in Hibernate-A medium to 100 mL. Sterilize by filtration and store at 4℃.

(f) Neurobasal medium

B27 supplement 2 mL, L-glutamine 250 µL, and Pen/Str 1 mL in Neurobasal-A to 100 mL. Sterilize by filtration and store at 4℃.

(g) Myelination medium (MyM)

Insulin stock (0.5 mg/mL) 400 µL, Hormone Mix stock (transferrin 1 mg/mL, putrescine 3.2 mg/mL, progesterone stock 12.5 µg/mL, and sodium selenite 10 µg/mL) 200 µL, T3 stock (45 µg/mL) 200 µL, hydrocortisone stock 40 µL, biotin stock (50 µg/mL) 8 µL, vitamin B_{12} stock (1.36 mg/mL) 8 µL, B27 supplement 15 µL, and ceruloplasmin stock (1 mg/mL) 4 µL in DMEM high-glucose medium to 40 mL. Sterilize by filtration and store at 4℃.

Table 1: Composition of density gradients

	Hibernate with phenol red	**Hibernate without phenol red**	**OptiPrep 1.32**
Grad. 1 (bottom layer)	7.443 mL		1.557 mL
Grad. 2 (second layer)		7.884 mL	1.116 mL
Grad. 3 (third layer)	8.109 mL		0.891 mL
Grad. 4 (top layer)		8.334 mL	0.666 mL

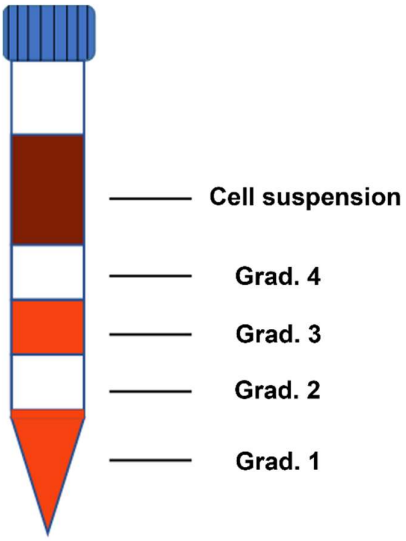

Fig. 5: Density gradient centrifugation

Four-layer density gradients were prepared by adding each gradient sequentially. To visualize the layers, Hibernate media with (Grad. 1 and Grad. 3) or without (Grad. 2 and Grad. 4) phenol red was used alternatively. The cell suspension was added on top of the gradients.

(h) Density gradient solution

Mix OptiPrep 1.32 with Hibernate medium (with or without phenol red) to prepare four 9 mL gradients (enough for four experiments; Table 1). Then, add 2 mL of Grad. 1 to each 15 mL conical centrifuge tube and add 2 mL of the next gradient on top of the previous one to create four density gradients (Fig. 5).

2.3. Methods

2.3.1. Mouse genotyping

Standard polymerase chain reaction (PCR) and agarose gel electrophoresis were used for mouse genotyping. The primers used for mouse genotyping are listed in Section 2.2.4, and the hotshot method was used to prepare the template DNA, according to a previously described method [110]. Briefly, 1 mm mouse tail was incubated in 75 µL of 1× base buffer at 95℃ for 30 min. Then, 75 µL of 1× neutralization buffer was added and mixed vigorously. Finally, 2 µL of the mixture was used as the template for PCR.

Each PCR reaction contains the following:	The PCR program was set as follows:
7 μL of H_2O	Step 1: 94℃ for 3 min
1.2 μL of Coral Load 10× PCR buffer	Step 2: 94℃ for 30 s
1.2 μL of primer mix (10 mM)	Step 3: 67℃ for 45 s
0.25 μL of dNTPs (10 mM)	Step 4: 72℃ for 45 s
0.24 μL of $MgCl_2$ solution	Step 5: Back to Step 2, 35 cycles
0.12 μL of Taq DNA polymerase	Step 6: 72℃ for 2 min
2 μL of template DNA	

After PCR was performed, 10 μL of the reaction solution was loaded to 1.5% agarose gel, and electrophoresis was performed at 100 V for 20 min. All genotypes were identified using the size of the PCR product, as illustrated in Fig. 6.

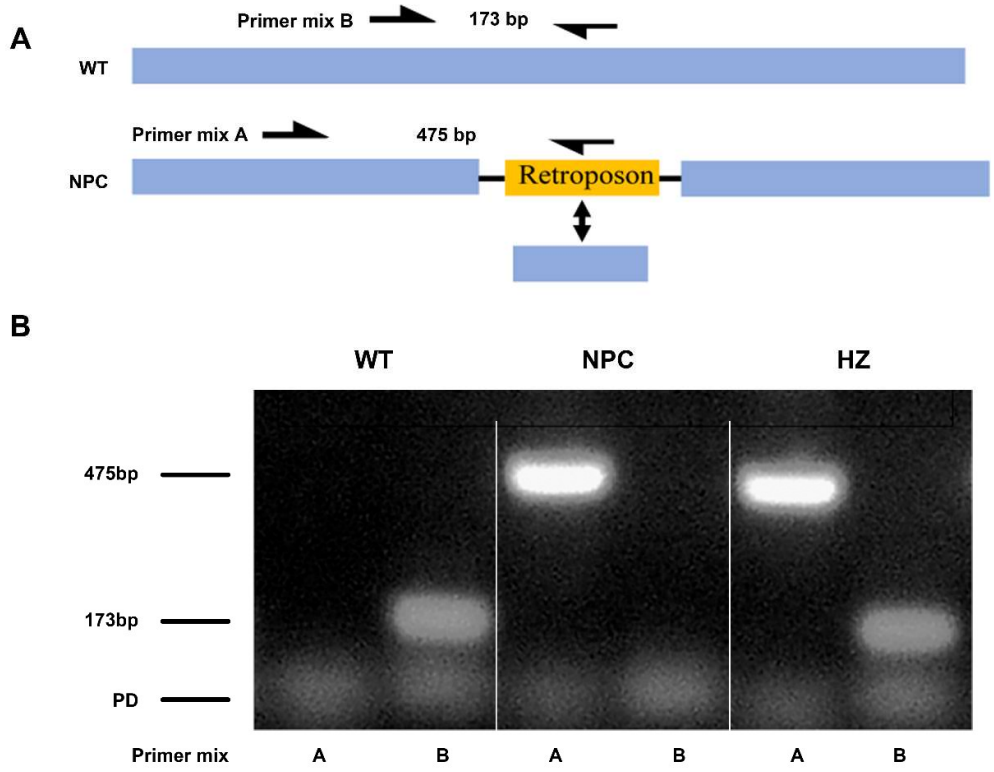

Fig. 6: Genotyping of NPC1$^{-/-}$ mice

(A) Sequence of *npc1* (blue) in WT and NPC1$^{-/-}$ mice. In NPC1$^{-/-}$ mice, 703 bp of the *npc1* sequence were replaced by 824 bp of retroposon-like DNA (yellow). The black arrows above each sequence indicate the locations of primers for genotyping. The length of the PCR product is 173 bp (Primer Mix B) in WT mice and 475 bp in NPC1$^{-/-}$ mice (Primer Mix A). (B) Electrophoresis results for genotyping. Both primer mixes, Primer Mix A and Primer Mix B, were used in the PCR reactions of each sample. The results of WT mice show only one band for Primer Mix B (173 bp), those of NPC1$^{-/-}$ mice show one band for Primer Mix A (475 bp), and those of heterozygous mice show two bands (173 and 475 bp). The weak bands in front of each lane are primer dimers (PDs).

2.3.2. Brain isolation

First, all mice were anesthetized with pentobarbital at different postnatal days. Then, their heads were decapitated by a pair of scissors and submerged in a prechilled PBS solution for a few minutes to cool down the brain. Microdissection scissors were used to cut the skin along the midline anteriorly toward the nose, muscles and connective tissues were split, and the exposed skull was cut from the foramen magnum by inserting the tips of the scissors gradually

along the midline until the nasion. It is important to point the tips of the scissors away from the brain to avoid damaging the brain. Two lateral incisions were made along the lambdoid suture until the temporal bones, and then the nasion was transected. Tweezers were then used to hold the nose part in a clean Petri dish, and another pair of tweezers were used to gently peel off the dissected bone. A few drops of prechilled PBS solution were applied to the exposed brain, and then the brain was transferred by a spatula into another Petri dish with ice-cold PBS. All detached brains were processed accordingly in the next steps.

2.3.3. Corpus callosum dissection

The forebrain part of the isolated brain was transected equally into five pieces, the second to fourth sections were flattened into the prechilled PBS in the Petri dish, and the first and last sections were discarded (Fig. 7A). Then, the following procedure was performed under a dissecting microscope. One 22-gauge syringe needle was used to fix the brain section, and another needle was used to dissect the corpus callosum from adjacent tissues (Fig. 7B). The dissected corpus callosum was then transferred into an Eppendorf tube, frozen in liquid nitrogen, and stored at −80℃.

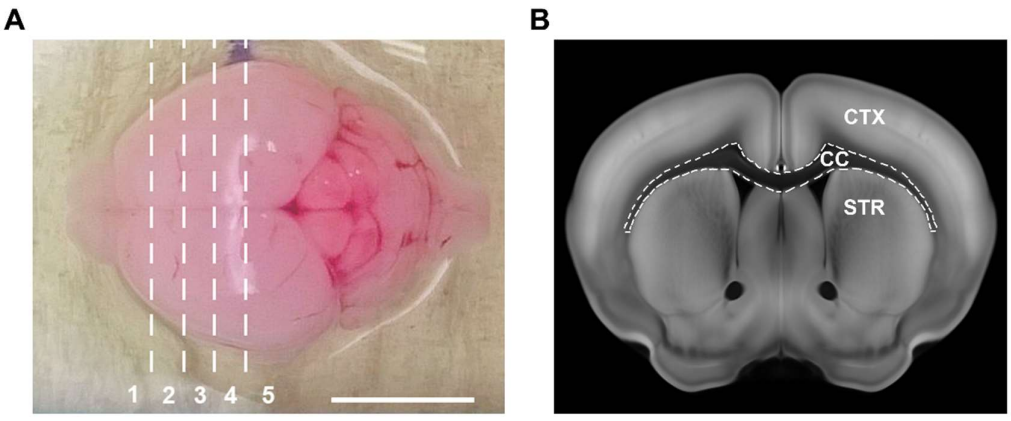

Fig. 7: Isolation of the corpus callosum

(A) Transections of the mouse brain. The forebrain was transected into five pieces along the dashed lines. (B) Isolation of the corpus callosum from the transections. The second to fourth sections were flattened, and the corpus callosum (CC) was disconnected from the cortex (CTX) and striatum (STR) along the dashed lines. Panel B is adapted from the Allen Brain Atlas (http://atlas.brain-map.org/). Scale bar: 1 cm in A.

2.3.4. Sample preparation for mass spectrometric analysis

Tissues were frozen in liquid nitrogen and ground rigorously using prechilled flame-polished glass rods. The ground samples were then homogenized in 150 µL of 8 M urea and 50 µL of SDC buffer (1% SDC in 0.1 M Triethylammonium bicarbonate buffer) and sonicated on ice. The protein concentration was measured using a BCA Protein Assay in a 96-well plate according to the user manual, and diluted BSA solution was used as the standard. Samples (100 µg protein from each sample) were digested using filter-aided sample preparation (FASP) [130]. Basically, all samples were placed in 10k centrifugal filter units (Amicon Ultra-0.5 Centrifugal Filter Unit), and the buffer was exchanged by 6 M urea, reduced by 20 mM dithiothreitol (DTT), alkylated by 40 mM iodoacetamide (IAA), and then digested by trypsin (enzyme-to-protein ratio = 1:50; Promega, Madison, WI, USA) in 400 µL of 100 mM ammonium bicarbonate buffer at 37℃ for 20 h. The digested peptides were then collected in water, lyophilized, and stored at −20℃ for mass spectrometric analysis.

2.3.5. NanoLC-MS/MS and data analysis

Tryptic peptides were dissolved in 0.1% formic acid (FA) and loaded into a nanoACQUITY ultra performance liquid chromatography (UPLC) system (Waters, Milford, MA, USA). A C18 trapping column (180 µm × 20 mm, 5 µm, 100 Å; Waters) and an analytical C18 column (Acclaim™ PepMap™ RSLC, 75 µm × 25 cm, 2 µm, 100 Å; Thermo Fisher Scientific, Waltham, MA, USA) were used to separate peptides. Then, UPLC was coupled with a Q Exactive™ Hybrid Quadrupole-Orbitrap™ Mass Spectrometer (Thermo Fisher Scientific). The positive voltage was set to 1.8 kV, the scan range *m*/*z* was set to 375–1,600 Th, the collision energy of HCD was 27%, and MS2 acquisition was performed in data-dependent mode by top 10. Data were processed using Xcalibur 4.0.27.13 (Thermo Fisher Scientific). Database searching and label-free quantification (LFQ) were performed using the MaxQuant platform (version 1.6.2.3, http://www.coxdocs.org/doku.php?id=maxquant:start). All raw files were searched with mouse proteome sequences from UniProt. “Unique plus razor peptides” was chosen for protein quantification [131]. The precursor mass tolerance was set to 20 ppm; the fragment mass tolerance was set to 0.5 Da; and the dynamic modification included oxidation (15.995 Da), acetyl (42.011 Da), and fixed modification carbamidomethyl (57.021 Da).

2.3.6. Data interpretation and comparison with other proteomic data

Data were uploaded to Perseus software, and online manuals were followed (version 1.6.2.1, http://www.coxdocs.org/doku.php?id=perseus:start). Basically, proteins labeled with "only identified by site," "reverse," and "potential contaminant" were removed from the data, and proteins were regarded as valid if they were identified from all samples in the WT or NPC group. Pearson's correlation was calculated with the default setting in the software. To obtain significantly expressed proteins, two-sample Student's *t*-test was used, and an S0 value of 1 and a false discovery rate (FDR) of 0.05 were set.

To elucidate the function of the identified proteins, valid proteins were analyzed using Gene Ontology Cellular Compartment (Go CC) term enrichment (GOTERM_CC_DIRECT) from the DAVID online tool (https://david.ncifcrf.gov/). Differentially expressed proteins were uploaded to the Gene Ontology Consortium (http://geneontology.org/) for Go CC, biological processes (Go BP), and Reactome pathway (Reactome) analysis, and both the protein count and FDR value of each term were obtained. The background of all the analyses was set to *Mus musculus*, and terms with an FDR value below 0.05 were listed.

We also compared our data to the published data of John et al. [57] and Sharma et al. (all data were obtained from Supplementary Table 2; https://www.nature.com/articles/nn.4160#supplementary-information) [132] to verify our results and assign the cell type specificity of the identified proteins, respectively. All histograms, pie charts, and Venn diagrams were produced by Microsoft Excel (Microsoft Corp., Redmond, WA, USA).

2.3.7. Western blot analysis

Briefly, tissues were first ground and incubated in 1 mL per 0.1 g tissue of cold RIPA buffer for 15 min, followed by homogenization by pipetting up and down a few times. For proteins extracted from cells, cultivated cells were washed with PBS, and RIPA buffer was applied directly to the culture plates. Finally, the lysate was collected and centrifuged at 15,000 ×*g* and 4℃ for 15 min, and the supernatant was collected and stored at −80℃.

Protein concentration was measured using the Pierce BCA Protein Assay (Thermo Fisher Scientific). Before loading to sodium dodecyl sulfate-polyacrylamide gel electrophoresis (SDS-PAGE), 5× Laemmli buffer was applied (which contains β-mercaptoethanol) to the samples, followed by incubation at 95℃ for 5 min to denature the

proteins. The samples were then loaded into either 18-well or 12-well 8–16% Criterion™ TGX Precast Midi Gel (Bio-Rad Laboratories, Hercules, CA, USA). Electrophoresis was performed at 80 V for 30 min followed by 200 V for 25 min using Criterion™ Cell (Bio-Rad Laboratories). Then, a Trans-Blot® Turbo™ Transfer Starter System (Bio-Rad Laboratories) was used to transfer proteins to the Midi nitrocellulose membrane. The membranes were then blocked using either 3% skim milk or 2% BSA in TBST buffer at room temperature for 1 h on a horizontal shaker. Primary antibodies were added to the blocking buffer and shaken overnight at 4℃. Then, the membranes were washed with TBST buffer for 5 min three times. Fluorescent conjugated secondary antibodies were added in blocking buffer to the membranes and incubated for 2 h at room temperature, followed by washing again with TBST buffer three times. Finally, the membranes were dehydrated and stored in a filter paper.

Semiquantitative Western blot analysis was performed using an Odyssey Infrared Imaging System (LI-COR Biosciences, Lincoln, NE, USA) according to a previously described protocol [133]. Odyssey software (version 1.2) was used to scan the membranes, and quantitation was performed using Image Studio Lite 4.0 (LI-COR Biosciences).

2.3.8. Real-time quantitative reverse transcription polymerase chain reaction

RNA was extracted using a RNeasy Plus Micro Kit (Qiagen, Hilden, Germany). All tissues were ground as outlined in Section 2.3.4, followed by homogenization using RPE buffer containing β-mercaptoethanol. To obtain RNA from cells, RPE buffer was directly added to the culture plates after washing with PBS buffer. Then, the lysate was centrifuged for 3 min at full speed to remove insoluble fragments. The supernatant was then transferred to a gDNA Eliminator and centrifuged to remove genomic DNA, followed by adding 100% ethanol to the flow-through fractions to precipitate the RNA. The mixture was then added to a RNeasy MinElute spin column, and RNA was bound to the column. Finally, the RNA was eluted in 14 µL of RNase-free water, and its concentration was measured using spectrophotometric analysis.

A QuantiTect Reverse Transcription Kit (Qiagen) was used to generate cDNAs. All cDNAs from different samples were diluted to 50 ng/µL as templates. Primers of target genes were designed using NCBI Primer-BLAST (https://www.ncbi.nlm.nih.gov/tools/primer-blast/index.cgi?LINK_LOC=BlastHome) and synthesized by Eurofins Scientific. FastStart Essential DNA Green Master and LightCycler® Nano (Roche Diagnostics, Basel, Switzerland)

were used for real-time quantitative reverse transcription polymerase chain reaction (qRT-PCR) according to the user manual.

2.3.9. Oligodendrocyte culture

Oligodendrocytes were isolated according to a previously described protocol [122,134]. Briefly, the brains of mice at P5 were dissected and transferred into cold MEM in a Petri dish. Cortices were split along the longitudinal fissure, and the corpus callosum was cut and the hippocampus removed. After being detached from the striatum, the remaining meninges were removed, and the cortices were diced into small pieces and gently transferred to a 15 mL conical centrifuge tube containing ice-cold MEM. After all the brains were prepared, MEM was aspirated, and 3 mL of papain solution was added to each brain to digest the tissues. The tubes were then incubated in a water bath for 25 min at 37℃. Then, 2 mL of DMEM-20S medium was added to the inactive papain, and the tissues were gently triturated using a sterile flame-polished glass Pasteur pipette approximately 10–15 times. The suspensions were then transferred to a new 15 mL conical tube, and 4 mL of DMEM-20S medium was added, followed by centrifugation at 300 ×*g* at room temperature for 5 min. The supernatants were then carefully aspirated, and 1 mL of warm DMEM-20S medium was added to resuspend the pellets. Cell suspensions were seeded into PDL-coated and medium-preequilibrated T25 flasks, and then the flasks were incubated in an incubator for 3-4 h to allow cells to attach to the PDL substrate. This was then followed by completely changing the medium to remove debris.

The medium was changed every three days, and insulin (5 μg/mL) was added at DIV7. At DIV9, the flasks were sealed and secured on a horizontal orbital shaker, shaken at 75 rpm for 1 h and the medium was changed to remove microglia. After incubation for another 3 h, the flasks were shaken again at 220 rpm for 16 h. Then, the cells were collected and filtered using a 70 mm nylon cell strainer and incubated on uncoated Petri dishes for 30–60 min to enrich OPCs. Nonbinding cells were collected in the medium and counted using a hemocytometer. For immunocytochemistry, 20,000 OPCs were seeded onto PDL-coated 13 mm coverslips. For Western blots, 200,000 cells were seeded into each well of a PDL-coated six-well plate. Then, the cells were cultured in MyM medium for six days before analysis. For neuron and oligodendrocyte co-cultures, 20,000 OPCs were seeded directly to the reaggregated neurons.

2.3.10. Neuron isolation and reaggregated neuron preparation

Primary neurons were isolated from the cortices of P1 mice according to a previously reported protocol [135]. Briefly, the cortices were dissected as described in Section 2.3.6, but MEM was replaced by a Hibernate medium during preparation. Density gradients were prepared using phenol red-free and phenol red media alternatively to visualize the different phases (Fig. 5). Then, after trituration with a flame-polished glass Pasteur pipette, homogenate tissues were loaded on top of the density gradient and centrifuged at 800 ×*g* for 15 min at room temperature. The second phase containing purified neurons was collected and transferred to 10 mL of Hibernate medium for centrifugation again at 200 ×*g* for 2 min to remove the density gradient solution. The pellet was resuspended by Hibernate medium and centrifuged again, then resuspended with prewarmed Neurobasal medium and counted using a hemocytometer. For immunostaining, 53,000 neurons (400 neurons/mm^2) were seeded onto 13 mm PDL-coated coverslips and cultured in Neurobasal medium, and the medium was changed every three days.

To prepare reaggregated neurons, 500,000 purified neurons in 0.5 mL of Neurobasal medium were seeded into each well of an uncoated four-well plate and incubated for 24 h. The cells were then gently resuspended and incubated for another 24 h to promote cell reaggregation. At DIV3, the cells were gently resuspended and transferred into 1.5 mL Eppendorf tubes. The tubes were left for 5 min at room temperature to allow the cells to settle down to the bottom, and then the supernatant, containing debris and nonaggregated neurons, was removed. The reaggregated neurons were resuspended and allowed to settle down again six times until no further debris was found under the microscope in the supernatant. Then, the reaggregated neurons were seeded onto 13 mm PDL-coated coverslips and cultured in the a Neurobasal medium for 12 days, and the medium was changed every three days.

2.3.11. Preparation of a CdM

At DIV12, after neurons were washed with prewarmed MEM twice, the medium was changed completely with MyM medium and incubated for 24 h. Then, the CdM was harvested by filtering the MyM medium from the neuron culture using a 0.22 μm filter to remove floating cells. Depending on the different genotypes of the cultivated neurons, the CdM was termed CdM-wt (from WT neurons), CdM-npc (from NPC1$^{-/-}$ neurons), and CdM-hz (from NPC1$^{+/-}$ neurons), respectively. Then, the CdM was concentrated using an Amicon ultra-15 mL-10 kDa cutoff centrifugal filter unit at 4℃ and stored at −80℃ until use.

2.3.12. Compounds and CdM treatment of oligodendrocytes

A stock solution of lovastatin was prepared in dimethyl sulfoxide (DMSO) to 2.5 mM and CD was prepared in PBS to 0.1 M. For treatment, different compounds were added to the medium at DIV1. Both 0.25 μM lovastatin and 0.1 mM CD were used as the final concentrations for oligodendrocytes. Then, DMSO was added to control and CD-treated oligodendrocytes to maintain their concentration under all conditions. In CdM-treated oligodendrocytes, concentrated CdM was diluted in MyM medium to the original concentration, and purified oligodendrocytes were seeded directly onto the diluted CdM. The cells were then cultured for six days without changing the medium.

2.3.13. Immunohistochemistry and immunocytochemistry

Fluorescence-labeled immunostaining of brain slices was performed using the free-floating method. Briefly, the brains were isolated and fixed in 4% paraformaldehyde overnight and embedded in (Optimal Cutting Temperature) OCT solution. Cryosections (30 μm) were cut using a microtome at −20℃ and collected in PBS. After fixing with 4% formaldehyde for 1 h, the brain slices were washed with PBS three times, 5 min each. Then, all slices were blocked in a blocking solution containing 10% goat serum and 0.4% Triton X-100 in PBS. The sections were then incubated overnight at 4℃ with the primary antibody in 5% goat serum and 0.08% Triton X-100 in PBS. After washing for 5 min with PBS three times, secondary antibodies were incubated for 1 h at room temperature. Finally, cell nuclei were counterstained with 4′,6-diamidino-2-phenylindole (DAPI) for 10 min. All incubation procedures were performed in a horizontal shaker at 400 rpm.

Cell fluorescence-labeled immunostaining was performed according to a previously described protocol [124]. Briefly, after washing with PBS, cells were fixed with 4% formaldehyde for 15 min and blocked with 10% goat serum and 0.4% Triton X-100 in PBS. Then, primary and secondary antibodies were used according to immunohistochemicaal methods, and coverslips were mounted with a VECTASHIELD Mounting Medium (with DAPI).

Fluorescence was assessed using a fluorescence microscopy system (Keyence, Osaka, Japan), and all images were randomly analyzed. For cell quantification, each coverslip was randomly imaged under a 10× objective and at least 600 cells from six coverslips were counted for each sample in one experiment.

2.3.14. Statistical analysis

The results obtained from independent specimens or experiments were treated as biological replicates. GraphPad Prism 7 software (GraphPad Software, San Diego, CA, USA) was used for all statistical analyses. Two-sample comparisons were analyzed using Student's two-tailed *t*-test, and multiple comparisons were analyzed using two-way analysis of variance (ANOVA) followed by the Šidák multiple comparisons test. All graphs are plotted as the mean ± standard error of the mean (SEM) unless stated otherwise, and statistical significance was assumed at $p < 0.05$ ($^{*}p < 0.05$, $^{**}p < 0.01$, $^{***}p < 0.001$, and $^{****}p < 0.0001$).

3. Results

3.1. Proteomic analysis revealed myelin disruption in NPC1$^{-/-}$ mice

3.1.1. Proteomic analysis of corpora callosa

To assess myelin deficiency in NPC, three replicates of corpora callosa from either WT or NPC1$^{-/-}$ mice at P12 were collected for nanoscale liquid chromatography coupled to tandem mass spectrometry analysis (Nano LC-MS/MS) analysis (Fig. 8A). In total, 3,114 proteins from all WT samples and 3,141 proteins from NPC samples were identified (Fig. 8B, green and pink parts in the Venn diagram), and 3,009 common proteins were detected from all WT and NPC1$^{-/-}$ samples (yellow part in Fig. 8B). Notably, the proteins that were only identified in one or two samples are mostly those with relatively low abundance (the lowest 30%). Therefore, only proteins detected from all the samples were used in the following analysis.

3.1.2. Similar proteomic patterns between WT and NPC1$^{-/-}$ mice

To estimate the quality of the proteomic data and the consistency of our sample preparation protocols, Pearson's correlation was calculated and the coefficients between replicates were compared. All the coefficients among the WT or NPC1$^{-/-}$ samples were found to be above 0.97, demonstrating high technical reliability in our analyses (Fig. 8C). Although myelination is significantly disrupted in the corpora callosa of NPC1$^{-/-}$ mice, the coefficients between the WT and NPC1$^{-/-}$ samples (Fig. 8C) were still higher than 0.9, indicating similar proteomic patterns between them [136].

We also compared our data with several published myelin proteomic results. Using a myelin-enriched fraction from mouse brains, Jahn et al. identified 344 proteins, including 26 well-known myelin proteins and 318 myelin-associated proteins [57]. Notably, our proteomic results from the corpus callosum also revealed most of these proteins: 21 myelin proteins and 273 myelin-associated proteins in the WT samples and 18 myelin proteins and 265 myelin-associated proteins in the NPC1$^{-/-}$ samples (Fig. 9A). Moreover, Go CC analysis (top 20 terms with the lowest FDR values, Fig. 9B) indicated that the 3,009 identified proteins were from different cell types. Although many proteins have been categorized into nonspecific cellular compartments (e.g., extracellular exosome, cytoplasm, membrane, and mitochondrion), various proteins have been classified into cell-type-specific compartments: 171 proteins in myelin sheaths (green part in Fig. 9B), 209 proteins in neuron projection, 229 proteins in

synapse, and 172 proteins in axon (red part in Fig. 9B). We also identified several astrocyte-specific proteins, such as glial fibrillary acidic protein (Gfap), aquaporin-4 (Aqp4), and cytosolic 10-formyltetrahydrofolate dehydrogenase (Aldh1l1) [23]. These results confirm the anatomical features of the corpus callosum, where not only myelin sheaths and axons but also other cellular compartments and cell types are located.

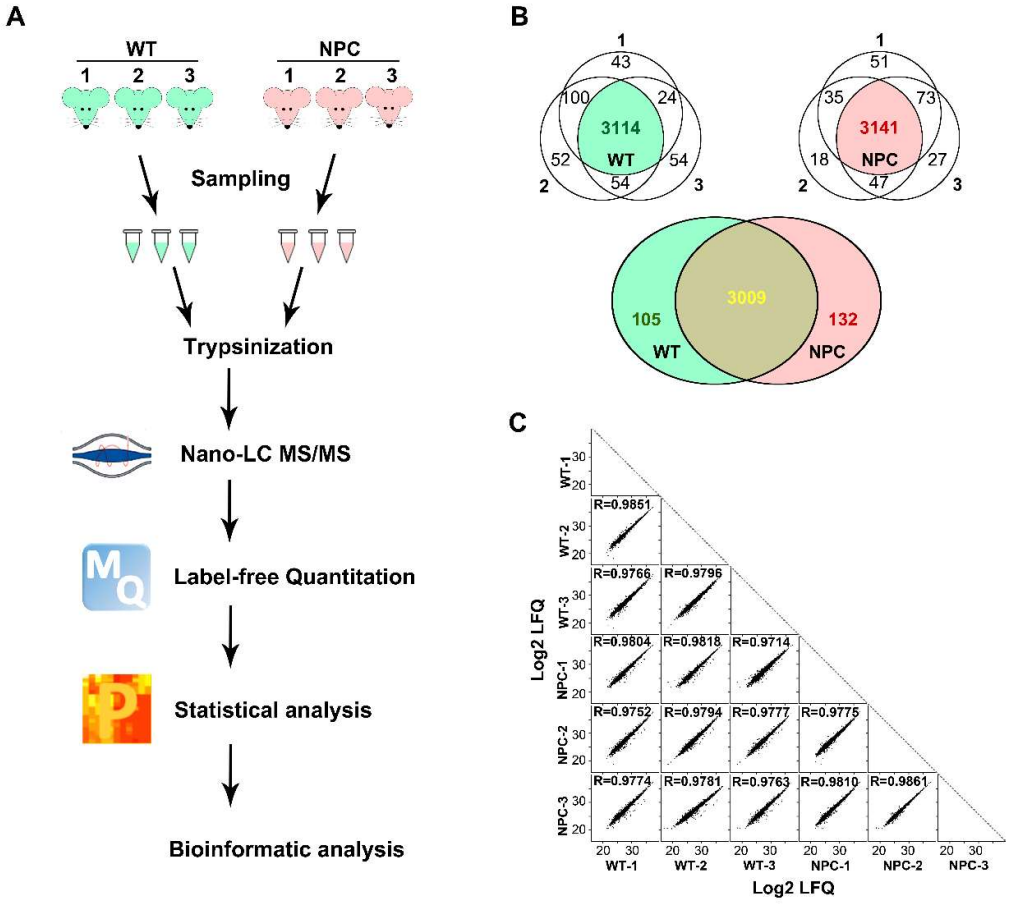

Fig. 8: Comparison of protein patterns in the corpus callosum of WT and NPC1$^{-/-}$ mice at P12

(A) Schematic diagram of the workflow for the proteomic analysis of three biological replicates of WT and NPC1$^{-/-}$ mice. (B) Venn diagram of the proteins identified from each sample. Valid proteins from each genotype are illustrated in green for WT samples and in pink for NPC samples. Common proteins from both WT and NPC mice are shown in yellow. (C) Scatterplots of $\log_2$ LFQ values of identified proteins between samples along with Pearson's correlations (*R* values).

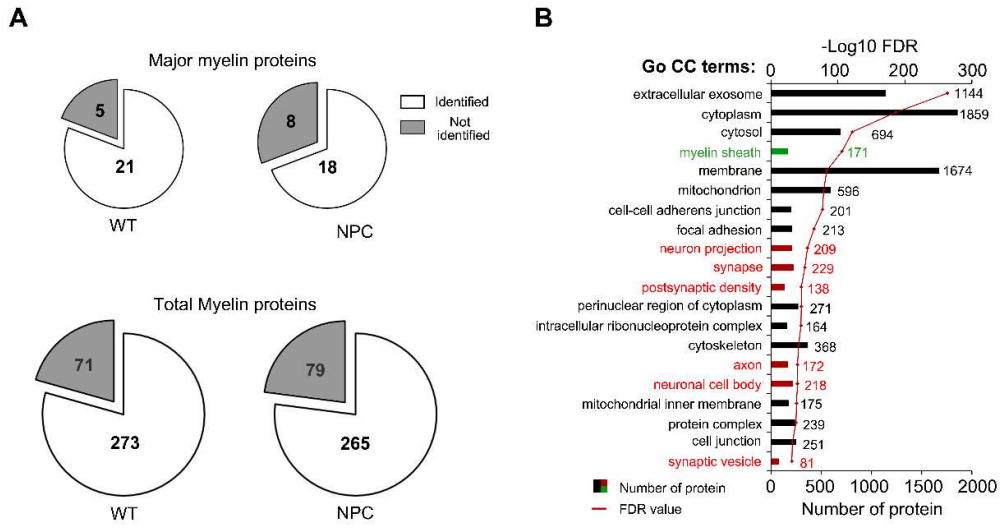

Fig. 9: Functional analyses of identified proteins

(A) The number of identified proteins was compared to the protein data obtained from the myelin-enriched fraction of Jahn et al. (2009). The number of the identified major or total myelin proteins is shown in the white part, whereas the number of those that have not been identified is shown in the gray part. (B) Go CC term enrichment of the identified proteins. The myelin-specific term is labeled in green, whereas neuron-specific terms are labeled in red. The numbers in front of the bars indicate the number of proteins in each term, and the red points represent the FDR values presented as $-\log_{10}$ values.

3.1.3. Differentially expressed proteins in NPC1$^{-/-}$ mice

Among all the identified proteins, the expression of 21 proteins was found to be significantly different (the two isoforms of Mbp were combined in this study) between the WT and NPC1$^{-/-}$ samples: 17 proteins were downregulated (red, Fig. 10A) and four proteins were upregulated in NPC1$^{-/-}$ mice (green, Fig. 10A). Go CC analysis was performed for differentially expressed proteins, and enrichment of myelin structural proteins, such as Plp1, Cnp, sirtuin 2 (Sirt2), Mbp, Mag, Mog, gelsolin (Gsn), and claudin 11 (Cldn11), was included in the term of the myelin sheath. Some of these were also categorized into specific myelin structures (e.g., Sirt2, Mbp, and Mag in compact myelin and Sirt2 and Mag in the Schmidt-Lanterman incisure; Fig. 11B). Gene Ontology Biological Processes (Go BP) analysis exhibited enrichment of proteins related

to development, myelination, and gliogenesis. The proteins Plp1, Bcas1, Sirt2, Mbp, Mag, 2-hydroxyacylsphingosine 1-β-galactosyltransferase (Ugt8), β-hexosaminidase subunit β (Hexb), Cldn11, Cnp, ceramide synthase 2 (Cers2), and plexin-B3 (Plxnb3) were included in the term of nervous system development. Moreover, Plp1, Bcas1, Sirt2, Mbp, Mag, Ugt8, Hexb, and Cldn11 were also included in axon ensheathment, and Cnp, Sirt2, Mag, and Hexb were included in gliogenesis (Fig. 11B). Additionally, the proteins Plp1, Mbp, Cnp, Mog, Mag, Sirt2, Cldn11, Enpp6, Bcas1, Rho-related GTP-binding protein RhoG (Rhog), and Gsn have been reported in myelin-enriched fractions [57]. Taken together, 12 downregulated proteins (i.e., Plp1, Mbp, Cnp, Mog, Mag, Sirt2, Cldn11, Enpp6, Bcas1, Rhog, Ugt8, and Gsn) and one upregulated protein (Hexb) in the corpus callosum of NPC1$^{-/-}$ mice either were myelin structural proteins or were involved in the regulation of myelination. Hence, this analysis confirms myelin disruption in NPC. Reactome pathway analysis revealed the enrichment of proteins in sphingolipid metabolism: proteins Gltp, Ugt8, Hexb, and Cers2 were involved in sphingolipid metabolism, and Gltp, Ugt8, and Hexb were involved in glycosphingolipid metabolism. Although the proteins PBDC1 (Pbdc1), Plxnb3, and chloride intracellular channel protein 4 (Clc4) have been found to be upregulated, their function is not related to myelination. Besides the protein Hexb, Ctsf and CtsD are lysosome proteases that participate in intracellular degradation. Moreover, C1qc, a subunit of complement C1q, has been found to be significantly upregulated in the corpus callosum of NPC1$^{-/-}$ mice.

To confirm the proteomic data, Western blot analyses were performed on corpora callosa from both WT and NPC1$^{-/-}$ mice at P12. The results showed that the protein levels of Bcas1, Enpp6, and Gltp were significantly decreased, with only 51.7% Bcas1, 41.2% Enpp6, and 32.2% Gltp in the corpus callosum of NPC1$^{-/-}$ mice when compared to WT mice (Fig. 10C, D). The protein Mbp was used as a positive control, which constituted only 9.8% in NPC1$^{-/-}$ mice compared to WT mice (Fig. 10C, D).

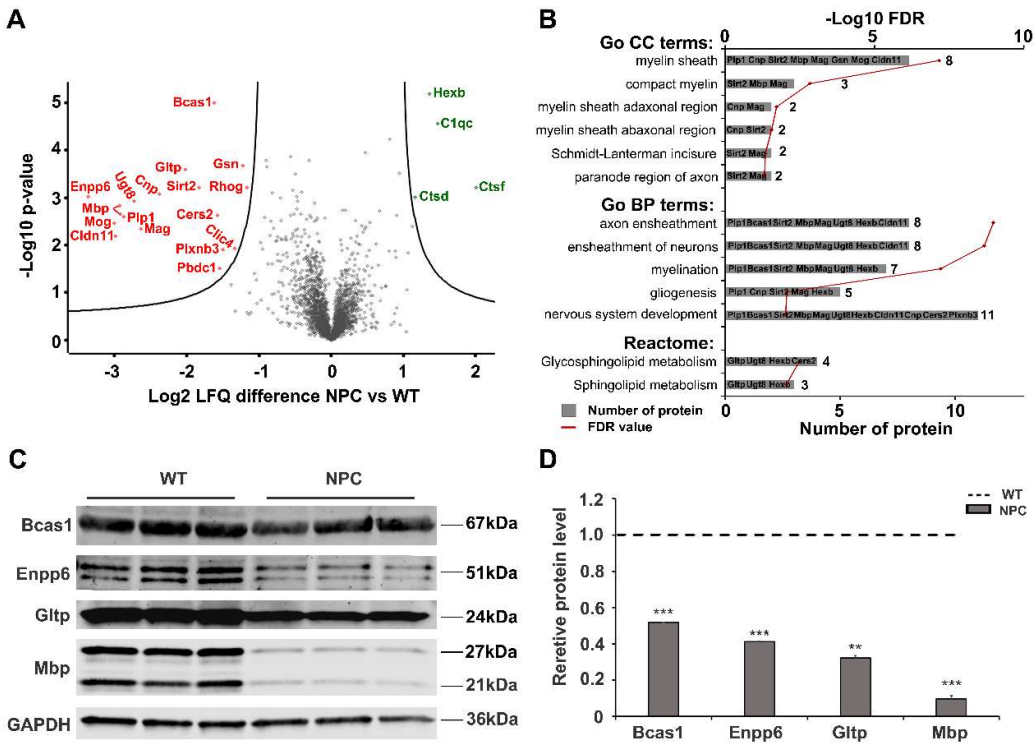

Fig. 10: Differentially expressed proteins between WT and NPC1$^{-/-}$ mice

(A) Volcano plot of $\log_2$ LFQ differences versus $-\log_{10}$ *p*-values of the common proteins between WT and NPC$^{-/-}$ mice. The downregulated proteins in NPC1$^{-/-}$ mice are shown on the left, with significant ones labeled in red, whereas the upregulated proteins are shown on the right, with significant ones labeled in green. (B) Go CC, Go BP, and Reactome enriched differentially expressed proteins, and their names are listed on the bars. Each red point marks an FDR value, presented as $-\log_{10}$ value. Western blots (C) and quantification (D) of differentially expressed proteins from the corpus callosum of mice. The value of each protein was normalized to the corresponding loading control, and the value of WT was set to 1. Three biological replicates were compared, and GAPDH was used as the loading control. Student's *t*-test was used. $^{*}p < 0.05$; $^{**}p < 0.01$; $^{***}p < 0.001$.

3.2. Hypomyelination in NPC1$^{-/-}$ mice

3.2.1. Reduced expression of major myelin proteins in NPC1$^{-/-}$ mice

To understand the mechanism of myelin disruption in NPC1$^{-/-}$ mice, corpora callosa were isolated from mice at different postnatal days and the expression level of myelin proteins was examined using Western blot analysis (Fig. 11A). In WT mice, the onset of myelination was indicated by the emergence of major myelin proteins, including MBP, MOG, and PLP. Notably, MBP formed clear bands as early as P8, whereas MOG formed a clear band at P9 and PLP at P10 in the corpus callosum. Therefore, P9 was considered as mostly the start point for myelination in the corpus callosum. Meanwhile, because of the continuous formation of myelin sheaths during development, the amount of MBP increased 10.5-fold at P20 and 14.1-fold at P65 when compared to P9 (Fig. 11B). Similar amplification results were observed in the expression of PLP and MOG (Fig. 11C, D). Because the formation of myelin in the corpus callosum can be traced *ab initio* and successive myelination in older mice can be monitored from the increased expression of major myelin proteins, the corpus callosum is considered an appropriate structure to study the progression and signal cascades of normal myelination as well as its deficiency.

In contrast to WT mice, in NPC1$^{-/-}$ mice, detectable MBP bands appeared at around P10, with those for MOG appearing at P12 and those for PLP barely appearing at P12, with a delay of around three days. It was also found that the expression of these proteins was markedly reduced when compared to WT mice at each time point. For example, the amount of MBP reached only about 19% that in WT mice at P65, with MOG and PLP reaching approximately 24% and 30%, respectively (Fig. 11B, D). On the basis of the Western blots, which showed that myelination in the corpus callosum started at around P9, immunostaining was performed on brain slices at both P8 and P9 in WT and NPC1$^{-/-}$ mice (Fig. 11). Perceptible MBP signals were found in the corpus callosum of P8 WT mice, which became stronger in fibrous form at P9 (Fig. 12A1, B1, C1, D1). However, such signals were mostly absent at P8 and very weak at P9 in NPC1$^{-/-}$ mice (Fig. 12A2, B2, C2, D2). Taken together, these results point out a delay in the onset of myelination in NPC1$^{-/-}$ mice accompanying the reduced expression of major myelin proteins at each time point. Therefore, it is believed that myelin deficiency in the corpus callosum of NPC1$^{-/-}$ mice is due to hypomyelination rather than demyelination.

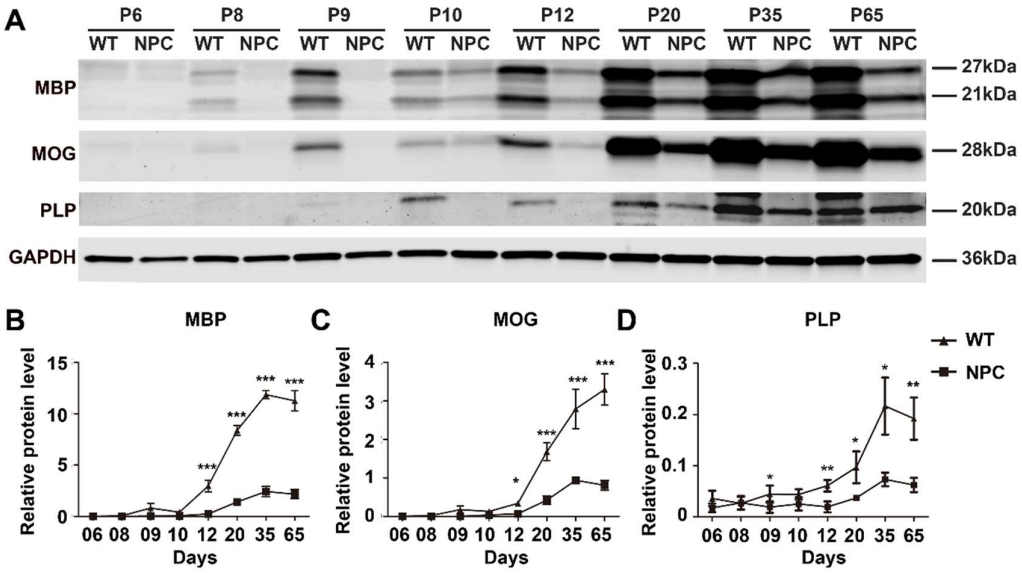

Fig. 11: Reduced expression of myelin proteins in the corpus callosum of NPC1$^{-/-}$ mice

Western blot analysis (A) and quantification (B) of differentially expressed proteins from the corpus callosum of mice. The expression of MBP, MOG, and PLP was compared between WT and NPC mice on different postnatal days. The value of each protein was normalized to the corresponding loading control (GAPDH). At least three biological replicates were compared (n = 6 for MBP, n = 3 for MOG, and n = 4 for PLP). Data are presented as mean ± SEM. Statistical significance was determined using Šidák-corrected two-way ANOVA. $^{*}p < 0.05$; $^{**}p < 0.01$; $^{***}p < 0.001$.

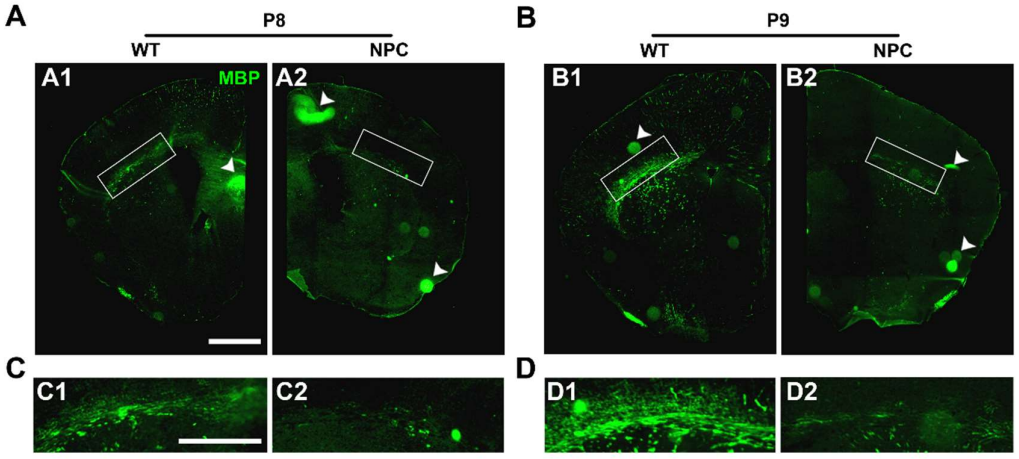

Fig. 12: Delayed myelination in the corpus callosum of NPC1$^{-/-}$ mice

MBP expression detected by immunohistochemistry in the brain sections of WT and NPC$^{-/-}$ mice at P8 and P9. The arrowheads indicate artificial bubbles. Panels C and D are magnified images of the boxes shown in panels A and B, respectively. Scale bar: 800 µm in A1 for A1, A2, B1, and B2; 400 µm in C1 for C1, C2, D1, and D2.

3.2.2. Impaired differentiation of oligodendrocytes in NPC1$^{-/-}$ mice

Myelin is a structure produced by oligodendrocytes in the CNS. Insufficient oligodendrocytes, resulting from either reduced proliferation or impaired migration of progenitor cells, result in hypomyelination. Therefore, we compared the expression of the premature oligodendrocyte marker NG2 in the corpus callosum using Western blots at different time points between WT and NPC1$^{-/-}$ mice (Fig. 13A). The results showed massive NG2 expression at P6 in both WT and NPC1$^{-/-}$ mice before the expression of myelin proteins (MBP, MOG, and PLP). Moreover, the amount of NG2 remained stable at earlier time points (from P6 to P20) and decreased slightly at P35 and P65, corresponding to the elimination of the extra oligodendrocytes at later stages of development [84]. In addition, no significant difference was found in the expression of NG2 at earlier stages between WT and NPC1$^{-/-}$ mice, despite a slight increase at P35 and P65 in NPC1$^{-/-}$ mice (Fig. 13B).

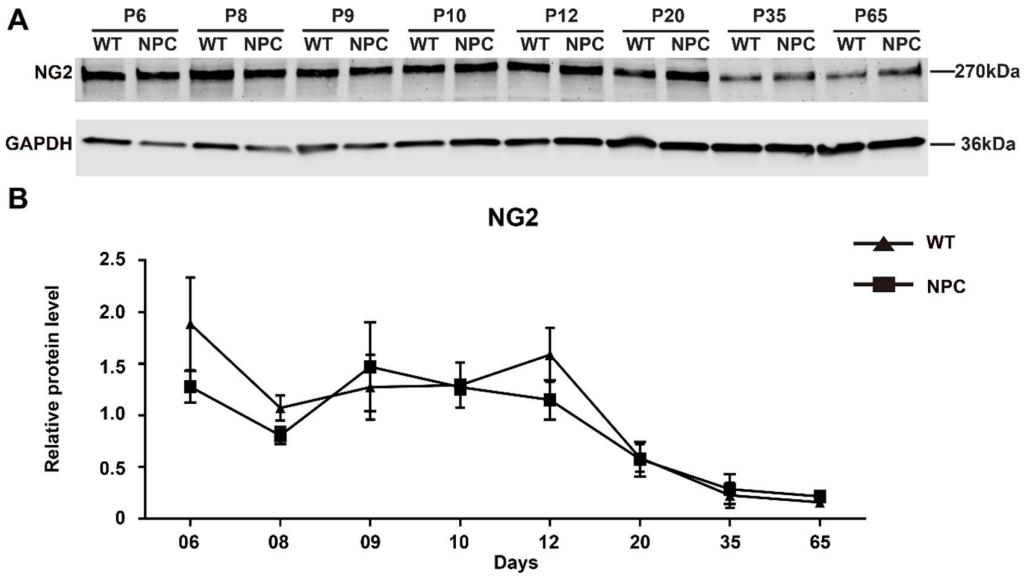

Fig. 13: Expression of NG2 in the corpus callosum of NPC1$^{-/-}$ mice

Western blot analysis (A) and quantification (B) of NG2 expression in the corpus callosum of mice. The expression of NG2 was compared between WT and NPC mice at different postnatal days, and the value of NG2 was normalized to the corresponding loading control (GAPDH). The quantification of NG2 is shown as a ratio of NPC to WT at each time point. Three biological replicates were compared. Data are presented as mean ± SEM. Statistical significance was determined using Šidák-corrected two-way ANOVA. No significant differences between WT and NPC were found.

Furthermore, the distribution of oligodendrocytes was compared directly by immunostaining on brain sections (Fig. 14). The data showed that Olig2-positive cells were distributed over the entire brain sections at P10 in both WT and NPC1$^{-/-}$ mice with a similar pattern (Fig. 14A, B), including the corpus callosum (Fig. 14C1, D1), and even in the molecular layer of the cortex (Fig. 14C2, D2), where myelination initiates much later. Therefore, neither the proliferation nor the migration of oligodendrocytes is disturbed in NPC1$^{-/-}$ mice, which suggests that hypomyelination in NPC1$^{-/-}$ mice does not result from the insufficient number or disturbed migration of oligodendrocytes.

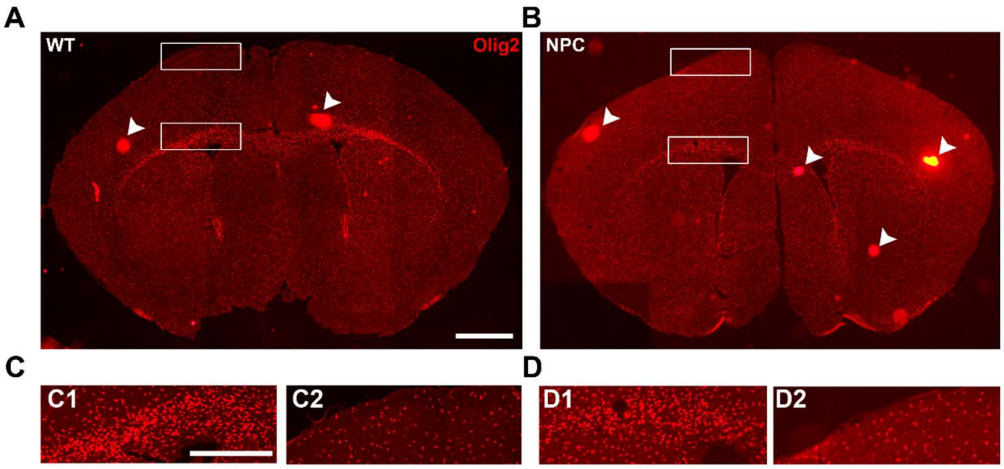

Fig. 14: Normal distribution of oligodendrocytes in NPC1$^{-/-}$ mice

Expression of Olig2 detected by immunohistochemistry in the brain sections of WT (A) and NPC$^{-/-}$ mice (B) at P10. The arrowheads indicate artificial bubbles. C1, C2 and D1, D2 are magnified images of the boxes shown in panels A and B, respectively. Scale bar: 800 µm in A for A and B; 400 µm in C1 for C1, C2, D1, and D2.

Generally, MBP is an indispensable myelin protein whose expression is sophistically regulated during myelination. Different conditions (e.g., inhibited transcription, blocking of the transport of RNA to distal processes, and/or delayed initiation after coming into contact with axons) affect MBP protein synthesis [137]. Therefore, we analyzed the transcription of MBP in the corpus callosum using qRT-PCR (Fig. 15). The results showed that the amount of MBP mRNA greatly decreased in NPC1$^{-/-}$ mice, with only 38.3% MBP detected at P8 and 25.0% at P65 compared to WT mice (Fig. 15A). In addition, similar reductions of 43.0% and 20.5% were found in the PLP transcription in NPC1$^{-/-}$ at P8 and P65, respectively (Fig. 15B). These results suggest that the deficiency of myelin formation observed in NPC1$^{-/-}$ mice occurs at earlier postnatal stages during myelination.

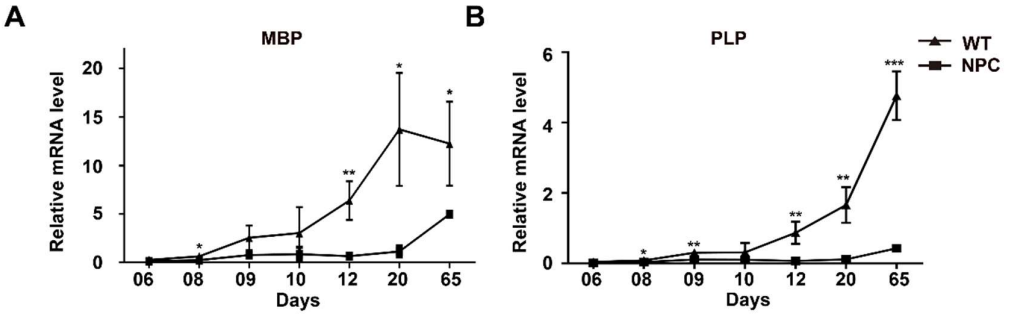

Fig. 15: Reduced transcription of MBP and PLP in the corpus callosum of NPC1$^{-/-}$ mice

Semiquantitative RT-PCR of MBP (A) and PLP (B) mRNA in the corpus callosum of WT and NPC1$^{-/-}$ mice at different postnatal days. All values were normalized to the corresponding internal control (PPIA) and are shown as a ratio of NPC to WT at each time point. Three biological replicates were compared. Data are presented as mean ± SEM. Statistical significance was determined using Šidák-corrected two-way ANOVA. $^{*}p < 0.05$; $^{**}p < 0.01$; $^{***}p < 0.001$.

Since the expression of major myelin structural proteins (MBP, PLP, and MOG) was found to decrease in the corpus callosum of NPC1$^{-/-}$ mice, the pattern of myelin-related transcription factors (e.g., Olig1, Olig2, and Sox10) was further evaluated (Fig. 16). The results of the Western blots showed that the expression of Olig1 and Olig2 remained relatively stable in the corpus callosum of WT mice, in contrast to the dramatically upregulated myelin structural proteins (Fig. 16A). Moreover, the amounts of both Olig1 and Olig2 proteins were found to be reduced in NPC1$^{-/-}$ mice from P9 onwards. In NPC1$^{-/-}$ mice, only 68.7% Olig1 and 56.3% Olig2 were observed at P9, whereas 13.2% Olig1 and 16.9% Olig2 were observed at P65, when compared to time-matched WT mice (Fig. 16C, D). However, although the expression of Sox10 was not significant at the early stages, it increased in older NPC1$^{-/-}$ mice (Fig. 16B). Such an increase in Sox10 in older NPC1$^{-/-}$ mice may be due to a compensatory effect. Both Olig1 and Olig2 are transcription factors that regulate the differentiation of oligodendrocytes [102,138]. Reduced expression of these proteins indicates disrupted oligodendrocyte differentiation, resulting in a reduction in the myelin protein expression and myelination impairment in NPC1$^{-/-}$ mice.

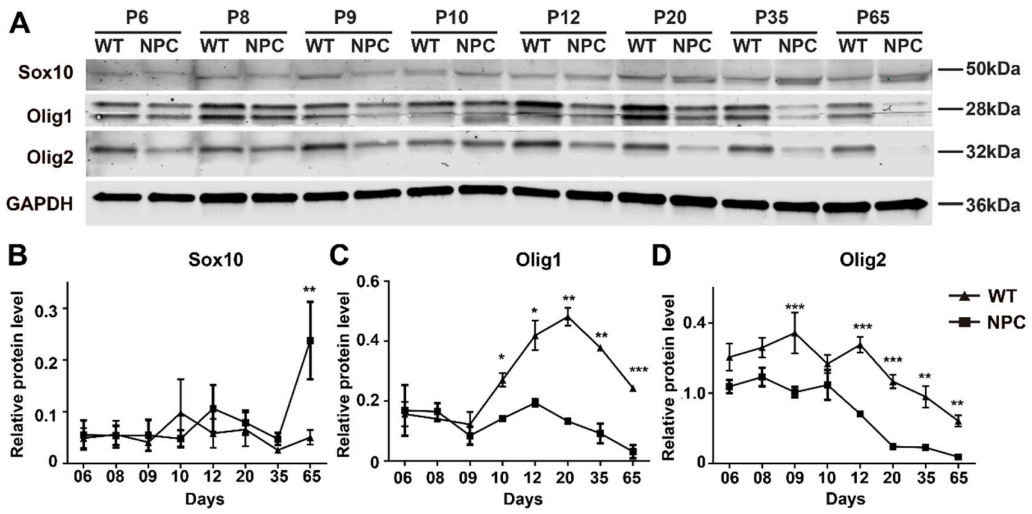

Fig. 16: Reduced Olig1 and Olig2 in the corpus callosum of NPC1$^{-/-}$ mice

Western blot analysis (A) and quantification (B) of differentially expressed proteins from the corpus callosum of mice. The expression of Sox10, Olig1, and Olig2 was compared between WT and NPC mice at different postnatal days. The value of each protein was normalized to the corresponding loading control (GAPDH). The quantification of these proteins is shown as a ratio of NPC to WT at each time point. At least three biological replicates were compared (n = 4 for Sox10, n = 3 for Olig1 and Olig2). Data are presented as mean ± SEM. Statistical significance was determined using Šidák-corrected two-way ANOVA. $^{*}p < 0.05$; $^{**}p < 0.01$; $^{***}p < 0.001$.

3.3. Establishing an *in vitro* myelination system

To investigate the cellular mechanisms of hypomyelination in NPC1$^{-/-}$ mice, an *in vitro* myelination system was established. According to the literature, P5 mice were used because OPCs are abundant at this stage and cells are relatively easier to disassociate than in older mice [124,134]. As described in Section 2.3, cells were seeded in PDL-coated flasks after disassociation, and astrocytes were allowed to proliferate and generate into a monolayer in the culture, whereas OPCs were allowed to grow on top of the feeding astrocyte layer (Fig. 17A). To increase the proliferation of OPCs, insulin was added to the medium at DIV7. Due to their weak attachment, OPCs were then harvested by shaking them off the astrocyte monolayer, while the monolayer remained intact in the flask (Fig. 17A, B).

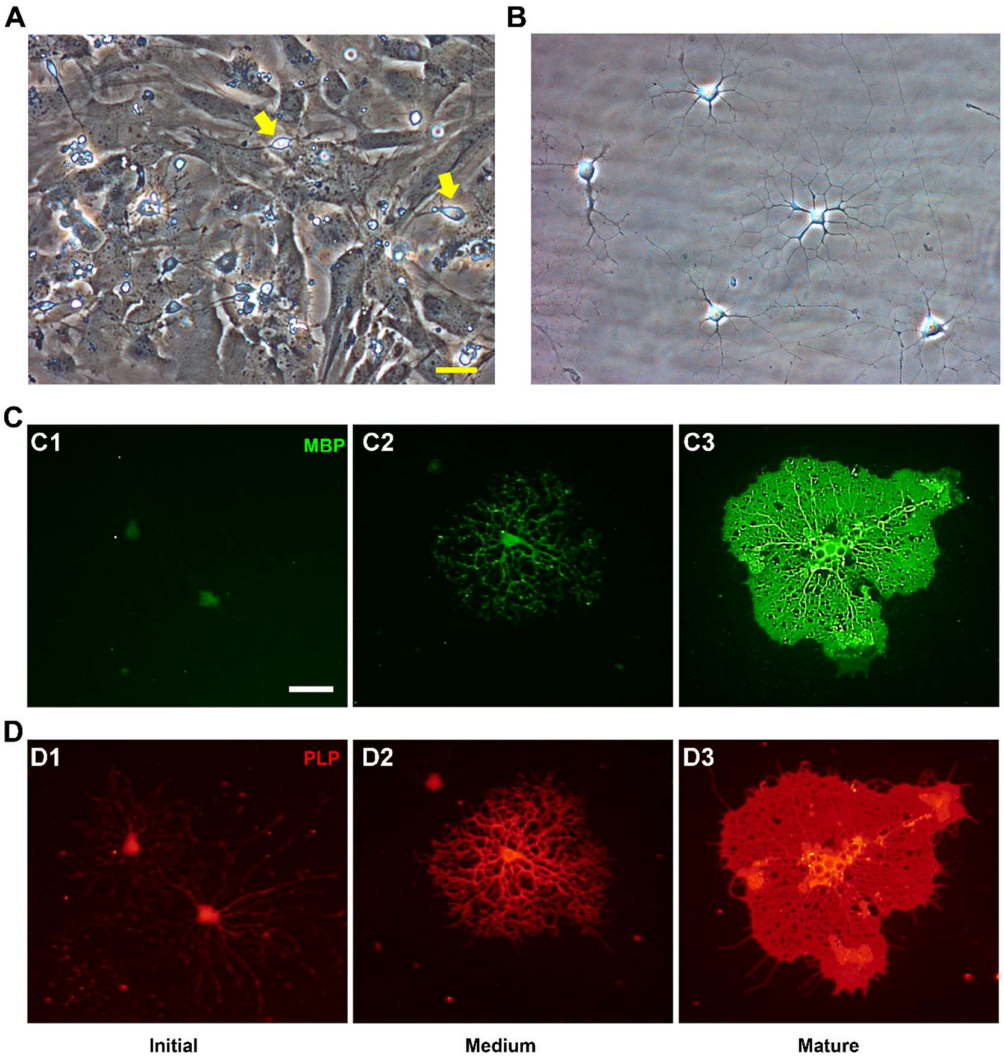

Fig. 17: Primary oligodendrocyte cultures and their morphology and categorization

(A) Growth of primary oligodendrocytes (arrows) above the monolayer of astrocytes at DIV9 under a bright-field microscope. (B) Purified oligodendrocytes on coverslips at DIV3. (C, D) Oligodendrocytes are categorized into an initial type (C1, D1), medium type (C2, D2), and mature type (C3, D3) according to their morphological complexity. Oligodendrocytes were stained with antibodies against MBP (green) and PLP (red). Scale bar: 40 µm in A for A and B; C1 for C1 to D3.

OPCs undergo differentiation spontaneously when cultured in a medium lacking growth factors [127]. After differentiation, oligodendrocytes develop dramatic morphological changes. For example, multiple processes are generated, and sheath-like structures expand from the cultured oligodendrocytes in the absence of axons. According to their morphology and expression of major myelin proteins, oligodendrocytes are categorized into three types (Fig. 17C, D): an initial type, a medium type, and a mature type. The initial type corresponds to early oligodendrocytes with a few processes that have recently exited the cell cycle (Fig. 17C1, D1). The medium type contains multiple and interconnected processes with distinctive expression of MBP and PLP (Fig. 17C2, D2). The mature type exhibits boosting MBP signals and a membrane-like structure that is similar to a myelin sheath (Fig. 17C3, D3).

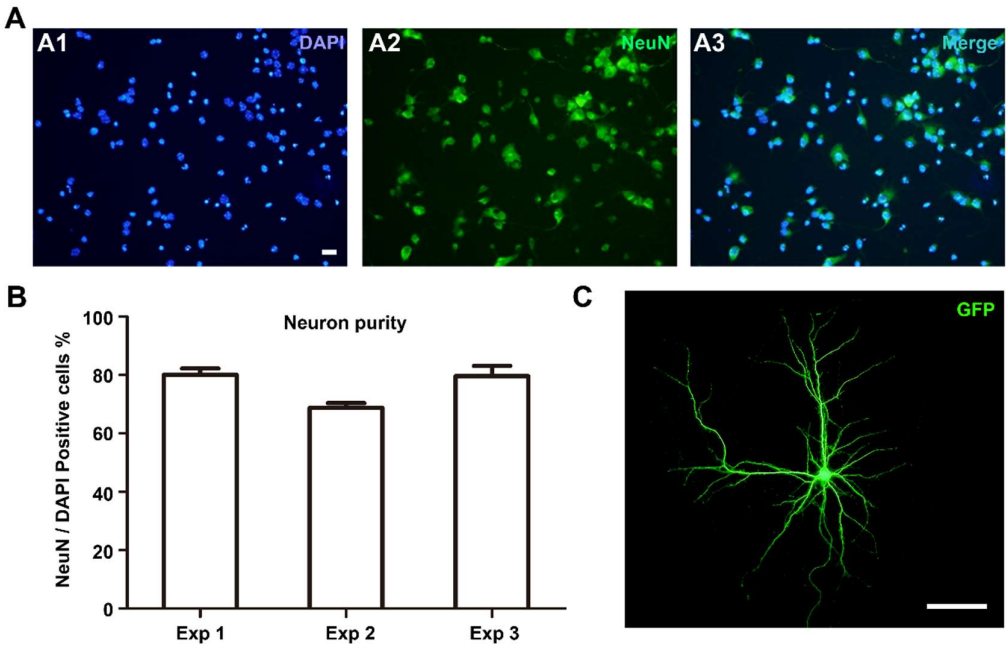

Fig. 18: Purity and morphology of cortical neurons

(A) Neurons were stained with an antibody against NeuN (green), and total cells were labeled with DAPI (blue) at DIV1. (B) The purity of cortical neurons was calculated from the ratio of NeuN-positive cells to the total number of DAPI-labeled cells at DIV1. Three independent neuron cultures (Exp 1, Exp 2, and Exp 3) were assessed. (C) Morphology of a typical cultivated cortical neuron. Neurons were transfected with GFP at DIV7 and imaged at DIV12. Scale bar: 40 µm in A1 for A1 to A3 and in C.

To test the capability of myelin sheath formation, primary oligodendrocytes were cocultured with primary cortical neurons, which were obtained from P1 mice using the density gradient centrifugation method, as described in Section 2.3. To test the purity of the primary neurons, immunostaining with an anti-NeuN antibody was performed along with DAPI co-staining for all cells (Fig. 18A). In the cultured system, more than 80% of the total cells were neurons at DIV1. It was found that those neurons can generate complex dendritic structures at DIV12, as observed in cells transfected with green fluorescent protein (GFP; Fig. 18B, C). Almost no oligodendrocytes were observed in the culture. Moreover, because axons from aggregated neurons are easier to be myelinated by oligodendrocytes [124], reaggregated neurons were prepared on an uncoated four-well plate for two days and seeded onto PDL-coated coverslips. It was found that the somas of the reaggregated neurons were highly concentrated and that their axons were extended radically outwards, whereas nonreaggregated neurons were found to generate processes arbitrarily (Fig. 19A, B).

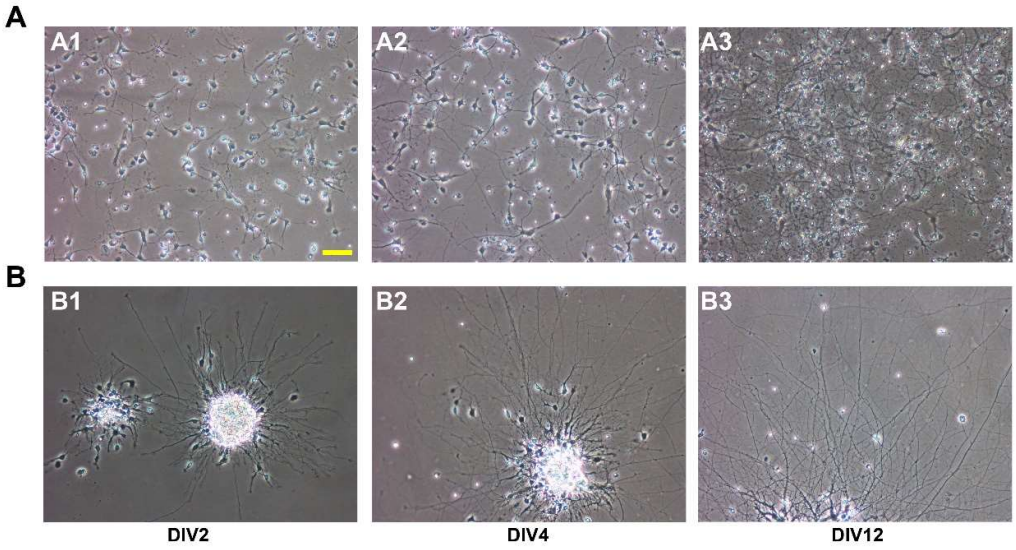

Fig. 19: Primary neurons in nonreaggregated and reaggregated cultures

Differences between primary neurons in nonreaggregated (A1–A3) and reaggregated (B1–B3) cultures at different time points. A1 and B1 show cells at DIV2, A2 and B2 show cells at DIV4, and A3 and B3 show cells at DIV12. Scale bar: 80 µm in A1 for all.

Five days after the primary oligodendrocytes were seeded into the DIV12 reaggregated neuron culture, myelin sheaths were detected using immunostaining (Fig. 20). Neurofilament (NF), an abundant neuronal cytoskeleton protein, was used to label axons, whereas MBP was used to label oligodendrocytes and myelin. In the coculture system, rod-like MBP-positive structures, indicating myelin sheaths, were found to be colocalized with lineal NF-labeled axons (Fig. 20A). Moreover, sodium channel protein type 8 subunit alpha (Nav1.6), a type of sodium channels concentrated on the node of Ranvier, and contactin-associated protein 1 (Caspr), a marker of the paranodal region [139], were found to be flanked in the coculture system (Fig. 20B). All of these results suggest that the primary oligodendrocytes prepared using this method can myelinate axons. Therefore, we believe that this coculture system can be used to study the mechanism of hypomyelination in NPC1$^{-/-}$ mice.

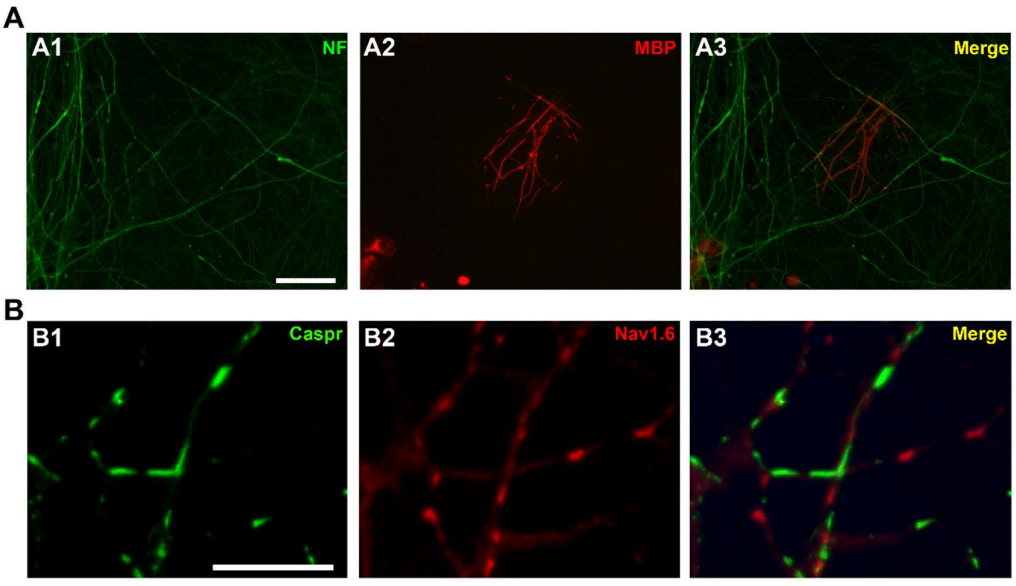

Fig. 20: Myelin formation in the neuron and oligodendrocyte coculture system
Colocalization of axons and myelin sheaths indicated by immunostaining with antibodies against NF (green) for axons from neurons and MBP (red) for oligodendrocytes in A, respectively, and the formation of the node of Ranvier indicated by immunostaining with antibodies against Caspr (green) for the paranodal region and Nav1.6 (red) for the node of Ranvier in B. Scale bar: 40 µm in A1 for A1 to A3 and in B1 for B1 to B3.

3.4. Inhibited maturation of NPC1$^{-/-}$ oligodendrocytes

Conditional knockout of *npc1* exclusively in neurons or oligodendrocytes disrupts myelination, proving the essential role of NPC1 protein in both cell types [36]. However, the mechanism underlying how a cholesterol transport protein affects myelination is still mostly unknown. To study this mechanism, oligodendrocytes from the cortices of both WT and NPC1$^{-/-}$ mice were cultured, since cortex myelination is severely disrupted in NPC1$^{-/-}$ mice. The percentages of mature cells were calculated in both WT and NPC1$^{-/-}$ oligodendrocyte cultures according to the method described in Section 3.3. At DIV6, approximately 18.5% of the cells were found to be of the mature type in WT oligodendrocytes, whereas the percentage was only 5.9% in NPC1$^{-/-}$ cells (Fig. 21A–C). Different proteins were extracted from cultivated oligodendrocytes, and the results showed significant reductions in the amounts of MBP, PLP, Olig1, and Olig2 in NPC1$^{-/-}$ oligodendrocytes when compared to WT oligodendrocytes by Western blot analysis (Fig. 21D). These data are consistent with the results obtained from the corpus callosum, wherein the differentiation of oligodendrocytes is affected in NPC1$^{-/-}$ mice.

Oligodendrocytes differentiate from OPCs that stop mitotically dividing and exit the cell cycle. To check whether such inhibited cell cycle exit of OPCs leads to reduced maturation of NPC1$^{-/-}$ oligodendrocytes, bromodeoxyuridine (BrdU), an analog of thymidine, was used to label proliferating cells. Briefly, BrdU was added at DIV1 to the medium and incubated with the cells for 24 h, and the percentages of BrdU-labeled proliferating cells were compared between WT and NPC1$^{-/-}$ oligodendrocytes. The results showed that only a small portion of the cells (5.2% in WT and 4.7% in NPC1$^{-/-}$ oligodendrocytes) were labeled by BrdU (Fig. 21E), with no significant difference between these two genotypes. Therefore, it was concluded that the cell cycle exit is not blocked in NPC1$^{-/-}$ oligodendrocytes but rather that the initiation of myelination is restricted.

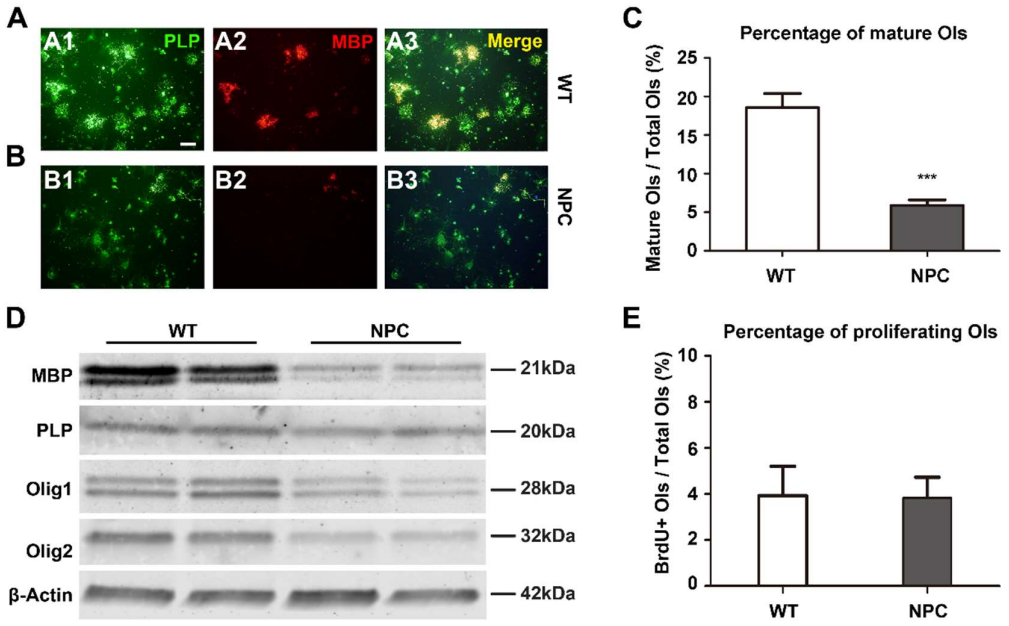

Fig. 21: Inhibited maturation in NPC1$^{-/-}$ oligodendrocytes

(A, B) Maturation of oligodendrocytes indicated by the immunostaining of cultivated oligodendrocytes at DIV6 with antibodies against PLP (green) and MBP (red). Nuclei were labeled with DAPI (blue). Scale bar: 80 µm in A1 for all. (C) The percentages of mature cells were calculated from the ratio of the number of mature cells (MBP-positive) to the total oligodendrocytes (PLP-positive) at DIV6 in WT or NPC1$^{-/-}$ oligodendrocytes. (D) Western blot analysis of MBP, PLP, Olig1, and Olig2 in cultivated oligodendrocytes at DIV6. β-Actin was used as the loading control. (E) Quantitation of proliferating oligodendrocytes by BrdU labeling. The percentages of proliferating oligodendrocytes were calculated from the ratio of the number of BrdU+/PLP+ double-positive cells to the total PLP-positive cells. In panels C and E, data were calculated from five independent experiments (more than 600 cells were counted under each condition in every experiment) and are presented as mean ± SEM. Statistical significance was determined using Student's two-tailed *t*-test. $^{*}p < 0.05$; $^{**}p < 0.01$; $^{***}p < 0.001$. No significant differences between WT and NPC mice were found in panel E.

3.5. Decreased response of NPC1$^{-/-}$ oligodendrocytes to CdMs

Signals from neurons modulate myelination. Besides contact signals, secretory factors from neurons are involved in the regulation processes. To evaluate the production of myelin regulatory factors from neurons and the responses of oligodendrocytes to them, CdMs prepared from primary neurons were used to culture primary oligodendrocytes. Briefly, CdM media were produced by conditioning MyM medium in neurons at DIV12 for 24 h and named according to the genotypes of the neurons: CdM-wt from WT neurons, CdM-npc from NPC1$^{-/-}$, and CdM-hz from heterozygotic neurons . In total, 20,000 oligodendrocytes were cultured at DIV1 with 0.5 mL of CdM, which was prepared from 100,000 neurons. The percentages of mature oligodendrocytes in different CdMs were compared at DIV6 (Fig. 22). It was observed that all CdMs significantly increased the percentages of mature WT oligodendrocytes, from 18.5% in normal MyM medium to 33.4% in CdM-wt, 29.8% in CdM-npc, and 41.0% in CdM-hz (Fig. 22A1, A2, A3, C). Therefore, it was concluded that mutations in NPC1 do not completely block the production of myelin regulatory factors by neurons.

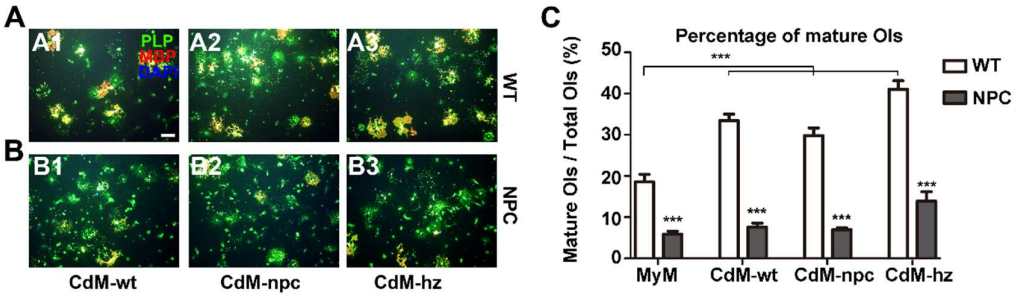

Fig. 22: Decreased response of NPC1$^{-/-}$ oligodendrocytes to CdMs

(A, B) Maturation of oligodendrocytes cultured in different CdMs. Oligodendrocytes were stained at DIV6 with antibodies against PLP (green) and MBP (red), whereas nuclei were labeled with DAPI (blue). Images from the same fields were merged. Colocalized PLP and MBP signals are shown in yellow. Scale bar: 80 µm in A1 for all. (C) Quantification of mature oligodendrocytes in different media. The percentages of mature cells were calculated from the ratio of the number of mature cells to the total oligodendrocytes at DIV6 in either WT or NPC1$^{-/-}$ oligodendrocytes. Data were calculated from five independent experiments (more than 600 cells were counted under each condition in every experiment) and are presented as mean ± SEM. Statistical significance was determined using Šidák-corrected two-way ANOVA. $^{*}p < 0.05$; $^{**}p < 0.01$; $^{***}p < 0.001$.

However, when NPC1$^{-/-}$ oligodendrocytes were cultured in CdMs, the percentages of mature cells reached only 7.0% in CdM-wt, 7.6% in CdM-npc, and 13.9% in CdM-hz, compared to 5.9% in MyM medium (Fig. 22B1, B2, B3, C). In contrast to WT oligodendrocytes, CdM treatment induced only slight promotion of maturation in NPC1$^{-/-}$ oligodendrocytes and most cells remained in the initial type, regardless of the CdM type. These data suggest that the myelination program in oligodendrocytes is disrupted and that even the stimuli of neuronal secretory factors cannot increase the percentage of mature NPC1$^{-/-}$ oligodendrocytes.

3.6. Involvement of Myrf in NPC1$^{-/-}$ mice

Oligodendrocyte maturation is controlled by different signaling pathways. To investigate the signals involved in hypomyelination in NPC1$^{-/-}$ disease, a few reported key factors were investigated. Myrf is a transcription factor which functions rely on the transport of its N-Myrf into the nucleus to regulate myelination. Therefore, we compared the expression of Myrf in the corpus callosum between WT and NPC1$^{-/-}$ mice (Fig. 23). It was found that full-length Myrf protein decreased gradually during development (from P8 to P65; Fig. 23A), whereas the active form, N-Myrf, increased from P8 to P20 and then decreased from P35 to P65 in WT mice. No significant difference in the levels of full-length Myrf and N-Myrf was found between WT and NPC1$^{-/-}$ mice, except for a slight decrease in N-Myrf in P65 NPC1$^{-/-}$ mice (Fig. 23A, B). Therefore, it was concluded that the expression and cleavage of Myrf are not affected by the dysfunction of NPC1 during development, although the reduction observed in P65 mice may represent the disrupted maintenance of myelination in older NPC1$^{-/-}$ mice.

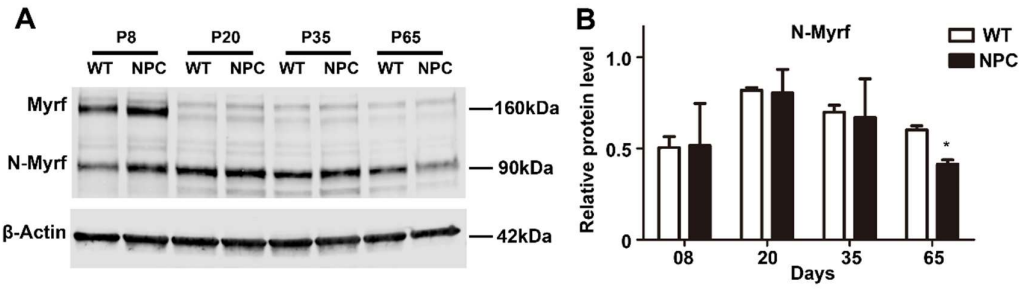

Fig. 23: Expression of Myrf in the corpus callosum of NPC1$^{-/-}$ mice

Western blot analysis (A) and quantification (B) of Myrf expression from the corpus callosum of mice. The expression of Myrf was compared between WT and NPC mice at different postnatal days. The value of N-Myrf was normalized to the corresponding loading control (β-actin). Three biological replicates were compared. Data are presented as mean ± SEM. Statistical significance was determined using Šidák-corrected two-way ANOVA. $^{*}p < 0.05$.

Furthermore, the translocation of N-Myrf was analyzed by immunostaining with different antibodies (Fig. 24). Both anti-C-Myrf and anti-N-Myrf antibodies, which can also bind full-length Myrf, were used to label oligodendrocytes. When double immunostaining was performed with an anti-MBP antibody, N-Myrf was detected in both the cytosol and nucleus, colocalizing with MBP and DAPI, respectively (Fig. 24A, C), whereas C-Myrf was detected only in the cytosol, colocalizing with MBP (Fig. 24B, D). At DIV5, N-Myrf was found to be transported into the nucleus of most WT and NPC1$^{-/-}$ oligodendrocytes, although the MBP signal was much weaker in NPC1$^{-/-}$ than in WT oligodendrocytes (Fig. 24A, C). These results indicate that the transportation of N-Myrf from the cytosol to the nucleus occurs at an early stage during the maturation of oligodendrocytes and is not affected in NPC.

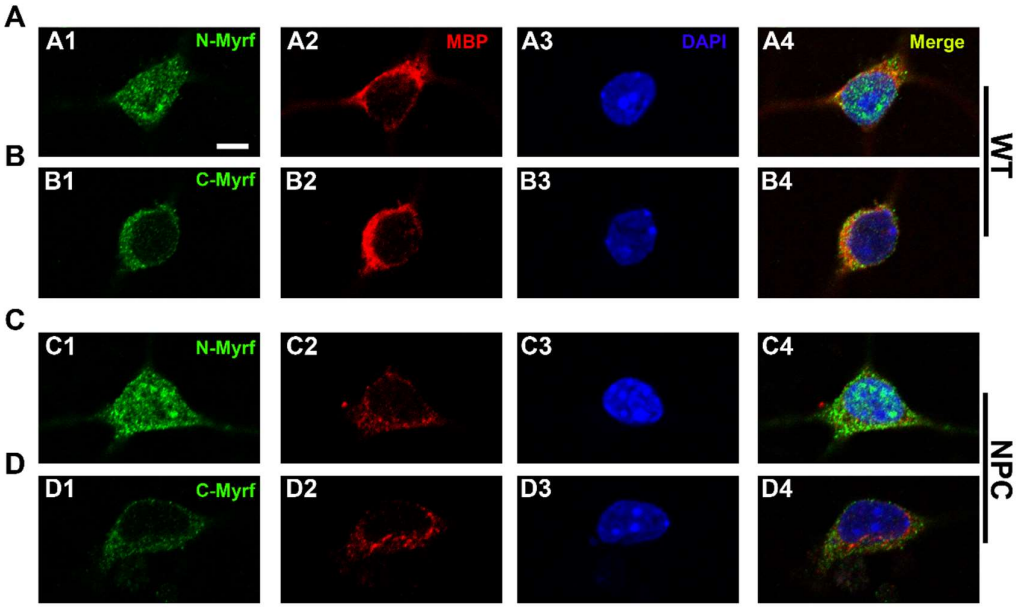

Fig. 24: Intact translocation of Myrf in NPC1$^{-/-}$ oligodendrocytes

The intracellular localization of Myrf is shown by immunostaining in cultured oligodendrocytes. Different antibodies were used to detect N-Myrf (green, A1, C1) or C-Myrf (green, B1, D1) and MBP (red, A2, B2, C2, and D2). Nuclei were labeled with DAPI (blue, A3, B3, C3, and D3). Scale bar: 10 µm in A1 for all.

3.7. Interrupted translocation of p57Kip2 in NPC1$^{-/-}$ oligodendrocytes

In contrast to Myrf, the role of p57Kip2 in the promotion of oligodendrocyte maturation depends on its transportation from the nucleus to the cytosol. Therefore, we investigated the expression and transport of p57Kip2 in the corpus callosum (Fig. 25). Western blot analysis showed that the expression of p57Kip2 gradually decreased nearly sixfold in WT mice at P65 compared to P6, indicating the progressive completion of myelination. Compared to WT mice, the amount of p57Kip2 in NPC1$^{-/-}$ mice was found to decrease slightly but not significantly (Fig. 25A, B). These data suggest that the expression of p57Kip2 is not affected in NPC1$^{-/-}$ mice.

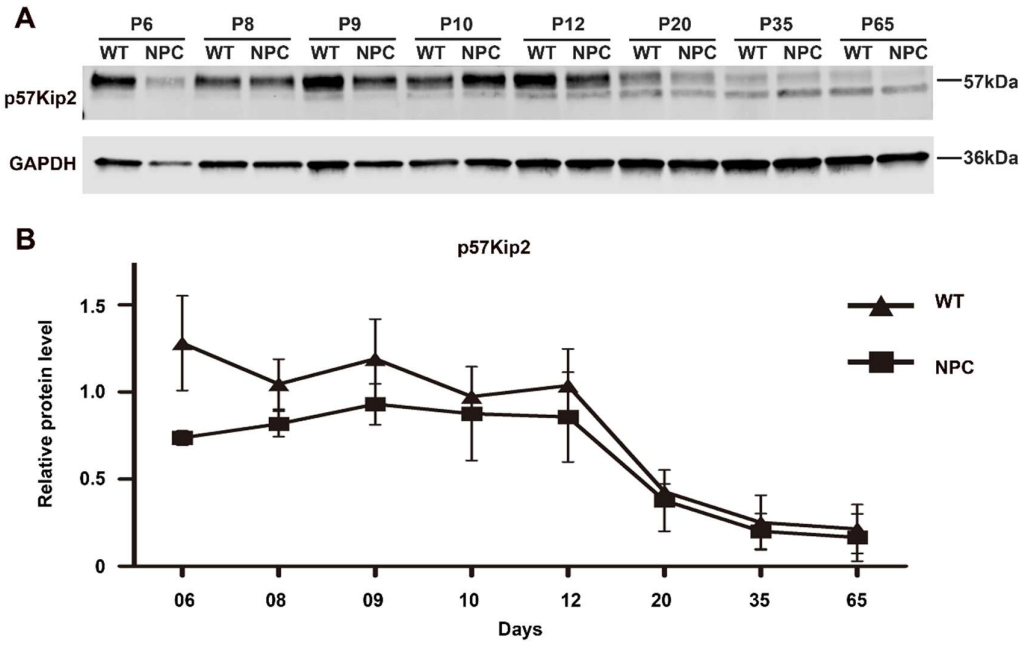

Fig. 25: Comparable expression of p57Kip2 in the corpus callosum of NPC1$^{-/-}$ mice

Western blot analysis (A) and quantification (B) of p57Kip2 expression from the corpus callosum of mice. The expression of p57Kip2 was compared between WT and NPC mice at different postnatal days. All values were normalized to the corresponding loading control (GAPDH). Three biological replicates were compared. Data are presented as mean ± SEM. Statistical significance was determined using Šidák-corrected two-way ANOVA. No significant differences between WT and NPC mice were found.

Furthermore, the location of p57Kip2 was analyzed by immunostaining on cultured oligodendrocytes at DIV6 (Fig. 26). This is because nuclear p57Kip2 inhibits the maturation of oligodendrocytes, but cytosolic p57Kip2 promotes their maturation [110]. Our results, therefore, confirm the strong correlation between the location of p57Kip2 and the maturation status of oligodendrocytes; in the initial type, p57Kip2 is located only in the nucleus; however, in the medium and mature types, it is also detected in the cytosol (Fig. 26A–C). We also quantified and compared cytosolic p57Kip2-positive cells between WT and NPC1$^{-/-}$ oligodendrocytes (Fig. 26D). The results showed that around 17.4% of the oligodendrocytes were cytosolic p57Kip2-positive in the NPC1$^{-/-}$ cells, compared to 28.9% in WT cells. This difference between WT and NPC1$^{-/-}$ oligodendrocytes became even more significant when a

CdM was used for culturing; such percentages increased from 17.4% to 27.1% in NPC1$^{-/-}$ cells and from 28.9% to 51.3% in WT cells. Thus, it was concluded that the translocation of p57Kip2 is disrupted in NPC1$^{-/-}$ oligodendrocytes.

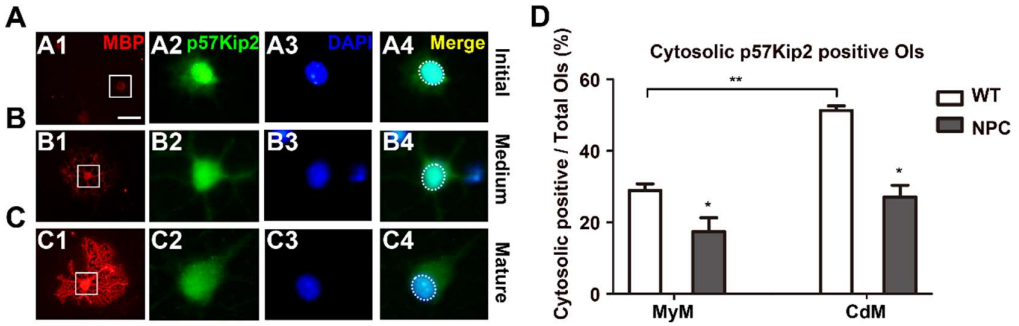

Fig. 26: Blockage of the nucleocytoplasmic transport of p57Kip2 in NPC1$^{-/-}$ oligodendrocytes

(A–C) The intracellular distribution of p57Kip2 was investigated by immunostaining in cultivated oligodendrocytes with antibodies against p57Kip2 (green) and MBP (red). Nuclei were labeled with DAPI (blue) in initial-type (A), medium-type (B), and mature-type (C) oligodendrocytes. The dashed cycles shown in A4, B4, and C4 mark the nuclei. Scale bar: 40 µm in A1 for all. (D) Percentages of cytosolic p57Kip2-positive oligodendrocytes at DIV6 in MyM medium or CdM. Data were calculated from three independent experiments (more than 600 cells were counted under each condition in every experiment) and are presented as mean ± SEM. Statistical significance was determined using Student's two-tailed *t*-test. $^{*}p < 0.05$; $^{**}p < 0.01$; $^{***}p < 0.001$.

3.8. β-Cyclodextrin and lovastatin reduce the accumulation of cholesterol in NPC1$^{-/-}$ mice

Accumulation of cholesterol and other lipids in the LE/LY is explicit to many NPC1$^{-/-}$ cell types (e.g., neurons, fibroblasts) [47,140] but has rarely been reported in oligodendrocytes. Filipin staining is frequently used in the diagnosis of NPC thanks to the specific affinity of filipin to unesterified cholesterol. Therefore, oligodendrocytes from DIV6 were labeled by filipin to estimate the accumulation of cholesterol. The results showed that NPC1$^{-/-}$ oligodendrocytes exhibit extensive filipin signals concentrated in the vesicle-like structures of the cytosol, but not in WT cells (Fig. 27A1, B1). The intensity of filipin staining of each cell

was then quantified, and the average intensities were compared between WT and NPC1$^{-/-}$ oligodendrocytes. Because the levels of cytosolic cholesterol dramatically increase during the maturation of oligodendrocytes, only the intensities of the initial type of oligodendrocytes were measured in each group. Quantitation of filipin intensity indicated an elevated level of cholesterol in NPC1$^{-/-}$ oligodendrocytes, with a onefold increase in the average intensity as compared to WT oligodendrocytes (Fig. 27C). Moreover, CdM stimulation exhibited no influence on filipin intensity in either WT or NPC1$^{-/-}$ oligodendrocytes compared to cells in MyM medium (Fig. 27A4, B4).

It has been proven that CD reduces the accumulation of cholesterol in NPC, possibly by mobilizing the accumulated cholesterol from the LE/LY to other cellular compartments [47]. As expected, filipin staining of CD-treated NPC1$^{-/-}$ oligodendrocytes revealed a dramatic reduction in the accumulation of cholesterol, indicated by the disappearance of most bright dots, and it was observed that the average filipin intensity decreased to a level similar to that in untreated WT cells (Fig. 27A2, B2, C). However, CD treatment had minor effects on WT oligodendrocytes (Fig. 27A2, C).

Although CD has been found to reduce the accumulation of cholesterol in NPC1$^{-/-}$ oligodendrocytes, the mechanism underlying this phenomenon remains equivocal. To directly reduce the accumulation of cholesterol by diminishing cholesterol synthesis, we used lovastatin at a concentration of 0.25 μM in the present study, which was reported to reduce the synthesis of cholesterol by 50% in neurons [141]. Similar to CD, lovastatin has been found to reduce the accumulation of cholesterol in NPC1$^{-/-}$ oligodendrocytes, indicated by small, weak dots on filipin staining (Fig. 27B3). Upon lovastatin treatment, the average filipin intensity was also found to be significantly reduced as compared to untreated NPC1$^{-/-}$ oligodendrocytes (from 62.0 to 45.5), but less dramatically to CD treatment (37.4; Fig. 27C). Furthermore, it was found that lovastatin treatment reduces the intensity of filipin in WT oligodendrocytes (from 32.7 to 23.1; Fig. 27A3, C). Since cholesterol is primarily derived from *de novo* synthesis in cultured oligodendrocytes, only inhibiting the synthesis of cholesterol can decrease its cellular content and reduce its accumulation in the LE/LY of NPC1$^{-/-}$ cells.

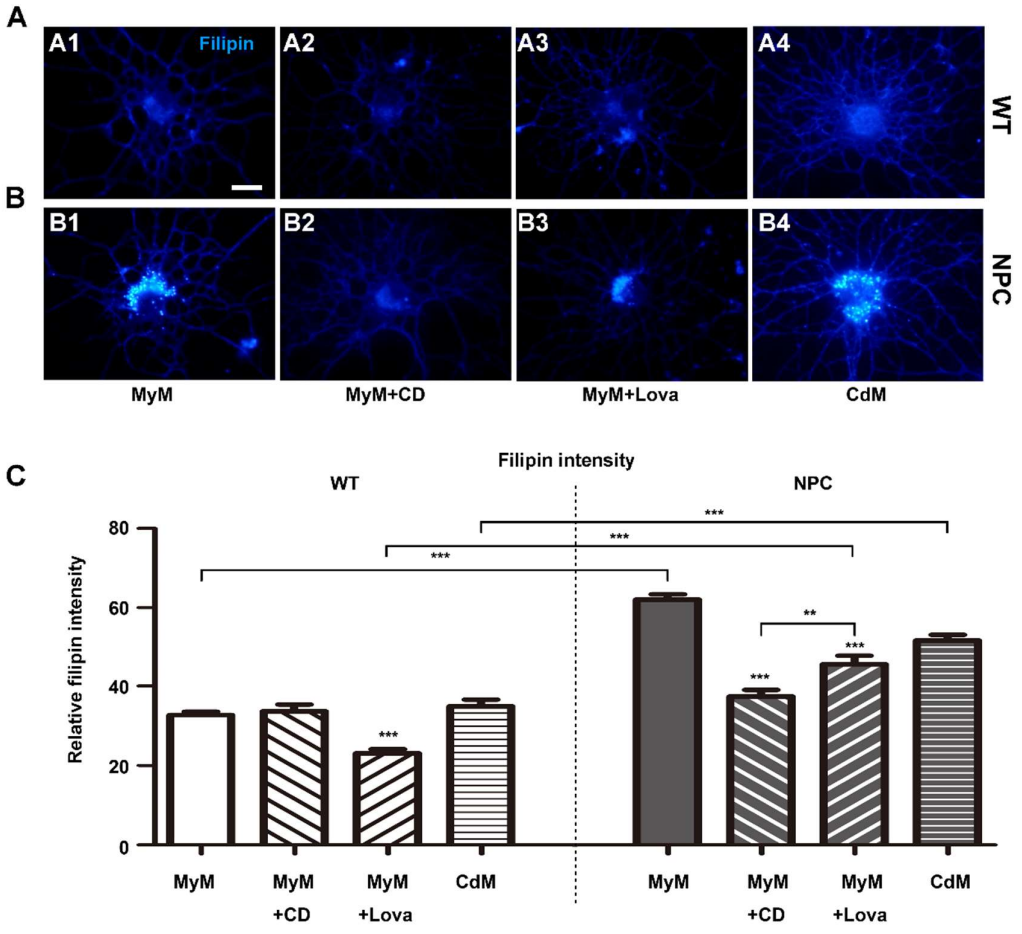

Fig. 27: CD and lovastatin reduce the accumulation of cholesterol in NPC1$^{-/-}$ oligodendrocytes

Filipin staining of WT (A) and NPC1$^{-/-}$ (B) oligodendrocytes with or without CD or lovastatin (Lova) treatment in MyM medium or in CdM at DIV6. Scale bar: 40 µm in A1 for all. (C) Quantification of the relative filipin intensity from A and B. Data were calculated from three independent experiments (the average filipin intensity was measured from more than 100 cells under each condition in every experiment) and are presented as mean ± SEM. Statistical significance was determined using Šidák-corrected two-way ANOVA. $^{*}p < 0.05$; $^{**}p < 0.01$; $^{***}p < 0.001$.

3.9. Restoring the maturation of oligodendrocytes by reducing the accumulation of cholesterol

CD treatment has several therapeutic effects on the accumulation of cholesterol in NPC1$^{-/-}$ oligodendrocytes (Fig. 27). To test whether this treatment subsequently influences the maturation of cells, the percentages of mature oligodendrocytes were calculated after CD treatment. The results showed that the percentages increased from 8.2% in untreated cells to 14.3% upon CD treatment in NPC1$^{-/-}$ oligodendrocytes in MyM medium. It was also found that CD treatment has a minor influence on the maturation of WT oligodendrocytes in MyM medium (Fig. 28A).

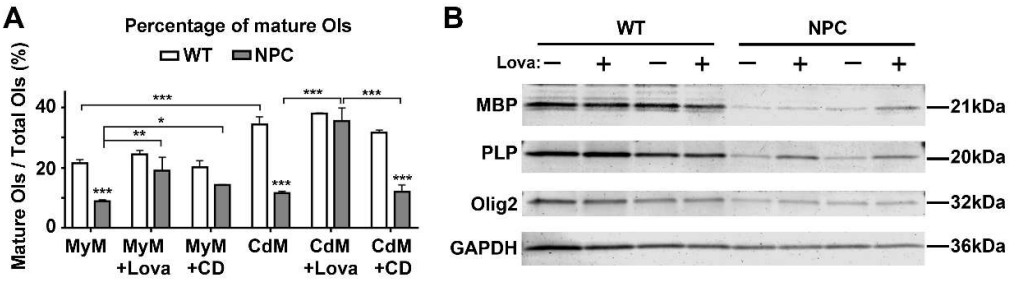

Fig. 28: Lovastatin treatment restores the maturation of NPC1$^{-/-}$ oligodendrocytes

(A) Quantification of mature oligodendrocytes with different treatments. The percentages of mature cells were calculated from the ratio of the number of mature cells to the total oligodendrocytes at DIV6. WT or NPC1$^{-/-}$ oligodendrocytes were treated with or without Lova or CD in different media (MyM medium or CdM). Data were calculated from three independent experiments (more than 600 cells were counted under each condition in every experiment) and are presented as mean ± SEM. Statistical significance was determined using Šidák-corrected two-way ANOVA. $^{*}p < 0.05$; $^{**}p < 0.01$; $^{***}p < 0.001$. (B) Western blot analysis of MBP, PLP, Olig1, and Olig2 in cultivated oligodendrocytes with or without Lova treatment at DIV6. β-Actin was used as the loading control.

Similar to CD, lovastatin has also been found to reduce the accumulation of cholesterol. Therefore, we evaluated the maturation of NPC1$^{-/-}$ oligodendrocytes upon lovastatin treatment. Notably, lovastatin treatment increased the percentage of mature NPC1$^{-/-}$ oligodendrocytes to 19.1%, which is considered significantly higher than those in untreated (8.8%) and even CD-

treated (14.2%) cells (Fig. 28A). Since mature-type oligodendrocytes have been found to increase in CdM as compared to MyM medium, oligodendrocytes cultivated in CdM were assessed with CD and lovastatin treatment. No significant increase was observed in CD-treated NPC1$^{-/-}$ oligodendrocytes (from 11.5% to 12.0%). However, after lovastatin treatment, the percentage of mature NPC1$^{-/-}$ oligodendrocytes reached 35.5%, similar to that in WT cells (38.0%) and nearly four times higher than those in CD-treated and untreated cells. However, lovastatin had no significant effect on the maturation of WT oligodendrocytes (Fig. 28A).

Upon different treatments, various proteins from purified oligodendrocytes were harvested at DIV6, and the expression of myelin proteins was analyzed using Western blot analysis (Fig. 28B). It was observed that the expression of myelin markers (MBP, PLP) increased in NPC1$^{-/-}$ oligodendrocytes upon lovastatin treatment, although the amounts were less than those in WT cells. Although lovastatin treatment reduced the filipin intensity (Fig. 27), the expression of myelin proteins did not change upon lovastatin treatment in WT groups.

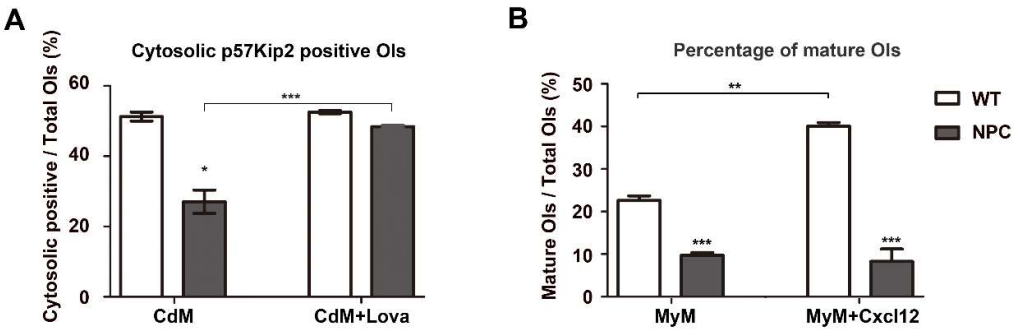

Fig. 29: Lovastatin promotes the nucleocytoplasmic transport of p57Kip2 independent of Cxcl12 signaling pathway in NPC1$^{-/-}$ oligodendrocytes

(A) Percentages of cytosolic p57Kip2-positive oligodendrocytes at DIV6 with or without lovastatin treatment in CdM. (B) Percentages of mature oligodendrocytes at DIV6 upon Cxcl12 stimulation in MyM medium. Data were calculated from five independent experiments (more than 600 cells were counted under each condition in every experiment) and are presented as mean ± SEM. Statistical significance was determined using Student's two-tailed *t*-test. $^{*}p < 0.05$; $^{**}p < 0.01$; $^{***}p < 0.001$.

To investigate the mechanism underlying the effects of lovastatin, we assessed the expression of Olig2 after treatment. Markedly increased expression of Olig2 was detected in

NPC1$^{-/-}$ oligodendrocytes upon treatment, although its amount was still less than that in WT cells (Fig. 28B). Since the intracellular transport of p57Kip2 is distinctly related to the maturation of oligodendrocytes [110] and interrupted translocation of p57Kip2 has been observed in NPC1$^{-/-}$ oligodendrocytes (Fig. 26), we evaluated the distribution of p57Kip2 in oligodendrocytes upon lovastatin treatment. The results showed that treatment promoted the nucleocytoplasmic transport of p57Kip2 in NPC1$^{-/-}$ oligodendrocytes and increased the percentage of cytosolic p57Kip2-positive NPC1$^{-/-}$ cells from 27.1% to 48.4%, similar to the level observed in WT cells under the same treatment. Nevertheless, lovastatin treatment had no effect on p57Kip2 transport in WT oligodendrocytes (Fig. 29A).

Cxcl12 is a chemokine that has been reported to promote p57Kip2 transport through the CXCR7 receptor and to enhance the maturation of oligodendrocytes [110,142]. It was found that, upon Cxcl12 treatment, the percentages of mature oligodendrocytes increased nearly twice to 40.05% in WT cells, but only by 7.97% in NPC1$^{-/-}$ cells (Fig. 29B). These results indicate that NPC1 dysfunction blocks the signals that transport p57Kip2 and consequently inhibits the maturation of NPC1$^{-/-}$ oligodendrocytes.

4. Discussion

Although myelin disturbance has been described in the NPC1$^{-/-}$ mouse model in the 1980s [35], the mechanism underlying how the dysfunction of the cholesterol transport protein influences myelination is still largely mysterious. In this study, we confirmed that hypomyelination occurs in NPC1$^{-/-}$ mice, indicated by the delayed initiation of myelination and decreased expression of myelin proteins (Figs. 11, 12). It was also observed that the expression of myelin-specific transcription factors decreased and that the maturation of primary NPC1$^{-/-}$ oligodendrocytes was inhibited and could not be promoted upon CdM stimulation (Figs. 16, 18, and 19). Furthermore, the nucleocytoplasmic transport of p57Kip2 was blocked (Fig. 26). The results showed that lovastatin decreases the accumulation of cholesterol in the LE/LY of NPC1$^{-/-}$ oligodendrocytes, increases the expression of Olig1 and Olig2, recovers the transport of p57Kip2 from the nucleus to the cytosol, and restores the maturation of oligodendrocytes (Figs. 26, 27, and 28).

4.1. Using the corpus callosum to monitor myelination

In this study, we used the corpus callosum to study myelin deficiency in NPC1$^{-/-}$ mice for the following reasons. (1) Myelin in the corpus callosum is severely disrupted in NPC1$^{-/-}$ mice. (2) Myelin comprises 50–60% of the dry weight of the white matter in the CNS, as estimated in the bovine brain [143]. Notably, the corpus callosum is the largest white-matter structure in the brain that primarily contains myelinated axons (e.g., more than 95% of the axons are myelinated in the human corpus callosum) [144], which project homotopically to the contralateral cortex, while their somas are located in layer II/III and layer V of the ipsilateral neocortex [145]. (3) Many researchers choose the corpus callosum to study myelination. For example, Nagy et al. electrically stimulated neurons in the corpus callosum at different frequencies and observed that the firing pattern of neurons tunes the response and behavior of OPCs [83]. The effects of Olig1 and Olig2 on oligodendrocyte differentiation have also been evaluated in the corpus callosum of Olig1$^{-/-}$ mice [101,146]. Meyer et al. pointed out that the oligodendrocytes in the corpus callosum provide energy to support axonal function via glucose in contrast to lactate in the optic nerve [147]. (4) Most importantly, the corpus callosum has a structure distinct from the adjacent tissues and can be distinguished and isolated under stereomicroscopy.

In the present study, we evaluated the expression of abundant myelin proteins using Western blot analysis to monitor myelination, since this technique is easier to perform than other methods, such as quantitation in immunohistochemical staining or electron microscopy [144]. According to the literature, myelin sheaths were first detected in the mouse brain at P11 [148]. Therefore, to monitor myelination starting from its initiation, the corpus callosum of mice at P6 to P65, especially at P8, P9, P10, and P12, was investigated. It was found that the patterns of myelin protein expression precisely reflect the processes of myelination during development: the vague appearance (from P8 to P10), dramatic increase (from P10 to P35), and steadiness (from P35 to P65) of the expression of myelin proteins represent the initiation phase, rapid phase, and completion of myelination in the corpus callosum, respectively. Additionally, in this study, immunostaining of brain slices confirmed the initiation of myelination, in which fibrous MBP-positive myelin structures, instead of punctate cell bodies, were present in the P9 corpus callosum (Fig. 12). Therefore, we defined the initiation of myelin formation to be around P9, two days earlier than what has been reported by Sturrock in 1980 [148], who compared myelination in the corpus callosum between P8 and P11 instead of P9. Importantly, in our study, we were able to used Western blotting to distinguish myelin protein expression patterns between two consecutive days (Fig. 11). Therefore, from our data, we propose that the corpus callosum is a good tissue model for studying molecular dynamics and signal cascades during myelination.

Myelination is coordinated by several interactions between neurons and oligodendrocytes and supported by astrocytes [149]. Many studies have used myelin-enriched fractions isolated using density gradient centrifugation to investigate myelination; however, these fractions contain compact myelin sheaths without the cytosolic fraction of oligodendrocytes and axons [57,73]. On the other hand, the corpus callosum contains multiple cell types involved in myelination; therefore, any protein changes besides oligodendrocytes can also be evaluated in the corpus callosum (Fig. 9).

4.2. Evaluating differentiation in primary oligodendrocytes

During myelination, the interaction between neurons and oligodendrocytes facilitates the wrapping of myelin sheaths on the right axons at the right time. Disruption of NPC1 in either neurons or oligodendrocytes affects myelination, which proves the necessity of NPC1 in both neurons and oligodendrocytes during myelination in mice [36]. However, the mechanism of

NPC1 in oligodendrocytes during myelination is still largely unknown. Thus, using a primary cell culture system, we focused on signal cascades in NPC1$^{-/-}$ oligodendrocytes.

To obtain primary mouse oligodendrocytes, we adopted the classical shaking method, which has originally been described for the isolation of rat OPCs [150], although the yield of oligodendrocytes obtained from mouse is lower than rat cells [134]. To test the quality of these isolated OPCs, we either cultured the isolated cells in a differentiation medium alone or cocultured them with primary cortical neurons. It was observed that these OPCs differentiated into oligodendrocytes, as revealed by the expression of specific lineage markers (PLP and MBP) and formed a typical morphology. The data obtained from our coculture system also revealed clear myelin sheaths, as indicated by the MBP-marked rod-like structures colocalized with NF and by the Nav1.6-labeled nodes of Ranvier flanked with Caspr-marked paranodes (Fig. 20). These results proved that the isolated primary oligodendrocytes preserve their physiological features and can be used to investigate the mechanisms of myelination *in vitro*.

It should be noted that the differentiation of oligodendrocytes is not synchronized in culture and, hence, can be quantified using the percentage of mature cells. Similar approaches have been reported by other researchers. For example, immature oligodendrocytes labeled with β-galactocerebroside and mature cells labeled with MBP have been used to investigate the function of PPAR-γ during lipid metabolism and oligodendrocyte differentiation [151]. Furthermore, Sholl analysis, a common morphological quantification method for assessing branching in neurons, has been used to evaluate the maturation of oligodendrocytes [143, 144]. Under proper circumstances, the size of oligodendrocytes may increase dramatically up to a hundred times, from an immature oligopolar structure to a mature membrane-like giant one. As a result of intercellular avoidance, the size of oligodendrocytes is highly related to the cell density. Therefore, Sholl analysis may underestimate the complexity of oligodendrocytes if the cells are not evenly distributed at a very low density.

A method based on the length, number, distribution, and size of the cells has been reported to categorize oligodendrocytes into five types, namely, low, medium-low, medium, medium-high, and high [152], which have been accepted and modified by others [111,142]. In this study, a system including three types (initial, medium, and mature) instead of these five types has been used to categorize oligodendrocytes, since the differences between the three medium types (medium-low, medium, and medium-high) are arbitrary and hardly

distinguishable. Besides the morphology of oligodendrocytes, the conspicuous increase observed in myelin proteins has been used as a parameter for cell type categorization.

4.3. Hypomyelination versus demyelination

Generally, defects in the formation of myelin during development result in hypomyelination. It has been reported that delayed myelin development is associated with a group of disorders referred to as hypomyelinating disorders [153]. For example, PMD, a prototype hypomyelinating disorder, is due to mutations in *Plp1*, whereas Pelizaeus–Merzbacher-like disease (PMLD) is due to mutations in *Gjc2* (gap junction protein γ2). Similar to NPC, mutations in solute carrier family 17 member 5 (SLC17A5) lead to the accumulation of sialic acid in the lysosome and, hence, to Salla disease (SD) [154]. In contrast, destruction or damage of preexisting myelinated structures leads to demyelination. Multiple sclerosis is one of the commonly known immune-mediated demyelinating diseases which cause, however, remains unclear [155]. Rapid correction of hyponatremia, the condition of low sodium level in the blood, causes osmotic demyelination syndrome [156].

In patients with NPC, a decrease in the volume of both the cerebellar gray and white matter has been reported and associated with impairments in saccadic gain and motor control [8,29]. In $NPC1^{-/-}$ mice, Takikita et al. described myelin disruption and suggested hypomyelination, but only a few time points were investigated and compared in the report [7]. In this study, we compared myelination in the corpus callosum of WT and $NPC1^{-/-}$ mice. The onset of myelination in WT mice, indicated by the emergence of myelin proteins, was observed at around P9, whereas in $NPC1^{-/-}$ mice, the onset was observed at P12, a delay of three days. Moreover, it was observed that the expression of myelin proteins in $NPC1^{-/-}$ mice greatly reduced compared to WT over time. Overall, our results confirm hypomyelination in $NPC1^{-/-}$ mice. Hence, it is important to focus on the signals that regulate myelin formation rather than degeneration in NPC.

4.4. Oligodendrocyte proliferation and migration in $NPC1^{-/-}$ mice

To wrap axons by myelin sheaths, OPCs are first generated and then migrate and differentiate into oligodendrocytes, which target axons and finally produce lipids and proteins to form insulating myelin structures. Disruption in any of the abovementioned steps results in hypomyelination. Conditional knockout of the L-type VOCCs isoform Cav1.2 in NG2-positive

OPCs affects cell proliferation and migration in early NG2 cells and also disrupts cell maturation at late stages, inducing significant hypomyelination in mice [157]. The knockout of G-protein-coupled receptor 56 (*Gpr56*) in mice decreases the proliferation of OPCs and leads to hypomyelination in the CNS. In addition, mutations in *Gpr56* in humans cause bilateral frontoparietal polymicrogyria (BFPP), in which myelination defects have been observed by magnetic resonance imaging (MRI) [158]. The overexpression of PDGF induces hyperproliferation of OPCs, and excess oligodendrocytes are eliminated via apoptosis at the immature stages during differentiation [159]. However, the elimination of extra cells is inhibited in semaphorin-4D-deficient mice, resulting in an increase in the cell number of oligodendrocytes in the cerebral cortex [160,161]. Abolishing bone morphogenetic protein receptor type IA (BMPR1A) reduces the number of immature oligodendrocytes in the brain at birth but significantly increases the number of mature and immature oligodendrocytes at P20 [159].

A question that has been raised in this study is whether the dysfunction of NPC1 reduces the number of OPCs, resulting in hypomyelination. Therefore, we compared the expression of NG2, a frequently used OPC maker, in the corpus callosum between WT and $NPC1^{-/-}$ mice. However, no difference was found at the early stages in $NPC1^{-/-}$ mice compared to WT mice. Notably, the downregulated expression of NG2 in the corpus callosum at P35 and P65 in WT mice (Fig. 11) indicates the completion of myelination in this region; however, the higher level of NG2 in older $NPC1^{-/-}$ mice suggests continuous proliferation of NG2-positive cells to compensate for the delayed myelination. Hughes et al. reported that NG2-positive cells continually survey the local environment, proliferate, and migrate to replace abolished cells in the cortex of adult mice [162]. Recently, it has also been observed that NG2-positive cells are multipotential and can differentiate into astrocytes and neurons *in vitro*, depending on extracellular signals [163]. In contrast, Kang et al. reported in their *in vivo* experiments that NG2-positive cells exhibit restricted lineage potential and only generate myelinating oligodendrocytes in the postnatal mouse brain and even remain committed to the oligodendrocyte lineage during neurodegeneration [164]. Other researchers have pointed out that oligodendrocytes have a redundant nature [84,85]. Kessaris et al. stated that three waves of oligodendrocytes are generated successively in the developing mouse brain and that any abolished population of oligodendrocytes can be compensated by others [75]. In addition, a massive number of oligodendrocytes are generated at the beginning of myelination to compete

over the limited survival factors, and those exceeding oligodendrocytes will be cleared later during development [77,86]. Therefore, changes in the number of oligodendrocytes are unlikely to cause hypomyelination in NPC1$^{-/-}$ mice.

After migrating from oligodendrogliogenic sites, oligodendrocytes become distributed throughout the entire CNS [165]. Protein defects affect the migration of oligodendrocytes. Ectopic activation of bone morphogenetic protein-4 (Bmp4) or transforming growth factor-β1 (Tgfβ1) accelerates the migration of OPCs into cortical areas [166]. Moreover, the absence of the receptor tyrosine-protein kinase ErbB4 in mouse embryos inhibits the migration of OPCs [167]. Blockage of cell migration has been reported in NPC1-deficient zebrafish [114]. To directly compare the migration of oligodendrocytes between WT and NPC1$^{-/-}$ mice, the distribution of Olig2-positive cells was evaluated in brain slices by immunostaining. At P10, Olig2-positive cells were detected in the entire brain, abundantly in the molecular layer of the cortex, no difference was observed between WT and NPC1$^{-/-}$ mice. Hence, it was concluded that the generation and migration of oligodendrocytes are not affected by the dysfunction of NPC1.

4.5. Differentiation of NPC1$^{-/-}$ oligodendrocytes

As it was observed that the number of OPCs is not altered and that the expression of myelin proteins and myelin-specific transcription factors is reduced, defects in the differentiation of OPCs were speculated. Generally, OPCs undergo simultaneous differentiation *in vitro*, although the process is rigorously controlled *in vivo*. For example, it has been suggested that homeobox protein Nkx-2.2 (Nkx2.2) controls the timing of OPC differentiation, possibly by directly repressing the expression of an inhibitory factor, namely, platelet-derived growth factor receptor alpha (Pdgfra) [168]. LINGO-1 inhibits the translocation and activation of receptor tyrosine-protein kinase erbB-2 (ErbB2) in lipid rafts to suppress the differentiation of oligodendrocytes. Knockdown of cyclin-dependent kinase 5 (Cdk5) in oligodendrocytes inhibits cell maturation and its knockout in mice reduces myelinated axons in the optic nerve and spinal cord but does not affect the number of OPCs [169].

In this study, we detected reduced expression of myelin proteins (MBP, PLP, and MOG) and transcription factors (Olig1, Olig2) in NPC1$^{-/-}$ corpus callosum and primary oligodendrocytes (Figs. 11, 13, and 20). We also observed that the maturation and

nucleocytoplasmic transport of p57Kip2 in primary NPC1$^{-/-}$ oligodendrocytes are inhibited (Fig. 26). All of these changes indicate the deficiency of NPC1$^{-/-}$ oligodendrocytes during differentiation.

4.5.1. Olig1

Olig1 is a basic helix-loop-helix (bHLH) transcription factor that is essential for the differentiation of oligodendrocytes. Olig1 regulates the transcription of the major myelin proteins MBP, PLP, and MAG. Abolished expression of myelin proteins and severely reduced myelination have been reported in Olig1-knockout mice [146]. The recovery of hypomyelination in the spinal cord but not in the brain of older Olig1-deficient mice suggests a specific role of Olig1 in myelination in the brain [101]. Moreover, ablation of Olig1 in OPCs inhibits cell differentiation and limits the ability of oligodendrocytes to repair demyelinated lesions in the CNS [170]. In NPC1$^{-/-}$ mice, it was found that the expression of Olig1 is reduced at P9, the time point of the initiation of myelination in the corpus callosum (Fig. 16), and that the transcription and translation levels of Olig1-controlled downstream myelin proteins (MBP, PLP) are also reduced (Figs. 8 and 15), consistent with the inhibited maturation in NPC1$^{-/-}$ oligodendrocytes (Fig. 21). Restoration of myelin proteins in the spinal cord has also been reported in older NPC1$^{-/-}$ mice [171], which is similar to the pattern observed in Olig1-knockout mice [101]. Therefore, reduced Olig1 is possibly a reason for hypomyelination in NPC1$^{-/-}$ mice.

4.5.2. Olig2

Homologous to Olig1, Olig2 is another key factor in the differentiation, maturation, and myelination of oligodendrocytes. Generally, oligodendroglial lineage cells fail to form in Olig2-knockout mice [172]. The overexpression of Olig2 in neural stem cells (NSCs) induces the expression of major myelin proteins and the development of mature oligodendrocytes. When transplanted in the corpus callosum of demyelinated mice, Olig2-transfected NSCs develop into remyelinating oligodendrocytes [173]. It has been suggested that Olig2 directs the transcription activator BRG1/Smarca4, an ATP-dependent SWI/SNF chromatin-remodeling enzyme, to oligodendrocyte-specific enhancers to transcribe myelin genes that promote the differentiation of oligodendrocytes and subsequent myelination in the CNS [105]. In NPC1$^{-/-}$ mice, the expression of Olig2 is reduced, similar to that of Olig1 (Fig. 16). However, in Olig1-deficient mice, compensated upregulation of Olig2 has been observed, explaining the recovery of hypomyelination in the spinal cord [101]. By abolishing Olig2 at different oligodendrocyte

stages, Mei et al. reported that the compensatory upregulation of Olig1 in Olig2-knockout immature oligodendrocytes enhances the maturation process and accelerates myelination [102]. Since no compensatory effects between Olig1 and Olig2 have been observed in NPC1$^{-/-}$ mice, the reduction of both proteins may indicate a disruption in their upstream signal.

4.5.3. Myrf

Myrf (initially termed MRF) was identified in postmitotic oligodendrocytes by transcriptomic analysis by Emery et al. in 2009. Knockout of Myrf within the oligodendrocyte lineage in mice reduces the expression of myelin genes and disrupts myelination but has no effect on premyelinating oligodendrocyte generation [104]. Importantly, the reduced expression patterns of MBP, PLP, and MOG, but not of Sox10, are similar to those in NPC1$^{-/-}$ mice, although the expression of NG2 is not affected in Myrf-knockout mice. Myrf regulates myelination by transporting its N-terminal domain into the nucleus, after cleavage from the transmembrane domain-containing region, to bind the enhancer regions of oligodendrocyte-specific and myelin genes [107,108]. Our previous data have shown that the transcription of Myrf is reduced in a different region in the CNS, especially in older NPC1$^{-/-}$ mice [171]. In the present study, we found that the amount of N-Myrf did not decrease in the corpus callosum of earlier NPC1$^{-/-}$ mice compared to age-matched WT mice, except at P65 (Fig. 23). Moreover, the transfer of N-Myrf into the nucleus was not disrupted in NPC1$^{-/-}$ oligodendrocytes, and strong N-Myrf signals were detected in the nuclei of most oligodendrocytes (Fig. 24), suggesting that the cleavage and nuclear transport of N-Myrf have not been affected in NPC1$^{-/-}$ oligodendrocytes. However, the amount of N-Myrf transported from the cytosol to the nucleus was not quantified in this study. Therefore, whether Myrf is involved in different pathological processes at the earlier stages should be further investigated. Moreover, Myrf is essential in the maintenance of myelin in the adult CNS, and its reduction in older mice may contribute to myelin disruption [174].

4.5.4. p57Kip2

The transport of proteins between the cytosol and the nucleus is a common mechanism to control myelination. For example, it has been reported that the transport of p57Kip2 [109,110] and Olig1 [101] from the nucleus to the cytosol and of NFAT [112] from the cytosol to the nucleus regulates the differentiation and maturation of oligodendrocytes. During the

differentiation and myelination of Schwann cells, the transfer of NFAT into the nucleus and its interaction with Sox10 activate Krox20, resulting in the expression of myelin genes [112]. For p57Kip2, although no difference was found in the expression of p57Kip2 protein in the corpus callosum between WT and NPC1$^{-/-}$ mice, nucleocytoplasmic transport was greatly reduced (Figs. 25 and 26), correlating with the inhibited maturation of oligodendrocytes. Any change in the subcellular distribution of p57Kip2 affects the differentiation of oligodendroglial cells in rats, mice, and humans both *in vivo* and *in vitro*. Moreover, the accumulation of p57Kip2 in the nucleus inhibits the differentiation of oligodendrocytes [110]. It has been suggested that Cxcl12 specifically activates the CXCR7 receptor to promote the transport of p57Kip2 and the maturation of oligodendrocytes [110,142]. However, in this study, it was found that Cxcl12 has no effect on the maturation of NPC1$^{-/-}$ oligodendrocytes (Fig. 29). Therefore, the nucleocytoplasmic transport of p57Kip2 was disrupted, which did not respond to stimulation with Cxcl12 in NPC1$^{-/-}$ oligodendrocytes.

4.6. Cholesterol accumulation in the LE/LY or deprivation in the membrane of NPC1$^{-/-}$ oligodendrocytes

Filipin-labeled cholesterol accumulation is the most characteristic feature in various NPC1-mutant cell types. Our results have also revealed intensely filipin-labeled NPC1$^{-/-}$ oligodendrocytes (Fig. 27). Despite the increased cholesterol levels observed in many NPC1$^{-/-}$ peripheral tissues, the amount in the brain did not differ from that of the WT controls [175]. The accumulation of cholesterol in the LE/LY of NPC1$^{-/-}$ cells is possibly due to an imbalance in intracellular distribution, as described in NPC1$^{-/-}$ neurons, where cholesterol heavily accumulates in cell bodies but decreases in distal axons [119]. In comparison to neurons, a massive amount of cholesterol is required in the distal myelin sheaths of oligodendrocytes during myelination. An insufficient level of cholesterol, resulting from abolishing its synthesis in oligodendrocytes, severely interrupts myelination [54]. The synthesis of cholesterol does not change in NPC1$^{-/-}$ cells (at least in the neurons [119]), but cholesterol resulting from *de novo* synthesis is accumulated in the LE/LY [176]. In primary cultured NPC1$^{-/-}$ neurons, the cholesterol accumulated in cell bodies is primarily derived from endogenous synthesis [119]. Although NPC1 dysfunction does not affect the supplementation of synthesized cholesterol, the incapability of transporting it outside the LE/LY limits the reuse of cholesterol after endocytosis or autophagy. Therefore, deprivation of myelin sheaths resulting from the occluded

mobilization of cholesterol from the LE/LY may cause hypomyelination in NPC1$^{-/-}$ oligodendrocytes.

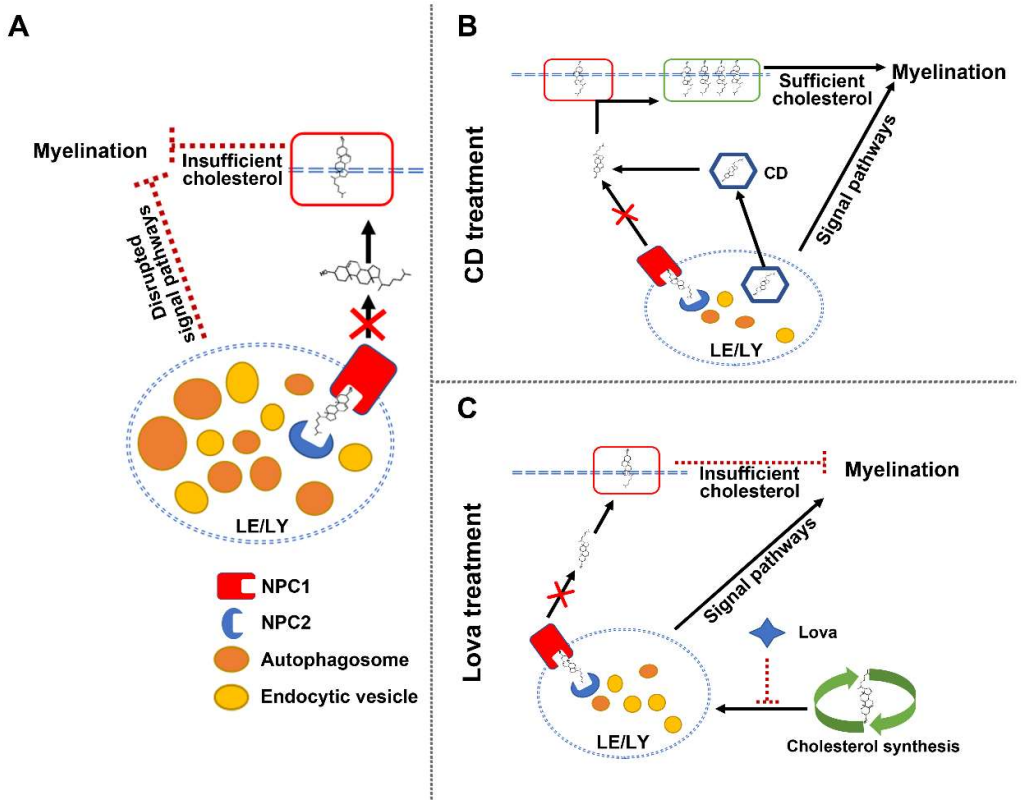

Fig. 30: Mechanisms underlying the effects of CD and lovastatin on myelination in NPC1$^{-/-}$ oligodendrocytes

(A) Schematic diagrams of inhibited myelination in NPC1$^{-/-}$ oligodendrocytes before treatment. (B, C) CD treatment reduces the accumulation of cholesterol in the LE/LY and/or transports cholesterol to myelin sheaths (B), whereas lovastatin (Lova) stimulation reduces only the accumulation of cholesterol by inhibiting its synthesis (C) to restore myelination.

It has been found that CD treatment reduces the filipin intensity and restores the maturation of NPC1$^{-/-}$ oligodendrocytes. The effect of CD may mediate by transporting cholesterol from the LE/LY to myelin sheaths (Fig. 30B). Treatment of *npc1* or *npc2* mutant fibroblasts with cholesterol-loaded CD significantly reduces the intensity of filipin. In general, CD treatment increases cholesterol esterification by acyl-coenzyme A (CoA):cholesterol acyltransferases (ACATs) [140]. These results show that CD mobilizes rather than extracts

accumulated cholesterol to other cellular compartments. However, inhibiting the synthesis of cholesterol by lovastatin reduces the accumulation of cholesterol and likewise restores the maturation of NPC1$^{-/-}$ oligodendrocytes (Fig. 30C). Notably, the mildly reduced cholesterol level due to lovastatin did not affect the maturation of WT oligodendrocytes, although a higher concentration of lovastatin may inhibit myelination in mice [48]. Therefore, after comparing the functions of CD and lovastatin in NPC1$^{-/-}$ oligodendrocytes, we suggest that cholesterol deprivation in the membrane is not the reason for the inhibited myelination in NPC1$^{-/-}$ oligodendrocytes, at least in the *in vitro* system. Besides degradation and recycling, the involvement of the LE/LY in different signaling pathways has been suggested [177,178]. Trajkovic et al. observed that PLP is initially transported to the LE/LY and that its redistribution to the plasma membrane is triggered by signals from neurons. They also suggested that oligodendrocytes may utilize the LE/LY to store large amounts of the membrane in a multilamellar and multivesicular fashion for myelin biogenesis [55]. Therefore, the signaling pathway disruption due to the accumulation of cholesterol in the LE/LY most likely lead to hypomyelination in NPC1$^{-/-}$ mice.

4.7. Other signaling pathways by lovastatin

In this study, CD treatment showed a stronger ability to reduce the accumulation of cholesterol than that of lovastatin. However, it was found that the percentage of mature NPC1$^{-/-}$ oligodendrocytes was lower with CD treatment than with lovastatin. Such differences cannot be explained by extracting excessive cholesterol in CD treatment since CD did not reduce the intensity of filipin in WT oligodendrocytes. Thus, lovastatin may also utilize other signaling cascades to promote myelination. Different statins, including lovastatin and simvastatin, regulate the processing of oligodendrocytes and improve their differentiation and remyelination via PPAR-γ and tumor suppressor phosphatase and tensin homolog (PTEN) signaling cascades in experimental autoimmune encephalomyelitis (EAE) [49]. Furthermore, it has been shown that simvastatin has time- and dose-dependent effects on myelin homeostasis and repair [179]. However, in the present study, lovastatin exhibited no significant effect on the maturation of WT oligodendrocytes (Fig. 28). In addition, it was observed that rosiglitazone (RZD), an agonist of PPAR-γ, promotes myelination only in WT oligodendrocytes, but not in NPC1$^{-/-}$ oligodendrocytes (data not shown). These results suggest that the effects of lovastatin in NPC1$^{-/-}$ oligodendrocytes were not from the PPAR-γ signaling cascade. Controversially, it has been found that lovastatin reduces hepatic and serum cholesterol levels but has no impact

on neurological symptoms in a small number of patients with NPC [180]. Treatment with the squalene synthase inhibitor (SSI) CP-340868 or lovastatin may inhibit myelin maturation in $NPC1^{-/-}$ mice [48]. Given the massive requirement of cholesterol during myelination, we used a lovastatin concentration of 0.25 μM, which reduces 50% of cholesterol synthesis in neurons, in our experiments [141]. Because cholesterol is self-sufficient in the CNS, cells are more susceptible to the inhibition of *de novo* cholesterol synthesis [181]. Different concentrations of lovastatin may have different effects (e.g., a low dose of 0.25 μM in our study versus a higher dose of 10 μM or higher in other studies) [49,179], resulting in different pathways.

4.8. Myelination regulated by neuronal secretory factors

Spatiotemporal restricted myelination depends on intrinsic programs from myelin-producing oligodendrocytes and extrinsic modulation from wrapped neurons. The neuronal electrical activity influences the proliferation of OPCs [80]. Axon selection for myelination is regulated via activity-dependent secretion [93]. In 1986, Bologa et al. reported soluble neuronal factors that regulate the production of MBP [94]. Generally, neuronal CdMs containing secretory factors promote the redistribution of PLP to the cellular membrane [55], induce the proliferation of OPCs [95], and promote the maturation of oligodendrocytes (Fig. 22). However, such factors in neuronal CdMs have not been identified so far.

In the present study, $NPC1^{-/-}$ oligodendrocytes did not respond to CdMs regardless of the genotype of the cultivated neurons; however, CdMs from $NPC1^{-/-}$ neurons promoted the maturation of WT oligodendrocytes. These results are inconsistent with the notion that *npc1* knockout exclusively in neurons is sufficient to disrupt myelination *in vivo* [36]. Possibly, npc*1* knockout only affects the neuron surface signals, but not the secretory factors. In addition, the procedures used to prepare CdMs are not performed under optimum conditions; molecules in the cytosol are released arbitrarily under nonphysiological conditions. Hence, whether the production of neuronal secretory factors is affected in $NPC1^{-/-}$ neurons will be answered when the factors are identified.

5. Summary

In this study, to investigate myelination, we applied mass-spectrometry-based differential quantitative proteomics to compare protein compositions in the corpus callosum of WT and NPC1$^{-/-}$ mice, identified most of the reported myelin proteins, and revealed a reduction in several myelin proteins in samples from NPC1$^{-/-}$ mice, proving the benefit of using the corpus callosum for investigating myelination. By comparing the expression of myelin structural proteins from the corpus callosum between WT and NPC1$^{-/-}$ mice at different time points, we found that the onset of myelination was delayed and confirmed hypomyelination in NPC1$^{-/-}$ mice. Furthermore, in NPC1$^{-/-}$ mice, we found that the expression level of the OPC markers NG2 and Sox10 was comparable to that in WT mice and that the distribution of oligodendrocytes in the brain was unaltered. Thus, it was concluded that the generation and migration of oligodendrocytes are not affected in NPC1$^{-/-}$ mice. Moreover, to investigate the cellular mechanism of hypomyelination in NPC1$^{-/-}$ mice, we established an *in vitro* myelination assay. Primary oligodendrocytes from either WT or NPC1$^{-/-}$ mice can wrap axons to form myelin sheaths. However, the percentage of mature cells in the culture system and upon the treatment of neuronal secretory factors significantly decreased in NPC1$^{-/-}$ oligodendrocytes. Moreover, the expression of the myelin-related transcription factors Olig1 and Olig2 was downregulated and the nucleocytoplasmic transport of p57Kip2 was inhibited in NPC1$^{-/-}$ oligodendrocytes. Therefore, loss of function of NPC1 disrupts the differentiation and maturation of NPC1$^{-/-}$ oligodendrocytes and eventually causes hypomyelination in NPC1$^{-/-}$ mice. Finally, to understand the involvement of cholesterol in hypomyelination in NPC, we treated NPC1$^{-/-}$ oligodendrocytes with lovastatin to inhibit the synthesis of cholesterol. We found that lovastatin reduces the accumulation of cholesterol in the LE/LY, increases the expression of Olig1 and Olig2, recovers the nucleocytoplasmic transport of p57Kip2, and restores the maturation of NPC1$^{-/-}$ oligodendrocytes. Therefore, we concluded that the accumulation of cholesterol in the LE/LY due to disrupted efflux, rather than its shortage in the plasma membrane, blocks essential myelin-regulated signaling pathways, inhibits the maturation of oligodendrocytes, and reduces the expression of myelin structural proteins, leading to hypomyelination in NPC1$^{-/-}$ mice.

6. References

1 Carstea, E. D. *et al.* Niemann-Pick C1 disease gene: Homology to mediators of cholesterol homeostasis. *Science* 277, 228-231, (1997).

2 Loftus, S. K. *et al.* Murine model of Niemann-Pick C disease: mutation in a cholesterol homeostasis gene. *Science* 277, 232-235, (1997).

3 Vance, J. E. & Karten, B. Niemann-Pick C Disease and Mobilization of Lysosomal Cholesterol by Cyclodextrin. *J Lipid Res*, (2014).

4 Vanier, M. T. [Niemann-Pick C disease: history, current research topics, biological and molecular diagnosis]. *Arch Pediatr* 17 Suppl 2, S41-44, (2010).

5 Crocker, A. C. & Farber, S. Niemann-Pick disease: a review of eighteen patients. *Medicine (Baltimore)* 37, 1-95, (1958).

6 Sarna, J. R. *et al.* Patterned Purkinje cell degeneration in mouse models of Niemann-Pick type C disease. *J Comp Neurol* 456, 279-291, (2003).

7 Takikita, S., Fukuda, T., Mohri, I., Yagi, T. & Suzuki, K. Perturbed myelination process of premyelinating oligodendrocyte in Niemann-Pick type C mouse. *J Neuropathol Exp Neurol* 63, 660-673, (2004).

8 Walterfang, M. *et al.* White and gray matter alterations in adults with Niemann-Pick disease type C: a cross-sectional study. *Neurology* 75, 49-56, (2010).

9 Niemann, A. Ein unbekanntes Krankheitsbild. *Jahrbuch für Kinderheilkunde* 79, 1–10, (1914).

10 Pick, L. Der Morbus Gaucher und die ihm ähnlichen Krankheiten (die lipoidzellige Splenohepatomegalie Typus Niemann und die diabetische Lipoidzellenhypoplasie der Milz). *Ergeb Inn Med Kinderheilkd* 29, 519–627, (1926).

11 Crocker, A. C. The cerebral defect in Tay-Sachs disease and Niemann-Pick disease. *J Neurochem* 7, 69-80, (1961).

12 Karten, B., Peake, K. B. & Vance, J. E. Mechanisms and consequences of impaired lipid trafficking in Niemann-Pick type C1-deficient mammalian cells. *Biochim Biophys Acta* 1791, 659-670, (2009).

13 Tang, Y., Li, H. & Liu, J. P. Niemann-Pick Disease Type C: from molecule to clinic. *Clin Exp Pharmacol Physiol* 37, 132-140, (2010).

14 Greer, W. L. *et al.* The Nova Scotia (type D) form of Niemann-Pick disease is caused by a G(3097)-> T transversion in NPC1. *American Journal of Human Genetics* 63, 52-54, (1998).

15 Naureckiene, S. *et al.* Identification of HE1 as the second gene of Niemann-Pick C disease. *Science* 290, 2298-+, (2000).

16 Infante, R. E. *et al.* NPC2 facilitates bidirectional transfer of cholesterol between NPC1 and lipid bilayers, a step in cholesterol egress from lysosomes. *P Natl Acad Sci USA* 105, 15287-15292, (2008).

17 Li, X. C., Saha, P., Li, J., Blobel, G. & Pfeffer, S. R. Clues to the mechanism of cholesterol transfer from the structure of NPC1 middle lumenal domain bound to NPC2. *P Natl Acad Sci USA* 113, 10079-10084, (2016).

18 Vanier, M. T. *et al.* Type C Niemann-Pick disease: spectrum of phenotypic variation in disruption of intracellular LDL-derived cholesterol processing. *Biochim Biophys Acta* 1096, 328-337, (1991).

19 Gondre-Lewis, M. C., McGlynn, R. & Walkley, S. U. Cholesterol accumulation in NPC1-deficient neurons is ganglioside dependent. *Curr Biol* 13, 1324-1329, (2003).

20 Li, H., Turley, S. D., Liu, B., Repa, J. J. & Dietschy, J. M. GM2/GD2 and GM3 gangliosides have no effect on cellular cholesterol pools or turnover in normal or NPC1 mice. *J Lipid Res* 49, 1816-1828, (2008).

21 Lloyd-Evans, E. *et al.* Niemann-Pick disease type C1 is a sphingosine storage disease that causes deregulation of lysosomal calcium. *Nat Med* 14, 1247-1255, (2008).

22 Simons, K. & Gruenberg, J. Jamming the endosomal system: lipid rafts and lysosomal storage diseases. *Trends Cell Biol* 10, 459-462, (2000).

23 Schulze, H., Kolter, T. & Sandhoff, K. Principles of lysosomal membrane degradation: Cellular topology and biochemistry of lysosomal lipid degradation. *Biochim Biophys Acta* 1793, 674-683, (2009).

24 Gillard, B. K., Clement, R. G. & Marcus, D. M. Variations among cell lines in the synthesis of sphingolipids in de novo and recycling pathways. *Glycobiology* 8, 885-890, (1998).

25 Kolter, T. & Sandhoff, K. Lysosomal degradation of membrane lipids. *Febs Letters* 584, 1700-1712, (2010).

26 Remmel, N., Locatelli-Hoops, S., Breiden, B., Schwarzmann, G. & Sandhoff, K. Saposin B mobilizes lipids from cholesterol-poor and bis(monoacylglycero)phosphate-rich membranes at acidic pH. Unglycosylated patient variant saposin B lacks lipid-extraction capacity. *Febs Journal* 274, 3405-3420, (2007).

27 Locatelli-Hoops, S. *et al.* Saposin A mobilizes lipids from low cholesterol and high bis(monoacylglycerol)phosphate-containing membranes: patient variant Saposin A lacks lipid extraction capacity. *J Biol Chem* 281, 32451-32460, (2006).

28 Oninla, V. O., Breiden, B., Babalola, J. O. & Sandhoff, K. Acid sphingomyelinase activity is regulated by membrane lipids and facilitates cholesterol transfer by NPC2. *J Lipid Res* 55, 2606-2619, (2014).

29 Walterfang, M. *et al.* Cerebellar volume correlates with saccadic gain and ataxia in adult Niemann-Pick type C. *Mol Genet Metab* 108, 85-89, (2013).

30 Love, S., Bridges, L. R. & Case, C. P. Neurofibrillary Tangles in Niemann-Pick Disease Type-C. *Brain* 118, 119-129, (1995).

31 Suzuki, K. *et al.* Neurofibrillary Tangles in Niemann-Pick Disease Type-C. *Acta Neuropathol* 89, 227-238, (1995).

32 Tanaka, J., Nakamura, H. & Miyawaki, S. Cerebellar involvement in murine sphingomyelinosis: a new model of Niemann-Pick disease. *J Neuropathol Exp Neurol* 47, 291-300, (1988).

33 Ong, W. Y. *et al.* Neurodegeneration in Niemann-Pick type C disease mice. *Exp Brain Res* 141, 218-231, (2001).

34 Totenhagen, J. W. *et al.* In vivo assessment of neurodegeneration in Niemann-Pick type C mice by quantitative T2 mapping and diffusion tensor imaging. *J Magn Reson Imaging* 35, 528-536, (2012).

35 Weintraub, H. *et al.* Neurological mutation characterized by dysmyelination in NCTR-Balb/C mouse with lysosomal lipid storage disease. *J Neurochem* 45, 665-672, (1985).

36 Yu, T. & Lieberman, A. P. Npc1 acting in neurons and glia is essential for the formation and maintenance of CNS myelin. *Plos Genetics* 9, e1003462, (2013).

37 Baumann, N. & Pham-Dinh, D. Biology of oligodendrocyte and myelin in the mammalian central nervous system. *Physiol Rev* 81, 871-927, (2001).

38 Zervas, M., Somers, K. L., Thrall, M. A. & Walkley, S. U. Critical role for glycosphingolipids in Niemann-Pick disease type C. *Curr Biol* 11, 1283-1287, (2001).

39 Stein, V. M. *et al.* Miglustat improves purkinje cell survival and alters microglial phenotype in feline Niemann-Pick disease type C. *J Neuropathol Exp Neurol* 71, 434-448, (2012).

40 Galanaud, D. *et al.* 24 month-treatment with miglustat of three patients with Niemann-Pick disease type C: follow up using brain spectroscopy. *Mol Genet Metab* 96, 55-58, (2009).

41 Alvarez, A. R. *et al.* Imatinib therapy blocks cerebellar apoptosis and improves neurological symptoms in a mouse model of Niemann-Pick type C disease. *Faseb Journal* 22, 3617-3627, (2008).

42 Lopez, C. A., de Vries, A. H. & Marrink, S. J. Molecular mechanism of cyclodextrin mediated cholesterol extraction. *PLoS Comput Biol* 7, e1002020, (2011).

43 Rosenbaum, A. I., Zhang, G., Warren, J. D. & Maxfield, F. R. Endocytosis of beta-cyclodextrins is responsible for cholesterol reduction in Niemann-Pick type C mutant cells. *P Natl Acad Sci USA* 107, 5477-5482, (2010).

44 Taylor, A. M., Liu, B., Mari, Y., Liu, B. & Repa, J. J. Cyclodextrin mediates rapid changes in lipid balance in Npc1(-/-) mice without carrying cholesterol through the bloodstream. *J Lipid Res* 53, 2331-2342, (2012).

45 Liu, B., Li, H., Repa, J. J., Turley, S. D. & Dietschy, J. M. Genetic variations and treatments that affect the lifespan of the NPC1 mouse. *J Lipid Res* 49, 663-669, (2008).

46 Davidson, C. D. *et al.* Chronic cyclodextrin treatment of murine Niemann-Pick C disease ameliorates neuronal cholesterol and glycosphingolipid storage and disease progression. *Plos One* 4, e6951, (2009).

47 Peake, K. B. & Vance, J. E. Normalization of cholesterol homeostasis by 2-hydroxypropyl-beta-cyclodextrin in neurons and glia from Niemann-Pick C1 (NPC1)-deficient mice. *J Biol Chem* 287, 9290-9298, (2012).

48 Reid, P. C. *et al.* Partial blockage of sterol biosynthesis with a squalene synthase inhibitor in early postnatal Niemann-Pick type C npcnih null mice brains reduces neuronal cholesterol accumulation, abrogates astrogliosis, but may inhibit myelin maturation. *J Neurosci Methods* 168, 15-25, (2008).

49 Paintlia, A. S., Paintlia, M. K., Singh, A. K., Orak, J. K. & Singh, I. Activation of PPAR-gamma and PTEN cascade participates in lovastatin-mediated accelerated differentiation of oligodendrocyte progenitor cells. *Glia* 58, 1669-1685, (2010).

50 Baron, W. & Hoekstra, D. On the biogenesis of myelin membranes: Sorting, trafficking and cell polarity. *Febs Letters* 584, 1760-1770, (2010).

51 Lee, Y. *et al.* Oligodendroglia metabolically support axons and contribute to neurodegeneration. *Nature* 487, 443-448, (2012).

52 Pfeiffer, S. E., Warrington, A. E. & Bansal, R. The oligodendrocyte and its many cellular processes. *Trends Cell Biol* 3, 191-197, (1993).

53 Czopka, T., Ffrench-Constant, C. & Lyons, D. A. Individual Oligodendrocytes Have Only a Few Hours in which to Generate New Myelin Sheaths In Vivo. *Dev Cell* 25, 599-609, (2013).

54 Saher, G. *et al.* High cholesterol level is essential for myelin membrane growth. *Nat Neurosci* 8, 468-475, (2005).

55 Trajkovic, K. *et al.* Neuron to glia signaling triggers myelin membrane exocytosis from endosomal storage sites. *J Cell Biol* 172, 937-948, (2006).

56 Saher, G. *et al.* Therapy of Pelizaeus-Merzbacher disease in mice by feeding a cholesterol-enriched diet. *Nat Med* 18, 1130-+, (2012).

57 Jahn, O., Tenzer, S. & Werner, H. B. Myelin proteomics: molecular anatomy of an insulating sheath. *Mol Neurobiol* 40, 55-72, (2009).

58 Klugmann, M. *et al.* Assembly of CNS myelin in the absence of proteolipid protein. *Neuron* 18, 59-70, (1997).

59 Werner, H. B. *et al.* A critical role for the cholesterol-associated proteolipids PLP and M6B in myelination of the central nervous system. *Glia* 61, 567-586, (2013).

60 Boison, D., Bussow, H., D'Urso, D., Muller, H. W. & Stoffel, W. Adhesive properties of proteolipid protein are responsible for the compaction of CNS myelin sheaths. *J Neurosci* 15, 5502-5513, (1995).

61 Griffiths, I. *et al.* Axonal swellings and degeneration in mice lacking the major proteolipid of myelin. *Science* 280, 1610-1613, (1998).

62 Garbern, J. Y. *et al.* Patients lacking the major CNS myelin protein, proteolipid protein 1, develop length-dependent axonal degeneration in the absence of demyelination and inflammation. *Brain* 125, 551-561, (2002).

63 Readhead, C., Schneider, A., Griffiths, I. & Nave, K. A. Premature arrest of myelin formation in transgenic mice with increased proteolipid protein gene dosage. *Neuron* 12, 583-595, (1994).

64 Readhead, C. & Hood, L. The dysmyelinating mouse mutations shiverer (shi) and myelin deficient (shimld). *Behav Genet* 20, 213-234, (1990).

65 Aggarwal, S. *et al.* Myelin membrane assembly is driven by a phase transition of myelin basic proteins into a cohesive protein meshwork. *PLoS Biol* 11, e1001577, (2013).

66 Barbarese, E. *et al.* Protein translation components are colocalized in granules in oligodendrocytes. *J Cell Sci* 108 (Pt 8), 2781-2790, (1995).

67 Ainger, K. *et al.* Transport and Localization of Exogenous Myelin Basic-Protein Messenger-Rna Microinjected into Oligodendrocytes. *J Cell Biol* 123, 431-441, (1993).

68 White, R. *et al.* Activation of oligodendroglial Fyn kinase enhances translation of mRNAs transported in hnRNP A2-dependent RNA granules. *J Cell Biol* 181, 579-586, (2008).

69 Colman, D. R., Kreibich, G., Frey, A. B. & Sabatini, D. D. Synthesis and Incorporation of Myelin Polypeptides into Cns Myelin. *J Cell Biol* 95, 598-608, (1982).

70 Lappe-Siefke, C. *et al.* Disruption of Cnp1 uncouples oligodendroglial functions in axonal support and myelination. *Nat Genet* 33, 366-374, (2003).

71 Li, C. *et al.* Myelination in the absence of myelin-associated glycoprotein. *Nature* 369, 747-750, (1994).

72 Brunner, C., Lassmann, H., Waehneldt, T. V., Matthieu, J. M. & Linington, C. Differential ultrastructural localization of myelin basic protein, myelin/oligodendroglial glycoprotein, and 2',3'-cyclic nucleotide 3'-phosphodiesterase in the CNS of adult rats. *J Neurochem* 52, 296-304, (1989).

73 Gopalakrishnan, G. *et al.* Lipidome and proteome map of myelin membranes. *J Neurosci Res* 91, 321-334, (2013).

74 Panfoli, I. *et al.* Myelin proteomics: the past, the unexpected and the future. *Expert Rev Proteomics* 11, 345-354, (2014).

75 Kessaris, N. *et al.* Competing waves of oligodendrocytes in the forebrain and postnatal elimination of an embryonic lineage. *Nat Neurosci* 9, 173-179, (2006).

76 Kirby, B. B. *et al.* In vivo time-lapse imaging shows dynamic oligodendrocyte progenitor behavior during zebrafish development. *Nat Neurosci* 9, 1506-1511, (2006).

77 Piaton, G., Gould, R. M. & Lubetzki, C. Axon-oligodendrocyte interactions during developmental myelination, demyelination and repair. *J Neurochem* 114, 1243-1260, (2010).

78 Rosenberg, S. S., Kelland, E. E., Tokar, E., De la Torre, A. R. & Chan, J. R. The geometric and spatial constraints of the microenvironment induce oligodendrocyte differentiation. *P Natl Acad Sci USA* 105, 14662-14667, (2008).

79 Howe, C. L. Coated glass and vicryl microfibers as artificial axons. *Cells Tissues Organs* 183, 180-194, (2006).

80 Barres, B. A. & Raff, M. C. Proliferation of oligodendrocyte precursor cells depends on electrical activity in axons. *Nature* 361, 258, (1993).

81 Demerens, C. *et al.* Induction of myelination in the central nervous system by electrical activity. *P Natl Acad Sci USA* 93, 9887-9892, (1996).

82 Coman, I., Barbin, G., Charles, P., Zalc, B. & Lubetzki, C. Axonal signals in central nervous system myelination, demyelination and remyelination. *J Neurol Sci* 233, 67-71, (2005).

83 Nagy, B., Hovhannisyan, A., Barzan, R., Chen, T. J. & Kukley, M. Different patterns of neuronal activity trigger distinct responses of oligodendrocyte precursor cells in the corpus callosum. *PLoS Biol* 15, e2001993, (2017).

84 Barres, B. A. *et al.* Cell death and control of cell survival in the oligodendrocyte lineage. *Cell* 70, 31-46, (1992).

85 Trapp, B. D., Nishiyama, A., Cheng, D. & Macklin, W. Differentiation and death of premyelinating oligodendrocytes in developing rodent brain. *J Cell Biol* 137, 459-468, (1997).

86 Simons, M. & Trajkovic, K. Neuron-glia communication in the control of oligodendrocyte function and myelin biogenesis. *J Cell Sci* 119, 4381-4389, (2006).

87 Foster, R. E., Connors, B. W. & Waxman, S. G. Rat optic nerve: electrophysiological, pharmacological and anatomical studies during development. *Brain Res* 255, 371-386, (1982).

88 Friede, R. L. Control of myelin formation by axon caliber (with a model of the control mechanism). *J Comp Neurol* 144, 233-252, (1972).

89 Tomassy, G. S. *et al.* Distinct Profiles of Myelin Distribution Along Single Axons of Pyramidal Neurons in the Neocortex. *Science* 344, 319-324, (2014).

90 Krasnow, A. M., Ford, M. C., Valdivia, L. E., Wilson, S. W. & Attwell, D. Regulation of developing myelin sheath elongation by oligodendrocyte calcium transients in vivo. *Nat Neurosci* 21, 24-28, (2018).

91 Kramer-Albers, E. M. & White, R. From axon-glial signalling to myelination: the integrating role of oligodendroglial Fyn kinase. *Cell Mol Life Sci* 68, 2003-2012, (2011).

92 Mensch, S. *et al.* Synaptic vesicle release regulates myelin sheath number of individual oligodendrocytes in vivo. *Nat Neurosci* 18, 628-630, (2015).

93 Hines, J. H., Ravanelli, A. M., Schwindt, R., Scott, E. K. & Appel, B. Neuronal activity biases axon selection for myelination in vivo. *Nat Neurosci* 18, 683-689, (2015).

94 Bologa, L., Aizenman, Y., Chiappelli, F. & de Vellis, J. Regulation of myelin basic protein in oligodendrocytes by a soluble neuronal factor. *J Neurosci Res* 15, 521-528, (1986).

95 Hardy, R. & Reynolds, R. Rat cerebral cortical neurons in primary culture release a mitogen specific for early (GD3+/04-) oligodendroglial progenitors. *J Neurosci Res* 34, 589-600, (1993).

96 Mitew, S. *et al.* Mechanisms regulating the development of oligodendrocytes and central nervous system myelin. *Neuroscience* 276, 29-47, (2014).

97 Jepson, S. *et al.* LINGO-1, a Transmembrane Signaling Protein, Inhibits Oligodendrocyte Differentiation and Myelination through Intercellular Self-interactions. *J Biol Chem* 287, 22184-22195, (2012).

98 Chen, Y. *et al.* The oligodendrocyte-specific G protein-coupled receptor GPR17 is a cell-intrinsic timer of myelination. *Nat Neurosci* 12, 1398-1406, (2009).

99 Barres, B. A., Lazar, M. A. & Raff, M. C. A novel role for thyroid hormone, glucocorticoids and retinoic acid in timing oligodendrocyte development. *Development* 120, 1097-1108, (1994).

100 Gupta, R. K., Bhatia, V., Poptani, H. & Gujral, R. B. Brain metabolite changes on in vivo proton magnetic resonance spectroscopy in children with congenital hypothyroidism. *J Pediatr* 126, 389-392, (1995).

101 Dai, J. X., Bercury, K. K., Ahrendsen, J. T. & Macklin, W. B. Olig1 function is required for oligodendrocyte differentiation in the mouse brain. *J Neurosci* 35, 4386-4402, (2015).

102 Mei, F. *et al.* Stage-specific deletion of Olig2 conveys opposing functions on differentiation and maturation of oligodendrocytes. *J Neurosci* 33, 8454-8462, (2013).

103 Hornig, J. *et al.* The Transcription Factors Sox10 and Myrf Define an Essential Regulatory Network Module in Differentiating Oligodendrocytes. *Plos Genetics* 9, (2013).

104 Emery, B. *et al.* Myelin gene regulatory factor is a critical transcriptional regulator required for CNS myelination. *Cell* 138, 172-185, (2009).

105 Yu, Y. *et al.* Olig2 targets chromatin remodelers to enhancers to initiate oligodendrocyte differentiation. *Cell* 152, 248-261, (2013).

106 Cahoy, J. D. *et al.* A transcriptome database for astrocytes, neurons, and oligodendrocytes: a new resource for understanding brain development and function. *J Neurosci* 28, 264-278, (2008).

107 Bujalka, H. *et al.* MYRF Is a Membrane-Associated Transcription Factor That Autoproteolytically Cleaves to Directly Activate Myelin Genes. *PLoS Biol* 11, (2013).

108 Li, Z. H., Park, Y. & Marcotte, E. M. A Bacteriophage Tailspike Domain Promotes Self-Cleavage of a Human Membrane-Bound Transcription Factor, the Myelin Regulatory Factor MYRF. *PLoS Biol* 11, (2013).

109 Heinen, A. *et al.* The cyclin-dependent kinase inhibitor p57kip2 is a negative regulator of Schwann cell differentiation and in vitro myelination. *P Natl Acad Sci USA* 105, 8748-8753, (2008).

110 Gottle, P. *et al.* Oligodendroglial maturation is dependent on intracellular protein shuttling. *J Neurosci* 35, 906-919, (2015).

111 Cheli, V. T., Santiago Gonzalez, D. A., Spreuer, V. & Paez, P. M. Voltage-gated Ca2+ entry promotes oligodendrocyte progenitor cell maturation and myelination in vitro. *Exp Neurol* 265, 69-83, (2015).

112 Kao, S. C. *et al.* Calcineurin/NFAT signaling is required for neuregulin-regulated Schwann cell differentiation. *Science* 323, 651-654, (2009).

113 Weider, M. *et al.* Nfat/calcineurin signaling promotes oligodendrocyte differentiation and myelination by transcription factor network tuning. *Nat Commun* 9, 899, (2018).

114 Schwend, T., Loucks, E. J., Snyder, D. & Ahlgren, S. C. Requirement of Npc1 and availability of cholesterol for early embryonic cell movements in zebrafish. *J Lipid Res* 52, 1328-1344, (2011).

115 Bi, X. & Liao, G. Autophagic-lysosomal dysfunction and neurodegeneration in Niemann-Pick Type C mice: lipid starvation or indigestion? *Autophagy* 3, 646-648, (2007).
116 Elrick, M. J., Yu, T., Chung, C. & Lieberman, A. P. Impaired proteolysis underlies autophagic dysfunction in Niemann-Pick type C disease. *Hum Mol Genet* 21, 4876-4887, (2012).
117 Wood, T. L. *et al.* mTOR: a link from the extracellular milieu to transcriptional regulation of oligodendrocyte development. *ASN Neuro* 5, e00108, (2013).
118 Shen, D. *et al.* Lipid storage disorders block lysosomal trafficking by inhibiting a TRP channel and lysosomal calcium release. *Nat Commun* 3, 731, (2012).
119 Karten, B., Vance, D. E., Campenot, R. B. & Vance, J. E. Cholesterol accumulates in cell bodies, but is decreased in distal axons, of Niemann-Pick C1-deficient neurons. *J Neurochem* 83, 1154-1163, (2002).
120 Karten, B., Vance, D. E., Campenot, R. B. & Vance, J. E. Trafficking of cholesterol from cell bodies to distal axons in Niemann pick C1-deficient neurons. *J Biol Chem* 278, 4168-4175, (2003).
121 Jarjour, A. A., Zhang, H., Bauer, N., Ffrench-Constant, C. & Williams, A. In vitro modeling of central nervous system myelination and remyelination. *Glia* 60, 1-12, (2012).
122 O'Meara, R. W., Ryan, S. D., Colognato, H. & Kothary, R. Derivation of enriched oligodendrocyte cultures and oligodendrocyte/neuron myelinating co-cultures from post-natal murine tissues. *J Vis Exp*, (2011).
123 Xiao, J. *et al.* Extracellular signal-regulated kinase 1/2 signaling promotes oligodendrocyte myelination in vitro. *J Neurochem* 122, 1167-1180, (2012).
124 Watkins, T. A., Emery, B., Mulinyawe, S. & Barres, B. A. Distinct Stages of Myelination Regulated by gamma-Secretase and Astrocytes in a Rapidly Myelinating CNS Coculture System. *Neuron* 60, 555-569, (2008).
125 Pang, Y. *et al.* Neuron-oligodendrocyte myelination co-culture derived from embryonic rat spinal cord and cerebral cortex. *Brain Behav* 2, 53-67, (2012).
126 Cheli, V. T., Gonzalez, D. A. S., Spreuer, V. & Paez, P. M. Voltage-gated Ca++ entry promotes oligodendrocyte progenitor cell maturation and myelination in vitro. *Exp Neurol* 265, 69-83, (2015).
127 Temple, S. & Raff, M. C. Differentiation of a bipotential glial progenitor cell in a single cell microculture. *Nature* 313, 223-225, (1985).
128 Szuchet, S., Polak, P. E. & Yim, S. H. Mature oligodendrocytes cultured in the absence of neurons recapitulate the ontogenic development of myelin membranes. *Dev Neurosci* 8, 208-221, (1986).
129 Vanier, M. T. Niemann-Pick disease type C. *Orphanet J Rare Dis* 5, 16, (2010).
130 Wisniewski, J. R., Zougman, A., Nagaraj, N. & Mann, M. Universal sample preparation method for proteome analysis. *Nat Methods* 6, 359-362, (2009).
131 Cox, J. *et al.* Accurate proteome-wide label-free quantification by delayed normalization and maximal peptide ratio extraction, termed MaxLFQ. *Mol Cell Proteomics* 13, 2513-2526, (2014).
132 Sharma, K. *et al.* Cell type- and brain region-resolved mouse brain proteome. *Nat Neurosci* 18, 1819-1831, (2015).
133 Hubner, R. *et al.* Differentiation of human neural progenitor cells regulated by Wnt-3a. *Biochem Biophys Res Commun* 400, 358-362, (2010).
134 Chen, Y. *et al.* Isolation and culture of rat and mouse oligodendrocyte precursor cells. *Nat Protoc* 2, 1044-1051, (2007).
135 Brewer, G. J. & Torricelli, J. R. Isolation and culture of adult neurons and neurospheres. *Nat Protoc* 2, 1490-1498, (2007).
136 Yang, F., Feng, X., Rolfs, A. & Luo, J. Lovastatin promotes myelin formation in NPC1 mutant oligodendrocytes. *J Neurol Sci* 386, 56-63, (2018).
137 Bauer, N. M. *et al.* Myelin Basic Protein synthesis is regulated by small non-coding RNA 715. *Embo Reports* 13, 827-834, (2012).
138 Meijer, D. H. *et al.* Separated at birth? The functional and molecular divergence of OLIG1 and OLIG2. *Nat Rev Neurosci* 13, 819-831, (2012).

139 Caldwell, J. H., Schaller, K. L., Lasher, R. S., Peles, E. & Levinson, S. R. Sodium channel Na(v)1.6 is localized at nodes of Ranvier, dendrites, and synapses. *P Natl Acad Sci USA* 97, 5616-5620, (2000).

140 Rosenbaum, A. I., Zhang, G., Warren, J. D. & Maxfield, F. R. Endocytosis of beta-cyclodextrins is responsible for cholesterol reduction in Niemann-Pick type C mutant cells. *P Natl Acad Sci USA* 107, 5477-5482, (2010).

141 Mailman, T., Hariharan, M. & Karten, B. Inhibition of neuronal cholesterol biosynthesis with lovastatin leads to impaired synaptic vesicle release even in the presence of lipoproteins or geranylgeraniol. *J Neurochem* 119, 1002-1015, (2011).

142 Gottle, P. *et al.* Activation of CXCR7 Receptor Promotes Oligodendroglial Cell Maturation. *Ann Neurol* 68, 915-924, (2010).

143 Norton, W. T. & Autilio, L. A. The lipid composition of purified bovine brain myelin. *J Neurochem* 13, 213-222, (1966).

144 Aboitiz, F., Scheibel, A. B., Fisher, R. S. & Zaidel, E. Fiber composition of the human corpus callosum. *Brain Res* 598, 143-153, (1992).

145 Zhou, J. *et al.* Axon position within the corpus callosum determines contralateral cortical projection. *P Natl Acad Sci USA* 110, E2714-E2723, (2013).

146 Xin, M. *et al.* Myelinogenesis and axonal recognition by oligodendrocytes in brain are uncoupled in Olig1-null mice. *J Neurosci* 25, 1354-1365, (2005).

147 Meyer, N. *et al.* Oligodendrocytes in the Mouse Corpus Callosum Maintain Axonal Function by Delivery of Glucose. *Cell Rep* 22, 2383-2394, (2018).

148 Sturrock, R. R. Myelination of the mouse corpus callosum. *Neuropathol Appl Neurobiol* 6, 415-420, (1980).

149 Ishibashi, T. *et al.* Astrocytes promote myelination in response to electrical impulses. *Neuron* 49, 823-832, (2006).

150 McCarthy, K. D. & de Vellis, J. Preparation of separate astroglial and oligodendroglial cell cultures from rat cerebral tissue. *J Cell Biol* 85, 890-902, (1980).

151 Roth, A. D. *et al.* PPAR gamma activators induce growth arrest and process extension in B12 oligodendrocyte-like cells and terminal differentiation of cultured oligodendrocytes. *J Neurosci Res* 72, 425-435, (2003).

152 Sperber, B. R. & McMorris, F. A. Fyn tyrosine kinase regulates oligodendroglial cell development but is not required for morphological differentiation of oligodendrocytes. *J Neurosci Res* 63, 303-312, (2001).

153 Barkovich, A. J. & Deon, S. Hypomyelinating disorders: An MRI approach. *Neurobiology of Disease* 87, 50-58, (2016).

154 Strehle, E. M. Sialic acid storage disease and related disorders. *Genet Test* 7, 113-121, (2003).

155 Yadav, S. K., Mindur, J. E., Ito, K. & Dhib-Jalbut, S. Advances in the immunopathogenesis of multiple sclerosis. *Curr Opin Neurol* 28, 206-219, (2015).

156 King, J. D. & Rosner, M. H. Osmotic demyelination syndrome. *Am. J. Med. Sci* 339, 561-567, (2010).

157 Cheli, V. T. *et al.* Conditional Deletion of the L-Type Calcium Channel Cav1.2 in Oligodendrocyte Progenitor Cells Affects Postnatal Myelination in Mice. *J Neurosci* 36, 10853-10869, (2016).

158 Giera, S. *et al.* The adhesion G protein-coupled receptor GPR56 is a cell-autonomous regulator of oligodendrocyte development. *Nat Commun* 6, 6121, (2015).

159 Calver, A. R. *et al.* Oligodendrocyte population dynamics and the role of PDGF in vivo. *Neuron* 20, 869-882, (1998).

160 Taniguchi, Y. *et al.* Sema4D deficiency results in an increase in the number of oligodendrocytes in healthy and injured mouse brains. *J Neurosci Res* 87, 2833-2841, (2009).

161 Yamaguchi, W., Tamai, R., Kageura, M., Furuyama, T. & Inagaki, S. Sema4D as an inhibitory regulator in oligodendrocyte development. *Mol Cell Neurosci* 49, 290-299, (2012).

162 Hughes, E. G., Kang, S. H., Fukaya, M. & Bergles, D. E. Oligodendrocyte progenitors balance growth with self-repulsion to achieve homeostasis in the adult brain. *Nat Neurosci* 16, 668-676, (2013).

163 Kondo, T. & Raff, M. Oligodendrocyte precursor cells reprogrammed to become multipotential CNS stem cells. *Science* 289, 1754-1757, (2000).

164 Kang, S. H., Fukaya, M., Yang, J. K., Rothstein, J. D. & Bergles, D. E. NG2+ CNS glial progenitors remain committed to the oligodendrocyte lineage in postnatal life and following neurodegeneration. *Neuron* 68, 668-681, (2010).

165 Mallon, B. S., Shick, H. E., Kidd, G. J. & Macklin, W. B. Proteolipid promoter activity distinguishes two populations of NG2-positive cells throughout neonatal cortical development. *J Neurosci* 22, 876-885, (2002).

166 Choe, Y., Huynh, T. & Pleasure, S. J. Migration of oligodendrocyte progenitor cells is controlled by transforming growth factor beta family proteins during corticogenesis. *J Neurosci* 34, 14973-14983, (2014).

167 Ortega, M. C. *et al.* Neuregulin-1/ErbB4 signaling controls the migration of oligodendrocyte precursor cells during development. *Exp Neurol* 235, 610-620, (2012).

168 Zhu, Q. *et al.* Genetic evidence that Nkx2.2 and Pdgfra are major determinants of the timing of oligodendrocyte differentiation in the developing CNS. *Development* 141, 548-555, (2014).

169 Yang, Y. *et al.* Cyclin dependent kinase 5 is required for the normal development of oligodendrocytes and myelin formation. *Dev Biol* 378, 94-106, (2013).

170 Arnett, H. A. *et al.* bHLH transcription factor Olig1 is required to repair demyelinated lesions in the CNS. *Science* 306, 2111-2115, (2004).

171 Yan, X. *et al.* Decreased expression of myelin gene regulatory factor in Niemann-Pick type C 1 mouse. *Metab Brain Dis* 26, 299-306, (2011).

172 Lu, Q. R. *et al.* Common developmental requirement for Olig function indicates a motor neuron/oligodendrocyte connection. *Cell* 109, 75-86, (2002).

173 Copray, S. *et al.* Olig2 overexpression induces the in vitro differentiation of neural stem cells into mature oligodendrocytes. *Stem Cells* 24, 1001-1010, (2006).

174 Koenning, M. *et al.* Myelin gene regulatory factor is required for maintenance of myelin and mature oligodendrocyte identity in the adult CNS. *J Neurosci* 32, 12528-12542, (2012).

175 Vanier, M. T. Lipid changes in Niemann-Pick disease type C brain: personal experience and review of the literature. *Neurochem Res* 24, 481-489, (1999).

176 Cruz, J. C. & Chang, T. Y. Fate of endogenously synthesized cholesterol in Niemann-Pick type C1 cells. *J Biol Chem* 275, 41309-41316, (2000).

177 Saftig, P. & Klumperman, J. Lysosome biogenesis and lysosomal membrane proteins: trafficking meets function. *Nat Rev Mol Cell Biol* 10, 623-635, (2009).

178 Jaishy, B. & Abel, E. D. Lipids, lysosomes, and autophagy. *J Lipid Res* 57, 1619-1635, (2016).

179 Miron, V. E. *et al.* Simvastatin regulates oligodendroglial process dynamics and survival. *Glia* 55, 130-143, (2007).

180 Patterson, M. C. *et al.* The effect of cholesterol-lowering agents on hepatic and plasma cholesterol in Niemann-Pick disease type C. *Neurology* 43, 61-64, (1993).

181 Bjorkhem, I. & Meaney, S. Brain cholesterol: Long secret life behind a barrier. *Arterioscler* 24, 806-815, (2004).

7. Abbreviations

ACATs	Acyl-coenzyme A (CoA): cholesterol acyltransferases
BCA	Bicinchoninic acid assay
BFPP	Bilateral frontoparietal polymicrogyria
bHLH	Basic helix-loop-helix
Bmp 4	Bone morphogenetic protein-4
BMPR1A	Bone morphogenetic protein receptor type IA
BrdU	Bromodeoxyuridine
Caspr	Contactin-associated protein 1
CC	Corpus callosum
CD	2-hydroxypropyl-β-cyclodextrin
Cdk5	Cyclin dependent kinase 5
CdM	Neuron-conditioned medium
CNP	2',3'-cyclic nucleotide phosphodiesterase
CTX	Cortex
DAPI	4′,6-diamidino-2-phenylindole
DMEM	Dulbecco's Modified Eagle's Medium
DNase	Deoxyribonuclease
dNTP	Deoxyribonucleotide triphosphates
EAE	Experimental autoimmune encephalomyelitis
EDTA	Ethylenediaminetetraacetic acid
EGTA	Ethylene glycol-bis (β-aminoethyl ether)-N, N, N', N'-tetraacetic acid
ER	Endoplasmic reticulum
ErbB2	Receptor tyrosine-protein kinase erbB-2
FAK	Non-receptor tyrosine kinase focal adhesion kinase
FGFs	Fibroblast growth factors
GAPDH	Glyceraldehyde-3-phosphate dehydrogenase
GFP	Green fluorescent protein
Gjc2	Gap junction protein γ2

GM2	Ganglioside GM2
GM3	Ganglioside GM3
GPR17	G-protein-coupled receptor 17
Gpr56	G protein-coupled receptor 56
HMG-CoA	3-hydroxy-3-methylglutaryl-CoA reductase
ID2/ID4	DNA-binding protein inhibitor ID-2
Krox20	E3 SUMO-protein ligase
LDL	Low-density lipoprotein
LE/LY	Late endosome/lysosome
LINGO1	Immunoglobulin domain-containing-1
Lova	Lovastatin
L-VOCCs	L-type voltage-operated Ca2+ channels
MAG	Myelin-associated glycoprotein
MBP	Myelin basic protein
MEM	Eagle′s minimum essential medium
MOG	Myelin-oligodendrocyte glycoprotein
MRI	Magnetic resonance imaging
MS	Multiple sclerosis
mTor	Serine/threonine-protein kinase mTOR
Myrf	Myelin gene regulatory factor
Nav1.6	Sodium channel protein type 8 subunit alpha
NeuN	RNA binding protein fox-1 homolog 3
NFAT	Nuclear factor of activated T-cells
NG2	Neural/glial antigen 2
Nkx2.2	Homeobox protein Nkx-2.2
NPC	Niemann-Pick Type C disease
NPC1L	NPC1-like protein-1
NPCs	Neural progenitor cells
NPD	Niemann-Pick disease type D
Olig1	Oligodendrocyte transcription factor 1

Olig2	Oligodendrocyte transcription factor 2
OPCs	Oligodendrocyte progenitor cells
P57Kip2	Cyclin-dependent kinase inhibitor 1C
PBS	Phosphate-buffered saline
PCR	Polymerase chain reaction
PD	Primer dimer
PDGF	Latelet-derived growth factor
Pdgfra	Platelet-derived growth factor receptor alpha
PDL	Poly-D-lysine
Pen/Str	Penicillin Streptomycin mixtures
PLP	Proteolipid protein
PMD	Pelizaeus-Merzbacher disease
PMLD	Pelizaeus–Merzbacher-like disease
PPAR-γ	Peroxisome proliferator-activated receptor-γ
PPIA	Peptidyl-prolyl cis-trans isomerase A
PTEN	Phosphatidylinositol 3,4,5-trisphosphate 3-phosphatase and dual-specificity protein phosphatase PTEN
RIPA	Radioimmunoprecipitation assay buffer
RZD	Rosiglitazone
SCAP	Sterol regulatory element-binding protein cleavage activating protein
SD	Salla disease
SDS	Sodium dodecyl sulfate
SEM	Standard error of the mean
Sema4D	Semaphorin-4D
SHH	Sonic hedgehog
Smarca4	Transcription activator BRG1
Smpd1	Acid sphingomyelinase
Sox10	SRY-related HMG-box 10
SQS	Squalene synthase
SSI	Squalene synthase inhibitor

STR	Striatum
T3	Triiodothyronine/thyroid hormone 3
TBS	Tris-buffered saline
TBST	TBS-Tween solution
Tgf β1	Transforming Growth Factor β1
TTX	Tetrodotoxin
VAMP2	Vesicle associated membrane protein 2
VOCCs	Voltage-operated Ca^{2+} channels
VSGP	Vertical supranuclear gaze palsy

8. Acknowledgements

Most of all, I would like to express my sincere gratitude to Professor Arndt Rolfs. He established the wonderful Albrecht-Kossel-Institut für Neuroregeneration, where we were working together to investigate different rare diseases. I would like to thank PD Dr. Jiankai Luo, who guided me into the research of Niemann-Pick type C disease and myelination. Being my supervisor, he encouraged brilliant ideas, advised various methods, boosted morale, criticized flaws, proofread thesis; beyond a supervisor, he assisted in VISA applications, negotiated with landlords, handled bureaucratical requests. Many thanks to other Ph.D. students and Post Docs for helping me a lot from the lab meetings, brainstorms, and discussions; our technicians for their continuous support and assistance. Thanks to our collaborators, Professor Andreas Wree, Professor Anja Bräuer and Professor Martin Witt from Institute of Anatomy, for hosting the regular NPC meeting, and sharing information and inspirations; Professor Hartmut Schlüter, Mrs. Parnian Kiani, Mr. Ramin Fazel and Mr. Yudong Guan, for their generous contributions in proteomic analysis.

I would like to thank all my friends. They came from different backgrounds, counties, and religions, however, the similarities gathered, and differences attracted each other to be friends. We created so many fantastic moments that imprinted in our memories: trips, sports, cooking, German classes, movie nights, city runs, theme parties, political debates. Life would be tedious without their presents.

I am so grateful to my parents, who support me unconditionally. Thank them for accepting my flaws and respecting my decisions. Thanks to my girlfriend and my dog. We build a home together to share joys and cure wounds.

In the end, I would like to thank the China Scholar Council for sponsoring my Ph.D. study, Dr. Junsong Liu, Dr. Hua Wang and Mr. Xichang Wang for being my financial guarantees, the TBI project. Without the finical support from them, I would not have the chance to finish my Ph.D. here in University of Rostock.

Declaration

Ich versichere eidesstattlich durch eigenhändige Unterschrift, dass ich die Arbeit selbstständig und ohne Benutzung anderer als der angegebenen Hilfsmittel angefertigt habe. Alle Stellen, die wörtlich oder sinngemäß aus Veröffentlichungen entnommen sind, habe ich als solche kenntlich gemacht.

Die Arbeit ist noch nicht veröffentlicht und ist in gleicher oder ähnlicher Weise noch nicht als Studienleistung zur Anerkennung oder Bewertung vorgelegt worden. Ich weiß, dass bei Abgabe einer falschen Versicherung die Prüfung als nicht bestanden zu gelten hat.

Rostock 02.06.2022 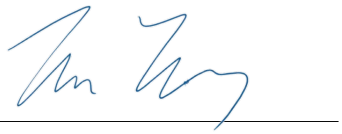

(Abgabedatum) (Vollständige Unterschrift)

Curriculum Vitae

Name: Fan Yang

Birth date and place: Aug. 21, 1986 in Rizhao, P. R. China

Tel: +4915907608698

E-Mail: timyang14@hotmail.com

Education:

2012 - Present: Ph.D. candidate (Dr. rer. hum.)
Albrecht-Kossel-Institute for Neuroregeneration (Akos),
University of Rostock
2009 - 2012: M.S. in Biochemistry and Molecular Biology
College of life Sciences, Jilin University, China
2004 - 2008: B.Ed. in Physical Education (Major)
College of Physical Education, Jilin University, China
B.S. in Biotechnology (Minor)
College of life Sciences, Jilin University, China

Publications:

1. A. Gläser, F. Hammerl, M. Gräler, S. Coldewey, C. Völkner, M. Frech, **F. Yang**, J. Luo , E. Tönnies, O. von Bohlen Und Halbach, N. Brandt, D. Heimes, A. Neßlauer, G. Korenke, M. Owczarek-Lipska, J. Neidhardt, A. Rolfs, A. Wree, M. Witt, A. Bräuer. Identification of Brain-Specific Treatment Effects in NPC1 Disease by Focusing on Cellular and Molecular Changes of Sphingosine-1-Phosphate Metabolism, Int J Mol Sci, 21 (2020) 4502.
2. **F. Yang**, Y. Guan, X. Feng, A. Rolfs, H. Schluter, J. Luo, Proteomics of the corpus callosum to identify novel factors involved in hypomyelinated Niemann-Pick Type C disease mice, Molecular brain, 12 (2019) 17.
3. **F. Yang**, X. Feng, A. Rolfs, J. Luo, Lovastatin promotes myelin formation in NPC1 mutant oligodendrocytes, J Neurol Sci, 386 (2018) 56-63.
4. X. Feng, B.M. Bader, **F. Yang**, M. Segura, L. Schultz, O.H.U. Schröder, A. Rolfs, J. Luo, Improvement of impaired electrical activity in NPC1 mutant cortical neurons upon DHPG stimulation detected by micro-electrode array, Brain Res, 1694 (2018) 87-93.
5. J. Lukas, C. Cozma, **F. Yang**, G. Kramp, A. Meyer, A.M. Nesslauer, S. Eichler, T. Bottcher, M. Witt, A.U. Brauer, P. Kropp, A. Rolfs, Glucosylsphingosine Causes Hematological and Visceral Changes in Mice-Evidence for a Pathophysiological Role in Gaucher Disease, Int J Mol Sci, 18 (2017) E2192.
6. X. Yan, **F. Yang**, J. Lukas, M. Witt, A. Wree, A. Rolfs, J. Luo, Hyperactive glial cells contribute to axonal pathologies in the spinal cord of Npc1 mutant mice, Glia, 62 (2014) 1024-1040.
7. X. Yan, J. Lin, V.A. Talabattula, C. Mussmann, **F. Yang**, A. Wree, A. Rolfs, J. Luo, ADAM10 negatively regulatesnegatively regulates neuronal differentiation during spinal cord development, Plos One, 9 (2014) e84617.